

Material Properties of Spider Silk

By

Mark J. Bonino

Submitted in Partial Fulfillment
of the
Requirements for the Degree of
Master of Science

Supervised by
Professor David R. Harding

Materials Science Program
The College
School of Engineering and Applied Sciences

University of Rochester
Rochester, NY

2003

Curriculum Vitae

The author was born in Rochester, NY on 26 May 1972. He attended St. John Fisher College from 1990 to 1994, and graduated with a Bachelor of Science degree in 1994. He came to the University of Rochester in the spring of 1995 as a staff employee at the Laboratory for Laser Energetics and began his part-time graduate studies in the Materials Science Program in the Spring of 1998. He pursued his research under the direction of Professor David R. Harding.

Acknowledgements

I would like to thank Dr. David R. Harding for his direction and insight during the term of this project. I also recognize and thank Messrs. E. Alfonso, L. Elasky, R. Gram, S. Noyes, D. Turner, and M. Wittman of the Laboratory for Laser Energetics' Target Fabrication Group for their technical assistance and J. Tidu of CEA, France for preparing diagrams. In particular, I thank L. Elasky for computer support and R. Gram for his experimental design format. I appreciate the support I received from Mr. B. McIntyre of the University of Rochester's Department of Optics for the SEM micrographs. I also value the support from C. Craig and H. Levi of Harvard University for the spider identification. I thank Chi Hwa Wu and Drs. Feng Yu Tsai and E. Alfonso for their moral support and T. Hicks for his motivating work ethic and assistance throughout the project. I also thank Mses. K. Freson and D. Hixson for their efforts in preparing this document. Finally, I thank my wife for her encouragement and patience, and I thank my parents and brothers for their continued confirmation.

Abstract

Spider silk has been employed to support direct-drive inertial confinement fusion (ICF) targets at the Laboratory for Laser Energetics. The silk's material properties such as stiffness, elasticity, high strength, energy to break and performance at cryogenic temperatures make it the only functioning small diameter material suitable to mount targets. Because silk is so important to ICF, these properties are quantified. A load cell and strain gauge were developed specifically for measuring silk (15gf full scale, 150% elongation). The design requirements for the load cell and strain gauge are discussed. Young's modulus, percent elongation, ultimate tensile strength and energy to break are quantified for room temperature and after heating the silk to 100°C. Upon comparing untreated silk and heat-treated silk, the stiffness, strength and energy to break were reduced after heating, while the elasticity did not change. To be specific, Young's modulus decreased from 2.2 ± 0.7 GPa to 0.6 ± 0.1 GPa, the strength decreased from 1244 ± 214 MPa to 382 ± 122 MPa and the energy to break decreased from $1.4 \pm 0.3 \times 10^5$ J/kg to $0.4 \pm 0.2 \times 10^5$ J/kg. The elasticity remained the same: $24.1 \pm 2\%$ for untreated silk and $24.3 \pm 5\%$ for heat-treated silk. Quantifying these properties will assist cryogenic target related issues such as fuel filling times and target vibration.

Table of Contents

1.0 Introduction	1
1.1 Spider Silk Background	1
1.2 Silk Applied to Inertial Confinement Fusion (ICF)	4
1.3 Objectives.....	5
1.4 Summary	5
1.5 Tables and Figures	7
1.6 References	10
2.0 Experimental and Equipment Design	12
2.1 Introduction	12
2.2 Tensile Testing Overview	12
2.3 Load Cell Design.....	15
2.4 Summary	17
2.5 Tables and Figures	18
2.6 References	23
3.0 Mechanical Material Properties	24
3.1 Introduction	24
3.1.1 Silk Diameter Variation and Experimental Uncertainty	25
3.2 Elastic Region	26
3.3 Inelastic Region.....	27
3.3.1 Percent Elongation	27
3.3.2 Hysteresis	28
3.3.3 Ultimate Tensile Strength and Final Modulus	29
3.3.4 Energy to Break.....	30
3.4 Summary	31
3.5 Tables and Figures	32
3.6 References	49
4.0 Elevated Temperature Testing	50
4.1 Introduction	50
4.2 Experimental Setup	51
4.3 Elastic Region	52
4.4 Inelastic Region.....	53

4.4.1 Percent Elongation	53
4.4.2 Ultimate Tensile Strength.....	53
4.4.3 Energy to Break.....	54
4.5 Summary	54
4.6 Tables and Figures	55
4.7 References	61
5.0 Summary	62
Appendix 1: Tensile testing data.....	64
A1.1 Calculations	64
A1.2 Untreated data.....	72
A1.3 Heat-treated data.....	87
A1.4 Hysteresis Data.....	96
Appendix 2: Silk Preparation Overview	102
A2.1 Sample Preparation.....	102
A2.2 Characterization.....	104
A2.3 Test Setup.....	104
A2.4 Appendix Figures	106

List of Tables

<i>Table 1 Mechanical properties for selected materials</i>	7
<i>Table 2 Operational limits of devices used for experimental setup</i>	18
<i>Table 3 Silk diameter measurements used for “averaged” values. The mean diameter is $1.00 \pm 0.09 \mu\text{m}$.</i>	32
<i>Table 4 Percent elongation at the yield point (defined as the value where the data begins to deviate from the initial slope).</i>	33
<i>Table 5 Young’s Modulus is $2.2 \pm 0.7 \text{ GPa}$. The stiffness decreases by a factor of 5 ($0.4 \pm 0.07 \text{ GPa}$) after the silk yields.</i>	34
<i>Table 6 Initial sample lengths and maximum percent elongation ($24.1 \pm 2\%$). Maximum strain was independent of initial length.</i>	35
<i>Table 7 Hysteresis data. The percentage of unrecovered strain decreases with every cycle. The internal energy lost as heat per cycle decreases since the percent strain remains constant (5%).</i>	36
<i>Table 8 Ultimate tensile strength ($1.2 \pm 0.2 \text{ GPa}$) and corresponding maximum load.</i>	37
<i>Table 9 The energy required to break a silk sample is $1.4 \pm 0.3 \text{ J/kg}$ ($\times 10^5$).</i>	38
<i>Table 10 Comparison of baseline material properties between experimental data and literature values.</i>	39
<i>Table 11 The silk heated to 100°C for 24 h. has a Young’s modulus of $0.6 \pm 0.1 \text{ GPa}$. The final modulus (after yielding) is $0.2 \pm 0.05 \text{ GPa}$.</i>	55
<i>Table 12 Strain at the yield point for silk heated to 100°C for 24 h is $1.2 \pm 0.2\%$.</i>	56
<i>Table 13 Properties of silk heated to 100°C for 24 h. The averaged experimental values are the following: percent elongation, $24.3 \pm 4.6\%$, ultimate tensile stress, $0.4 \pm 0.1 \text{ GPa}$, energy to break, $4 \pm 2 \times 10^4 \text{ J/kg}$.</i>	57
<i>Table 14 Dragline silk material properties between untreated and heat-treated silk (100°C for 24 h.)</i>	58

List of Figures

Figure 1 Spider silk structure: (A) photograph of a golden orb weaver (<i>Nephila</i> , sp.), (B) a segment of dragline silk, (C) silk matrix containing β -pleated sheets (Gray rectangles) and α -helices (lines surrounding rectangles), (D) β -pleated sheets (gray) are accordion-shaped, crystalline structures that are created by α -helices undergoing shear during the initial extrusion through the spider's spinneret. This concept is based on that of the silkworm. ⁴	8
Figure 2 Photograph of a cryogenic compatible target mount. Silk spans the 250 μm diameter beryllium wire frame. Notice the four silk strands supporting the 920 μm diameter capsule. Silk strands are approximately 1 μm in diameter.	9
Figure 3 Schematic of a fundamental tensile testing device. The sample is in between two fixed grips (green boxes).	19
Figure 4 Conceptual design of tensile testing apparatus.	20
Figure 5 LabView architecture of tensile testing program.	21
Figure 6 Continuation of LabView code.	22
Figure 7 A single strand of spider silk shown at 50,000 times magnification. The diameter is 834.1 nm. The surface texture is difficult to image due to the low electrical conductivity of the silk. The upper limit is 10 keV; any more will burn through the sample.	40
Figure 8 Four strands of silk grouped together illustrate batch-to-batch variability.	41
Figure 9 Typical stress-strain data. The silk yields at approximately 1% strain; the maximum strain is 20%. Notice after the silk ruptures, the data plateaus at 600 MPa. This indicates two parallel silk strands were loaded.	42
Figure 10 Complete recovery is exhibited when load is removed, demonstrating the elasticity of the Hookean region. The viscoelastic nature of the silk is also seen as the loading and unloading data is not overlapping. (The gap shown at the end of the unloading cycle is lost data during the test.)	43
Figure 11 Schematic of silk harvesting technique, as seen from left to right. (Top sequence) The spider attaches a dragline from a substrate and falls to the surface below. Once the silk dragline is long enough, the silk is attached to the nearby fixture with 2 parallel beams. The silk is drawn into contact with the beams that contain an adhesive on the surface. A spool reels the fresh silk into smaller, more manageable sections for testing. (Bottom sequence) Silk being applied to the cryogenic target mount. The reel contains 9 sections of silk. One section at a time is added to a temporary fixture (center) for maneuverability. The beryllium mount is moved into position and the silk is attached to the frame.	44

Figure 12 SEM micrograph showing one of the nine samples measured for quantifying the variation of silk diameter over a 30 cm strand. The micrograph shows 2 parallel strands of silk.	45
Figure 13 Schematic of Powellscope metrology station measuring the length of a silk sample. In the first step, focus is on the glue joint connecting the silicon carbide fiber to the silk. The stage is translated downward, while recording the displacement. The translation ends at the glue/post intersection. The total displacement is measured seven times and then an average initial length is reported for each sample.....	46
Figure 14 Hysteresis curves. The calculated area between the loading and unloading curves is (internal) energy lost. In order to make this calculation, raw data is used in the form of load and displacement. The load (mgf) and displacement (μm) data multiplied together to yield energy (J). As each cycle is completed, the strain remains constant. Also notice as cycles are completed, the loading slope increases in the limit of the initial slope.....	47
Figure 15 SEM micrograph of silk with two parallel strands over the length.	48
Figure 16 Heating sequence. Before heating, the silk matrix consists of long flexible α -helixes and rigid crystalline β -sheets. β -sheets are discontinuities in an α -helix microstructure. When heated, a fraction of the β -sheets melt, decreasing the total number of β -sheets in the matrix. As a result, the microstructure has fewer discontinuities. When stressed, there are fewer local mismatches that would cause resistance otherwise. The result is less-stiff silk compared to untreated silk.....	59
Figure 17 Stress-strain data comparing untreated and heat-treated silk (heated to 100 °C). Notice the reduced initial slope for heat-treated silk compared to the untreated silk. Both types retain elasticity greater than 20% strain.	60
Figure 18 Top view as looking through the Wild microscope. The two spokes hold the silk in place while the UV glue cures to the aluminum post and the silicon-carbide fiber (SiC). The small circle in the right diagram is the vacuum chuck used to position the SiC. Once the glue is cured, the silk is cut from the spokes, leaving the silk attached to the post. The silk is now easily handled using the operator's fingers.	106
Figure 19 Flowchart of experimental process	107

1.0 Introduction

1.1 Spider Silk Background

For many decades, biologists and material scientists have been fascinated with the favorable mechanical properties of spider silk. Its resilience, elasticity, tensile strength and energy to break are equivalent or superior to those of common metallic and non-metallic structural materials. For example, *Table 1* compares modulus, strength and energy to break of similar materials.¹ Compare Kevlar, the material used for bulletproof vests, to spider silk: although spider silk tensile strength is a factor of four less than Kevlar (3.4-4.1 GPa), the energy it takes to break silk is about three times greater ($1 \times 10^5 \text{ Jkg}^{-1}$). AISI 1080 high carbon steel music wire (annealed condition) has an elongation up to 25% and a tensile strength of 0.6 GPa (89 ksi),² while spider silk has an elongation to rupture of 30% and a tensile strength of 1 GPa.¹ Based on these values, silk has greater elasticity than steel music wire and has a comparable tensile strength. Silk is also biodegradable. It becomes clear why spider silk has been such a researched material.

Spider silk is a general term for any web-like fiber that the animal prepares as a net, or a cocoon for harnessed prey, or even a dragline to lower itself. To be specific, the orb-web-weaving female common garden spider produces seven different types of silk: (1) dragline and structural silk (major ampullate glands), (2) structural thread and auxillary spiral (minor ampullate glands), (3) core fibers of capture spiral (fili- or flagilliform glands), (4) aqueous coating and glycoprotein glue

for capture spiral (aggregate glands), (5) tough outer silk of egg sac (cylindrical glands), (6) soft inner silk of egg sac and silk for swathing prey (aciniform a/b glands), and (7) cement silk for joints and attachment (piriform glands).³ Only types (1) and (3) have been studied in detail.¹ Silk is made from keratin, a protein found in hair, horn and feathers.⁴ An extrusion process beginning in the major ampullate gland makes dragline silk. Vollrath reports highly viscous α -keratin is formed from grandula ducts to create a liquid crystalline dope.⁵ The liquid is extruded through a nozzle that creates shear, causing the molecular helices to stack onto each other. The result is an accordion-shaped molecule encased in an amorphous jacket of rubber-like material. The helical stacks are referred to as β -pleated sheets and make up a local crystalline region within the random remaining amino acid chains, as illustrated in *Figure 1*.⁴ The amorphous regions are made from glycine and called “ α -helices”, while the β -pleated sheets are alanine-based proteins. The crystalline regions provide strength and the amorphous regions provide flexibility, and in turn, high energy to break.

Most researchers have been interested in how to reproduce this biopolymer synthetically. In 1976, Work pioneered the modern-day study of silk. Work’s research involved anesthetizing spiders to discover if the animal consciously controlled the silk dimensions, and in turn its properties.⁶ A correlation was formed favoring higher strength silk from a conscience silk donor. Gene sequencing is currently being investigated to explain silk’s robust properties.^{7, 8} The Jelinski effort at Cornell University during the 1990’s studied the structural aspects of silk by employing X-ray diffraction techniques (both small angle⁹ and wide angle¹⁰).

Jelinski's works showed that the dry silk matrix of *Nephila* species contains both amorphous (88%) and crystalline (12%) regions.

Although there have been numerous efforts to discover a synthetic technique to fabricate silk, the applications of silk are just beginning. One reason spider silk has not caught on is due to the spider's predatory nature, making it more difficult to handle.¹¹ The alternative is using silk from silkworms, which produce lower strength material to that of spiders. Research at Tufts University continues in an effort to apply silk as an alternate material for medical sutures. Silk possesses many positive aspects related to this application: (1) *tensile strength* – to match the clinical repair, (2) *knot strength* – the amount of force required to cause a knot to slip, (3) *elasticity*, (4) *memory* – change in stiffness over time; the better the suture, the less memory, (5) *degradability* – ability to be metabolized by host once its repair function has been completed, (6) *tissue reactivity* – non-irritant, and (7) *infection free*.¹¹ Two possible military applications are bulletproof vests and parachute chord. Silk from the major ampullate gland not only serves as dragline silk, but also as a capture thread. This silk is used to stop unexpected prey in mid-flight. High extensibility at high velocity makes silk a strong candidate for both of these situations.¹² The textile industry has patented a technique for reinforcing a fiber with spider silk. The silk in a helical pattern orbits the fiber. Once the silk is added, the combined pair of the fiber/silk is sewn into fabric.¹³ For 30 years, the astronomers at the University of Victoria, Canada have employed spider silk.¹⁴ They are using silk as a thin crosshair reticule for the Schmid telescope. Another group who use silk are members of the Inertial Confinement Fusion (ICF) community. Brinker *et al.*, describe the application of silk

with respect to a low mass target mount.¹⁵ Strands of silk are used as suspension lines keeping a spherical, gas-filled capsule stationary during a laser driven implosion.¹⁶ This application motivates the majority of this thesis.

1.2 Silk Applied to Inertial Confinement Fusion (ICF)

At the Laboratory for Laser Energetics (LLE) silk is used to provide a stable, cryogenically compatible, low mass mount for targets used on the OMEGA Laser System. A direct-drive laser fusion target at LLE is a millimeter diameter capsule, or shell, filled with deuterium and tritium fuel (DT). The DT fuel is fused to produce helium and energy upon being imploded by the 60 OMEGA laser beams. *Figure 2* illustrates this type of mounting system. This mounting scheme requires material of low atomic number in order to minimally affect the implosion. X-rays from high-Z materials can prematurely heat the core before the shock wave arrives. This causes an insufficient temperature difference in the capsule. Without a great temperature difference, the capsule will not achieve the pressures needed to fuse the deuterium and tritium. Along with a low atomic number, the ideal mount needs to be low mass. A bulky mount attached to the shell can cause a mass perturbation and a non-uniform implosion. A dense material has more inertia and will not accelerate as quickly, causing a non-uniform implosion. The elastic properties of silk also are advantageous for practical reasons. During handling, a silk target mount is more forgiving than a rigid stalk-mounted target. Even after a sharp impulse, the silk returns to rest in a fraction of a second. More importantly, the capsule remains suspended. The silk

retains its properties in cryogenic environments. The silk becomes stiffer when frozen but still supports targets at temperatures between 10 and 20 K.

1.3 Objectives

In this study, a common brown spider native to northeastern America, *Statoda triangulosa* (Walckenaer), was chosen to produce the silk.^{17,18} Its dragline silk is used for these experiments. The spider's diet in captivity primarily consisted of common houseflies, crickets and water. Diet trends are beyond the scope of this study. Silk samples are tested within 8 days of being harvested. This study does not involve techniques of creating a synthetic substitute to nature's creation. What it describes is how this natural biopolymer is applied in ways other than the life supporting function and quantifies its material properties.

The objectives of the study are threefold:

1. Engineer a load cell capable of measuring strain and tensile properties of spider silk.
2. Establishment of silk's mechanical properties using the load cell/strain gauge apparatus at room temperature.
3. Measurement of the silk's mechanical properties after being held at an elevated temperature.

1.4 Summary

Although the silk mounting format has been established at LLE, many quantitative results are missing. Mechanical properties such as percent elongation, elastic modulus, strength and energy to break will be attained and compared to

literature values. These properties will give a better understanding as to why this material is currently applied to ICF.

1.5 Tables and Figures

Table 1 Mechanical properties for selected materials¹

Material	Modulus (N m⁻²)	Strength (N m⁻²)	Energy to break (J kg⁻¹)
Spider frame silk	1×10^{10}	1×10^9	1×10^5
KEVLAR	1×10^{11}	4×10^9	3×10^4
Cellulose fibers	3×10^{10}	8×10^8	9×10^3
High tensile steel	2×10^{11}	2×10^9	1×10^3
Tendon	1×10^9	1×10^8	5×10^3
Bone	2×10^{10}	2×10^8	3×10^3
Rubber	ca. 10^6	1×10^8	8×10^4
Viscid silk	3×10^6	5×10^8	1×10^5

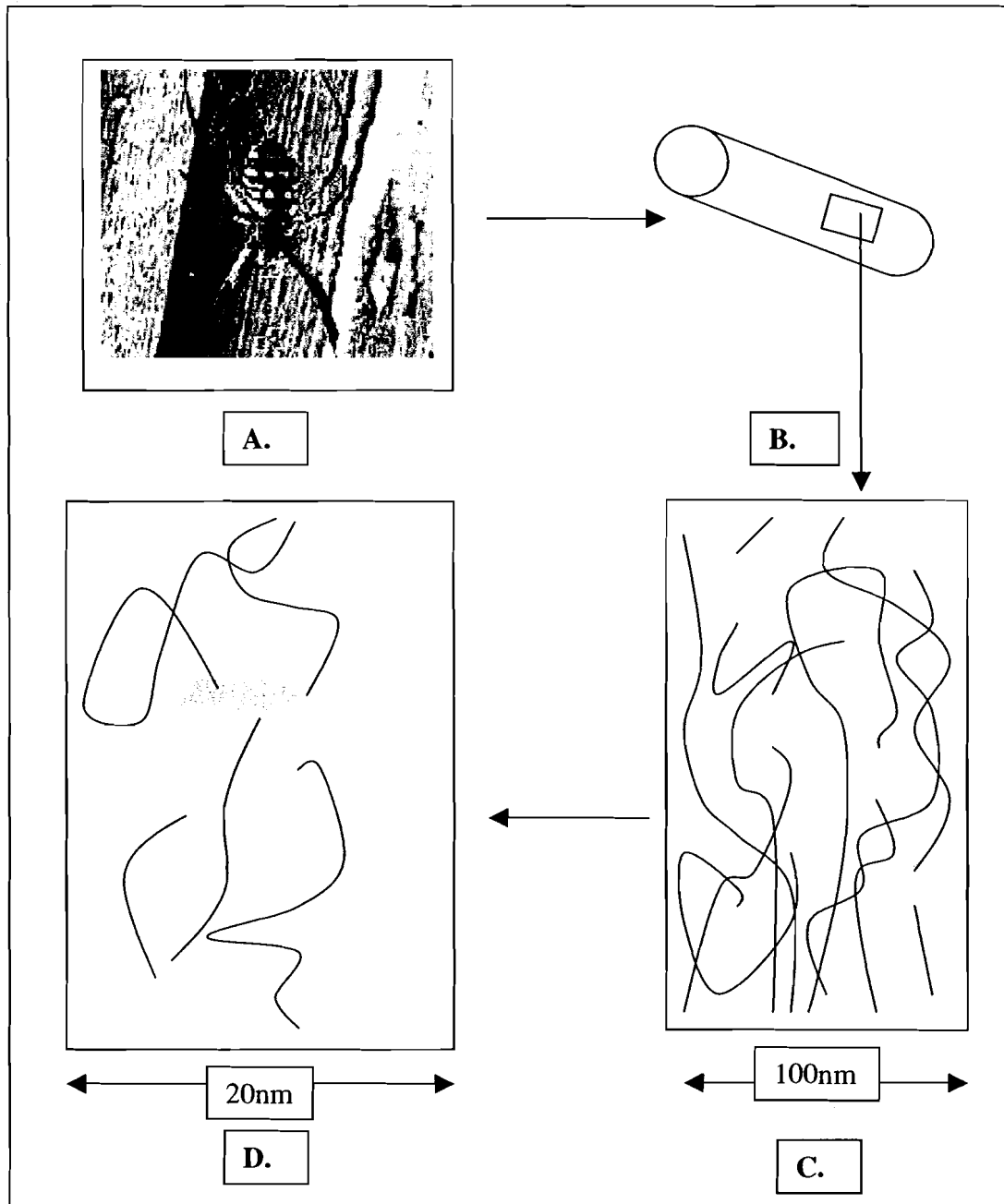


*Figure 1 Spider silk structure: (A) photograph of a golden orb weaver (*Nephila*, sp.), (B) a segment of dragline silk, (C) silk matrix containing β -pleated sheets (Gray rectangles) and α -helices (lines surrounding rectangles), (D) β -pleated sheets (gray) are accordion-shaped, crystalline structures that are created by α -helices undergoing shear during the initial extrusion through the spider's spinneret. This concept is based on that of the silkworm.⁴*

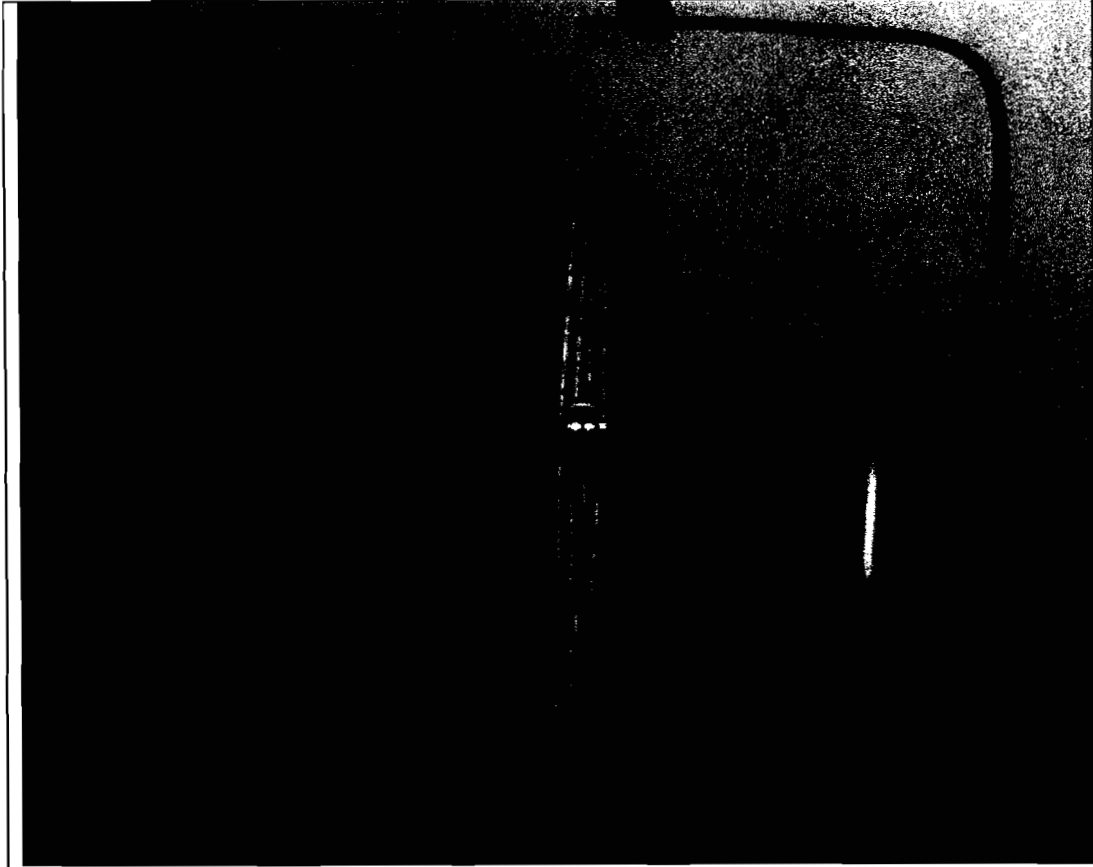


Figure 2 Photograph of a cryogenic compatible target mount. Silk spans the 250 μm diameter beryllium wire frame. Notice the four silk strands supporting the 920 μm diameter capsule. Silk strands are approximately 1 μm in diameter.

1.6 References

¹ J.M. Gosline, M.E. DeMont and M.W. Denny, "The Structure and Properties of Spider Silk," *Endeavour*, New Series, **10**, No.1 (1986).

² William F. Smith, *Principles of Materials Science and Engineering* (New York: McGraw Hill), 469 (1986).

³ F. Vollrath, "General Properties of Some Spider Silks," *ACS Symposium Series*, (Silk Polymers), **544**, 17-28 (1994).

⁴ F. Vollrath, "Spider Webs and Silks," *Scientific American*, 70-76 (March 1992).

⁵ Fritz Vollrath and David P. Knight, "Liquid crystalline spinning of spider silk," *Nature*, **410**, 541-548 (29 March 2001).

⁶ R.W. Work, "The Force-Elongation Behavior of Web Fibers and Silks Forcibly Obtained from Orb-Web-Spinning Spiders," *Textile Research Journal*, 485-492 (July 1976).

⁷ C.Y. Hayashi, N.H. Shipley, and R.V. Lewis, "Hypotheses that correlate the sequence, structure, and mechanical properties of spider silk proteins," *International Journal of Biological Macromolecules*, **24**, 271-275 (1999).

⁸ J. Gatesy, C. Hayashi, D. Motriuk, J. Woods, and R. Lewis, "Extreme Diversity, Conservation, and Convergence of Spider Silk Fibroin Sequences," *Science Magazine*, **291** (5513), 2603-2605 (30 Mar. 2001).

-
- ⁹ Z. Yang et al., "Small Angle X-Ray Scattering of Spider Dragline Silk," *Macromolecules*, **30**, 8254-8261 (1997).
- ¹⁰ David T. Grubb and Lynn W. Jelinski, "Fiber Morphology of Spider Silk: The Effects of Tensile Deformation," *Macromolecules*, **30**, 2860-2867 (1997).
- ¹¹ Gregory H. Altman, et al., "Silk-based Biomaterials," *Biomaterials*, **24**, 401-416 (2003).
- ¹² "Technology: Warding off bullets by a spider's thread," *New Scientist*, **136** (issue 1847), 18 (14 Nov 1992).
- ¹³ United States Patent: US 6412261 B1: Method of Reinforcing a Fiber with Spider Silk (2 July 2002).
- ¹⁴ JB Tatum, "Spider Threads," *A&G*, **43**, 5.8 (Oct.2002).
- ¹⁵ B.A. Brinker, et al., "Inertial fusion target mounting methods: New fabrication procedures reduce the mounting support perturbation," *Journal of Vacuum Science Technology A1* (2), 941-944 (Apr – June 1983).
- ¹⁶ R. Stephen Craxton, Robert L. McCrory, and John M. Soures, "Progress in Laser Fusion," *Scientific American*, **255**, 68-79 (August 1986).
- ¹⁷ G.B. Edwards, spider identifications (14 Sept. 1982).
- ¹⁸ C.Craig and H.Levi, spider identifications (11 Mar. 2003).

2.0 Experimental and Equipment Design

2.1 Introduction

This chapter covers the theoretical and practical details of the tensile testing apparatus. The relationships of percent elongation, stress, ultimate tensile stress and energy to break are described to interpret the information that can be gathered from performing a simple tensile test. This chapter also details the experimental design.

2.2 Tensile Testing Overview

The tensile test is the fundamental way the strength of a material is determined. A schematic is shown in *Figure 3*.¹ A sample under test is placed between the two grips. (One side of the sample is clamped in a load cell and the other is fixed.) The sample is pulled by the crosshead, driven by the lead screws on either side. (This setup can perform measurements in compression as well as in tension.) The load cell measures a voltage that corresponds to a mass (in kgf). An extensometer is placed on the sample across the two ends near the grips, measuring the displacement (in fractions of meters). The raw data acquired is load against displacement. From here, stress and strain data are generated. This test is performed uniaxially, preventing any torque from being introduced.

Many basic mechanical properties can be obtained from the tensile test. The first is the modulus of elasticity, defined by Hooke's law. It is analogous to the spring constant, k , in the following equation:

$$F = -kx, \quad (1-1)$$

where F is the applied force and x is the displacement. Equation 1-1 illustrates the linear relationship between the applied force and displacement. Similarly, the stress (σ) and strain (ϵ) are defined. The amount of stress applied is proportional to the amount of strain on an object. The elastic modulus is the constant of proportionality between stress and strain, as shown in equation (1-2).

$$\sigma = E\epsilon \quad (1-2)$$

where σ and E have dimensions of force per unit area, (Nm^{-2} or Pa) and ϵ is dimensionless (m/m). (Specifically, σ is the engineering stress, defined as the load divided by the original cross-sectional area. Strain is defined as the engineering strain throughout this work.)

A material tested in this region of the stress-strain curve is referred to as linear elastic. If a sample is loaded and unloaded in this region, it will return to its original length and cross-sectional area. More importantly, permanent deformation has not occurred. Hooke's law is only valid for small deformations. Any large deformation usually becomes non-linear, and this law does not apply.

The point at which the slope changes from linearity is called the yield point. At this point, the material is being strained beyond its elastic region. Any

deformation after this point is plastic, meaning once unloaded, the sample will not return to its original length.

The yield stress or strain can be rather ambiguous due to the nature of the data. The American Society for Testing and Materials (ASTM) has a convention for American structural design defining the yield strength as 0.2% offset from the linear slope of the data. This point of the data was chosen because a definite amount of permanent deformation has occurred.² In this study, the ASTM standard D3822 is referenced to define the yield strength as a horizontal line connecting a point from where the initial slope begins to deviate from a straight line and the vertical axis. Yield strain is the vertical line drawn from the deviation from linearity to the strain axis.

In order to test the strength of a material, the tensile loading will continue until a sample ruptures. For metals, the stress-strain curve will reach a peak before rupture. This point is the largest load the sample can withstand before necking occurs. The maximum load defines the ultimate tensile strength, or loosely known as strength.

$$\sigma_{UTS} = \frac{P_{MAX}}{A_0}, \quad (1-3)$$

where P_{max} is the maximum load and A_0 is the original cross-sectional area.

Percent elongation is defined as:

$$\varepsilon = \frac{(l - l_0)}{l_0} * 100, \quad (1-4)$$

where l_0 is the initial sample length and l is the length in tension. Strain is a figure of merit for the ductility of a material. For reference, AISI 1080 steel (annealed

condition) has an elongation at break of 25%, low-density polyethylene film (LDPE) ranges between 320% and 600% before breaking, and silicone rubber breaks between 100% and 800% elongation.

The area under the stress-strain curve is the amount of energy stored in the sample during the tensile test. To calculate this value, the energy is defined as:

$$E_f = \int_0^{\epsilon_{\max load}} P d\epsilon, \quad (1-5)$$

where P is the load, $\epsilon_{\max load}$ is the corresponding strain associated with the σ_{UTS} . In this study, energy to break is defined by the following equation:

$$E_f = \sum_{n=0}^i (l_{i+1} - l_i) \cdot \left(\frac{P_i + P_{i+1}}{2} \right) \quad (1-6)$$

This method sums a number of rectangles whose width is equal to the distance δ between successive displacement data points and whose height is the average of the neighboring load values.

2.3 Load Cell Design

Many materials are tested using an Instron tensile tester. This instrument is standardized according to the ASTM. Measuring silk strength properties is not as straightforward. A single strand of silk will rupture at loads approaching 100 mgf. Therefore, a very sensitive load cell was used. A design criterion for any load cell is the minimum-breaking load equal to 30% to 60% of full scale. (For example: 100 mgf breaking load requires a minimum of 300 mgf full scale.) Since this type of device was not commercially available, it was necessary for a custom apparatus to be developed specifically for the application. The load cell test setup referenced the

ASTM D3822 (The Standard Test Method for Tensile Properties of Single Textile Fibers³) by using a constant rate of traverse. In other words, the crosshead speed was constant throughout the span of the test. The load cell portion is achieved using a Mettler-Toledo analytical balance (maximum load 15 gf with resolution of ± 0.1 mgf). An Oriol controller (Model 18010), with resolution of $1\mu\text{m}$, runs the crosshead displacement to a maximum of 25 mm. *Table 2* details the instruments involved and their corresponding limits.

The basic concept of this load cell design is the following: a pre-mounted silk sample is glued to a mass, resting on a scale. The sample, pulled by the translating stage, removes mass from the scale while the load and displacement data are collected with LabView data acquisition software. *Figure 4* shows the key components of the test setup. The testing procedure is as follows: A silk sample is glued between a 0.25" outer diameter aluminum tube, referred to as a post, and a silicon carbide fiber ($17\mu\text{m}$ diameter, 0.1 mg). The mounted silk sample is inserted into the crosshead port with the sample aligned over the center of the balance. (Mounting sequence is detailed in A2.1 Sample Preparation.) The silicon carbide fiber (SiC) acts as a plumb bob that keeps the sample aligned vertically, exhibiting uniaxial stress. The SiC end of the silk is attached to the anchor (2.84 g) by means of 5-minute curing epoxy. The purpose of the anchor is to resist the tensile force drawn by the silk. Once the glue is cured, testing begins. The silk is stretched and the load decreases on the scale. The load signal is interfaced through serial port zero into the LabView data acquisition program.

The load reading from the Mettler scale is interfaced to the computer by a bi-directional module (Mettler Option 12 data interface). This device allows the transmission of data between the scale and the serial port. A voltage is simultaneously acquired from the translation stage controller. This transistor-transistor-logic (TTL) signal is interfaced to the software through the National Instruments data acquisition board (68-Pin Shielded Connector Block). The software code was designed (author Luke Elasky) to acquire and synchronize both signals and plot a load-displacement curve in real time. The program code is shown in *Figure 5* and *Figure 6*.

2.4 Summary

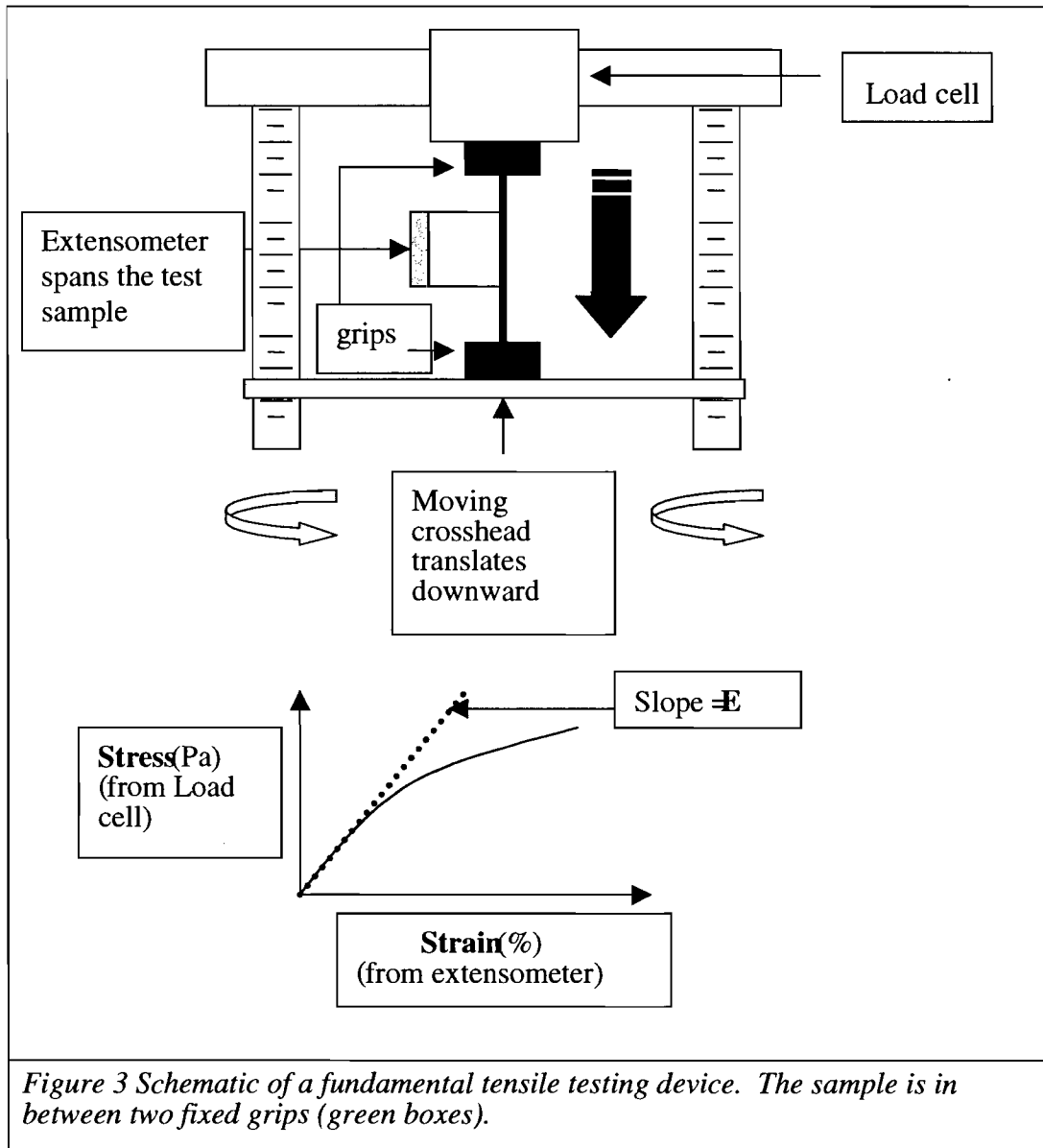
The equations in Chapter 2.2 Tensile Testing Overview are necessary for calculating the mechanical properties of the silk. More importantly, these equations relate the key factors of the tensile test to the mechanical properties. Here are the key points related to material terminology:

- *Elasticity* is analogous to *percent elongation*
- *Strength* is analogous to maximum load and ultimate tensile strength (*UTS*)
- Material *stiffness* is analogous to *modulus*
- *Toughness* is analogous to *energy to break*

2.5 Tables and Figures

Table 2 Operational limits of devices used for experimental setup.

Device	Operational Limits
Mettler AE100 Balance	0 to 15 g full scale, 0.1 mg resolution
Oriel Motor Mike and Controller (Model 18010)	0.5 $\mu\text{m/s}$ crosshead speed, 0.1 μm resolution
Cohu Solid State Camera and Navitar Macro lens (for sample viewing and alignment)	10x magnification
Powellscope Metrology Station	5 μm resolution
Wild Stereo Microscope (preparing samples)	6-50x magnification, 18 μm /reticle division @ 50x mag.
Centurion Vacuum Oven	30" Hg at 500°C
Scanning Electron Microscope	2 nm resolution



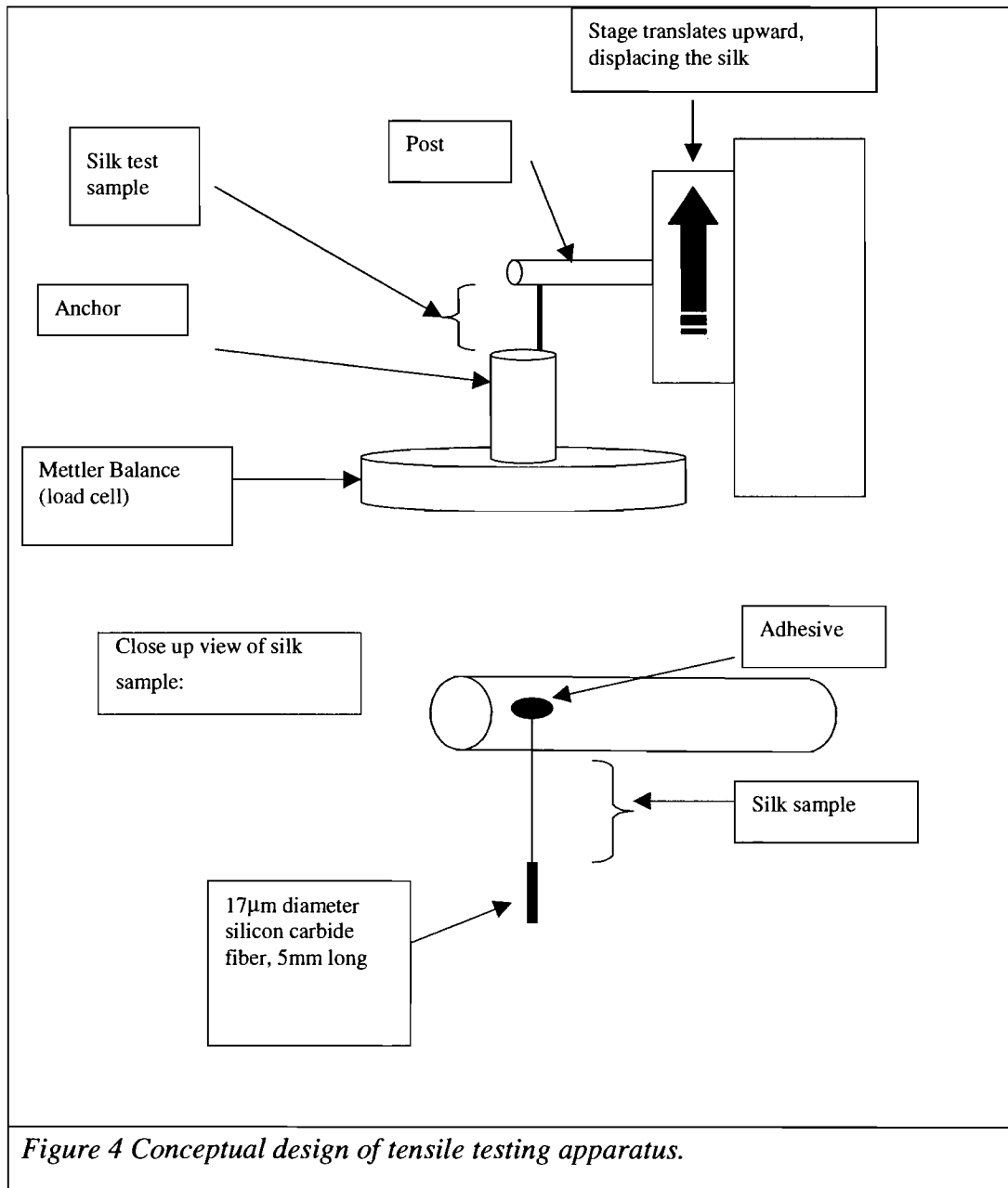


Figure 4 Conceptual design of tensile testing apparatus.

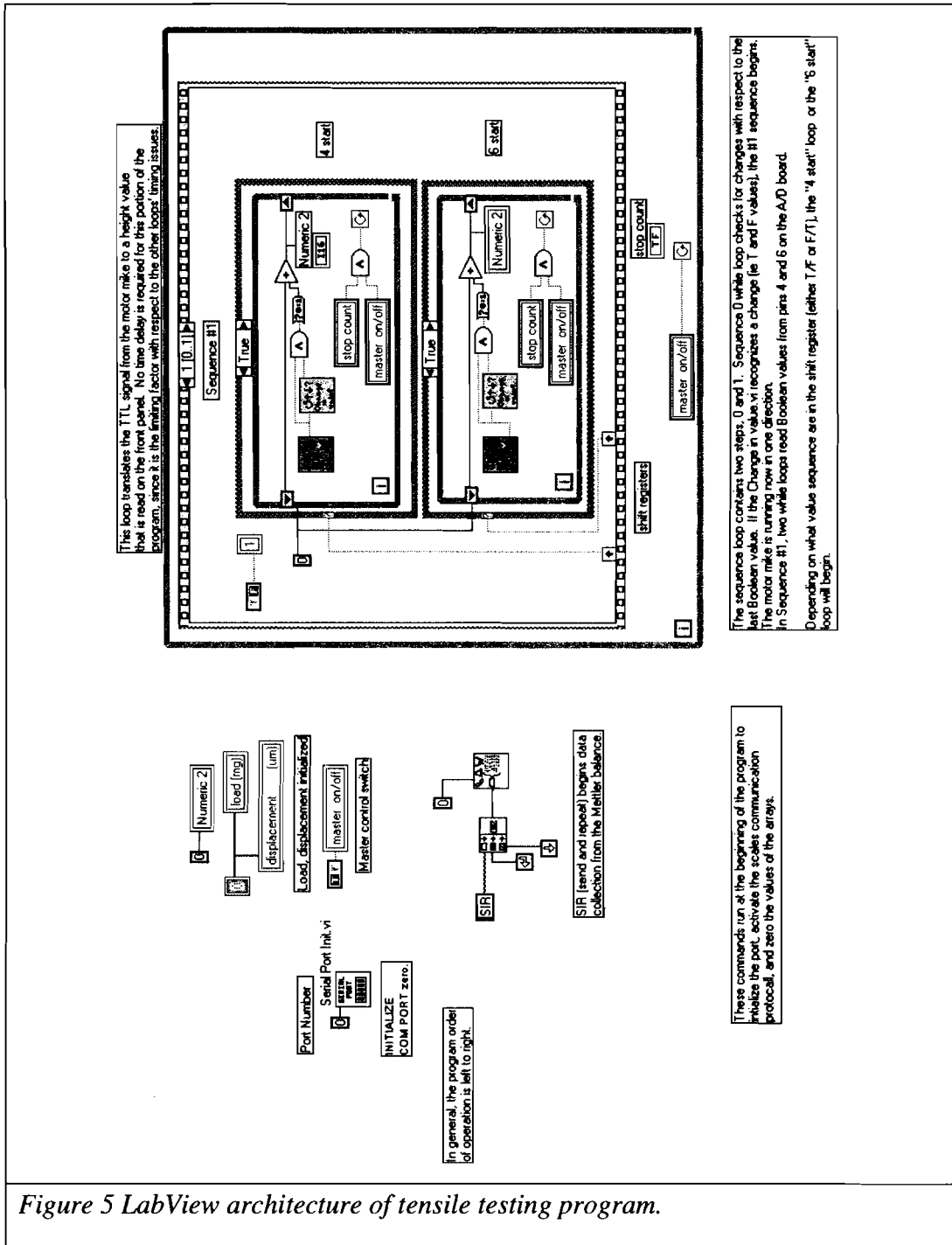


Figure 5 LabView architecture of tensile testing program.

2.6 References

¹ C.J. McMahon, Jr. and C.D. Graham, Jr., *Introduction to Engineering Materials: The Bicycle and the Walkman*, (Philadelphia: Merion Books, 1992), 28.

²William F. Smith, *Principles of Materials Science and Engineering* (New York: McGraw Hill, 1986), 251.

³ ASTM D 3822-01, "Standard Test Method for Tensile Properties of Single Textile Fiber," *Book of Standards Vol. 07.02*, 140-149, (2001).

3.0 Mechanical Material Properties

3.1 Introduction

Mechanical material properties of spider silk were established by interpreting data from the tensile testing apparatus. The following three regions can categorize all stress-strain data: (1) the elastic region, (2) the inelastic region, and (3) the region after maximum loading. The elastic region spans the data set from initial loading to the onset of yielding. In this area, the data follows a linear curve defined by Hooke's law (Equation 1-1). The region spanning the yield stress through the ultimate stress is referred to as the inelastic region. Permanent deformation occurs as the material is strained beyond its elastic region. The final area is the section beyond the ultimate stress. The material has reached its loading limit and quickly degrades until it ultimately fails.

This chapter is divided into discussions of the three stress-strain regions. The properties related to each region are discussed based on the data gathered from tensile testing. Before discussing the properties associated with the linear region, experimental variability is addressed.

Spider silk exhibited batch to batch variation between individual tensile tests. For example, the number of strands of silk per sample were as few as one (*Figure 7*) and as great as four (*Figure 8*). This variability was not controlled for this

experiment. It was more successful to name these items as uncertain variables and to address them through statistics. The diameter of the silk also varied between batches, which may be a product of the spider diet or some other environmental impact. Measuring a large sample of silk puts this variability into perspective.

3.1.1 Silk Diameter Variation and Experimental Uncertainty

Silk diameter is the major source of uncertainty for calculating the values of strength, modulus and energy to break. During the experiment, measurements of the silk diameter were not always easy to attain. SEM photomicrographs of silk were taken periodically to make measurements needed for quantifying the material properties. After working with silk during this project, two questions needed to be answered: (1) how much does the silk diameter vary over a 30 cm length (30 cm was chosen based on the length of silk used from each harvest), and (2), based on this value, is it necessary to measure each test sample for its diameter. The first question is answered in the following experiment.

The silk diameter was measured to find the variation over a 30 cm strand. *Figure 11* illustrates the silk harvesting sequence. A 1-cm section was selected from the top, middle, and bottom of the 30 cm dragline strand. Three SEM photographs were taken of each of the three samples to measure the silk diameter (see *Figure 12*). Based on this information, the variation in diameter over the length was determined. The mean of the nine samples was $0.842 \mu\text{m}$ per strand, with a standard deviation of $0.05 \mu\text{m}$. The change in diameter over the 30 cm length was deemed acceptable.

A statistical basis was adopted to answer to the second question. Over the two years of testing, four spiders (same species) were used, yielding 29 measurements of silk diameters (*Table 3*). (Twenty-nine diameter measurements ranged between 0.72 μm and 1.42 μm per sample.) The mean diameter was $1.00 \pm 0.09 \mu\text{m}$ (95% confidence). A comparison between measured and averaged values of ultimate tensile strength was drawn to conclude if using average diameter values was statically significantly to the actual measured values. Actual diameter measurements yielded $1.2 \pm 0.3 \text{ GPa}$ ($n=8$) and the averaged values yielded $1.3 \pm 0.4 \text{ GPa}$ ($n=7$). Since these values overlap, this method of substituting averaged diameter values for unmeasured silk diameters will be used throughout the course of the text.

Other conditions that affect the experiment are silk harvesting rate, temperature, and relative humidity. The harvesting rate ranged from 8 to 12 cm/s, depending on the rate at which the spider produced silk. It is reported that the harvesting rate (5 and 10cm/s) affects the stiffness by a factor of two.¹ The temperature and relative humidity (RH) were ambient laboratory conditions; $21 \pm 2 \text{ }^\circ\text{C}$ and 24% to 56% RH. According to Gosline *et al.*, water has a large affect on the properties of silk.² Silk will contract up to 50% when immersed in water, and Young's modulus decreases by three orders of magnitude. In this work, none of these conditions were deemed extreme enough to impact the experiment.

3.2 Elastic Region

The initial slope of the load-displacement data is the elastic modulus, also known as Young's modulus. The silk is loaded to an average of 1.4% strain (based

on *Table 4*) and then changes slope, as seen in *Figure 9*. At the inflection point in the data, the material yields plastically. The long protein chains have reached the end of the elastic region and begin permanent deformation. *Figure 10* illustrates a silk sample that was strained to 0.9% and then returned to its initial length. The slope was the same during loading and unloading, confirming that it is an elastic region.

Calculating the modulus requires knowing the initial cross-sectional area of the silk fiber. The average diameter of 1.00 μm is used to make these calculations. Young's modulus is 2.2 ± 0.7 GPa; values are shown in *Table 5*. The modulus is reported with 95% confidence. The literature values range from 6.9 to 10 GPa.^{3,4,5} The literature compares dragline silks from a number of different species: (*Pisauridae (Euprosthenspe)*, *Tetragnathidae (N. edulis)*, *Theridiidae (L. mactaus)*, *Araneidae (C. citricola)*).

3.3 Inelastic Region

In the inelastic region, plastic deformation occurs. The long protein chains are pulled along each other and the data takes on a new slope, referred to as the final modulus. If the silk was unloaded after the yield point, permanent strain is not recovered. Therefore, the data will not return to the origin. Practically speaking, the sample has been plastically deformed and will not return to its initial length upon unloading.

3.3.1 Percent Elongation

The percent elongation is calculated for each sample by measuring the initial length of the silk first. After the sample is mounted on the post, it is situated in the

Powellscope metrology station, as drawn in *Figure 13*. The Powellscope has a vertical stage that translates 2.5 cm (1 μm resolution). It also uses a microscope to view the sample at higher magnification. The sample was measured 7 times in order to accurately find the length, l_0 . The initial length of the samples varied between 9 and 18 mm, with the average length being 10 mm. The shorter length caused the sample to rupture after 1 h instead of 2.5 h. Based on data in *Table 6*, there is no correlation between initial length and maximum strain. The value of percent elongation is $24 \pm 2\%$ (95% confidence). The literature values range from 24% to 40%, depending on the species of spider.^{3,4,6}

3.3.2 Hysteresis

Silk was exercised through a hysteresis cycle to see if the linear region was repeatable and to determine the recoverable strain. The silk was cycled five times to 5% strain and after the 5th cycle, the sample was loaded to failure. Each cycle showed the following trends: (1) the loading data became closer to the unloading data (area between curves decreased), (2) the slope after yielding became steeper, making the yield point less well defined, and (3) the unrecoverable strain decreased from 1.8% to 0.5%. The first cycle showed the largest difference in area under the curve between loading and unloading. The area under the curve is energy stored in the silk. If the silk lost no internal energy during the cycle, the loading path would match the unloading path. In the first cycle, the energy lost is greater than 50%. This energy is lost due to atomic bonds breaking. Cycling the silk creates a stiffening mechanism whose limit is a line parallel to the initial slope. With each cycle, the data follow the

track towards the initial slope. At the same time, the unrecoverable strain decreased. The first cycle unloaded to 1.8% unrecoverable strain. After 5 consecutive cycles, the unrecoverable strain decreased to 0.5%. Since each cycle was strained to the same nominal percentage, the work done to deform the silk was greatest after the first cycle. All subsequent cycles required smaller amounts of work to deform the silk matrix. Observations are summarized in *Table 7* and *Figure 14*. It is noteworthy to mention that the material followed a different path between loading and unloading. This observation is explained by the viscoelastic nature of the silk. If the curves were collinear, the material would be linear elastic. This is not the case for silk. There is a time-dependent property associated with the silk, which is characteristic of a viscoelastic solid.⁷ Denny recorded similar observations.⁸

3.3.3 Ultimate Tensile Strength and Final Modulus

The ultimate tensile strength (UTS) is determined by two factors: the original cross-sectional area of the sample and the maximum load. *Table 8* shows the UTS for the 15 measured silk samples. The mean UTS is 1.2 ± 0.2 GPa. For comparison, literature values range between 1.06 to 1.6 GPa, again depending on the species.^{3,4,6}

The modulus after yielding, referred to as the final modulus, was measured to document the stiffness differences between the elastic and plastic regions. The elastic region is stiffer than the plastic region, but the elongation is far greater in the plastic zone. The ratio of initial to final modulus is 2.2 to 0.4 GPa, differing by a factor of five. In the microstructure the α -helices (from *Figure 1*) have extended past their

elastic limit and are moving along each other. The β -sheets add resistance to the tensile force, much like a dislocation would in a solid.

3.3.4 Energy to Break

The energy it takes to rupture a sample is the most outstanding material property of the silk. The units of this property are J/kg, meaning the amount of energy to break the sample per unit mass. Competing materials listed in *Table 1* show comparable stiffness. However, silk has a greater percent elongation, which directly contributes to the amount of energy stored in the silk.

On a micro-level, as the silk is being loaded, the protein chains move along each other. The microstructure is analogous to a container of long rubber bands sliding past each other. The sample will continue loading until the strands come to the end or interfere with other strands. If the strands interfere, a knot forms causing a stress concentration. The knot will not pass, so the strand is forced to extend until it ruptures. Eventually, many of these events occur and the silk fails. This break occurs on average at 24% elongation. The energy to break, defined by the area under the load-displacement curve, becomes very large because of the combination of the maximum load and the large elasticity. This is the intriguing property that makes silk scientifically interesting. The energy to break is $1.4 \pm 0.3 \text{ J/kg} (\times 10^5)$, reported in *Table 9*. For comparison, literature values range from 1 to $2.2 \times 10^5 \text{ J/kg}$.

Once the silk has reached its UTS, it continues to be stretched, but quickly loses tensile properties. The sample shows a greatly reduced load as the constant pull rate continues. An interesting observation was made regarding this region of the data.

Once the load begins a sharp descent to zero milligrams, it stops at a load equal to one half UTS. This observation is supported by the presence of two parallel silk lines. The load value is exactly half of the value prior to the major decrease in load, as seen in the load-displacement data in *Figure 9* and in the SEM micrograph shown in *Figure 15*. After the silk ruptures, the sample is viewed under a microscope. Silk was found attached to both grips. This implies that the sample fractured at the sample midpoint and was not pulled away from the glue bond.

3.4 Summary

Table 10 summarizes comparisons between experimental data and the literature values. The maximum strain is equal to the lower reported limit of the literature values. Young's modulus is smaller by a factor of 3 to 5 times. The tensile strength and the energy to break values agree. In general, the values are in agreement; *Table 10* values are the benchmark.

3.5 Tables and Figures

Table 3 Silk diameter measurements used for “averaged” values. The mean diameter is $1.00 \pm 0.09 \mu\text{m}$.

Sample date	Diameter/strand (μm)
101200	0.72
101200	0.73
102000	1.37
102000	1.42
102000	1.41
102000	1.32
102000	1.33
102000	1.32
102000	1.38
102000	1.36
022401	0.805
022401	0.895
022401	0.755
022401	0.81
022401	0.835
022401	0.82
022401	0.876
022401	0.871
022401	0.909
031001	0.900
031001	0.951
031001	0.915
031001	0.972
031001	0.958
032302	0.88
032302	0.946
032302	0.919
032302	0.885
032302	0.900

Table 4 Percent elongation at the yield point (defined as the value where the data begins to deviate from the initial slope).

Data title	Percent Elongation at Yield Strain
092200	1.5
101200_2	1.2
101300	1.5
102000_1	1.4
102000_2	0.9
102000_3	1.2
111600_1	1.9
111600_2	1.6
111700_4	2
112200_1	1
112200_2	1.3

Table 5 Young's Modulus is 2.2 ± 0.7 GPa. The stiffness decreases by a factor of 5 (0.4 ± 0.07 GPa) after the silk yields.

Data Title	Young's Modulus (GPa)	Final Modulus (GPa)
092200	1.5	0.43
101200	2.0	NA
101300	2.0	0.29
102000_1	1.3	0.36
102000_2	2.9	0.3
102000_3	1.5	0.45
111600_1	1	0.29
111600_2	0.9	0.24
111700_4	2.3	0.49
112200_1	6.2	0.62
112200_2	2.5	0.54
031001_4	2.3	0.56
031101_1	2.3	0.51
031101_2	2.2	0.33

Table 6 Initial sample lengths and maximum percent elongation ($24.1 \pm 2\%$). Maximum strain was independent of initial length.

Data Title	Initial Length, l_0 (mm)	Maximum Percent Elongation (%)
092200	11.86	20.3
101200_2	12.90	22.5
101300	13.46	26.6
102000_1	17.96	27.2
102000_2	11.22	19.8
102000_3	15.94	24.6
111600_1	9.91	21.5
111600_2	10.25	22.2
111700_4	8.77	31.9
112200_1	9.83	24.2
112200_2	9.95	21.4
031001_4	9.595	26.1
031101_1	9.358	26.6
031101_2	9.933	23

Table 7 Hysteresis data. The percentage of unrecovered strain decreases with every cycle. The internal energy lost as heat per cycle decreases since the percent strain remains constant (5%).

Data Title	Strain at Peak (%)	Percent Unrecovered Strain	Recoverable Energy (%)
H032302	5.1	1.8	39
H032302A	5.3	1.3	47
H032302B	4.9	0.8	56
H032302C	4.9	0.6	59
H032302D	5	0.5	62

Table 8 Ultimate tensile strength (1.2 ± 0.2 GPa) and corresponding maximum load.

Data title	Maximum load (mgf)	UTS (GPa)
090800	152.5	1.9
092200	184.1	1.1
101200	171.7	1.0
101300	122.9	1.5
102000_1	311.3	1.1
102000_2	216.1	0.7
102000_3	319.7	1.1
111600_1	112.9	0.7
111600_2	104.1	0.6
111700_4	122	1.5
112200_1	134.6	1.7
112200_2	99	1.2
031001_4	187.9	1.7
031101_1	180.9	1.6
031101_2	139.8	1.2

Table 9 The energy required to break a silk sample is $1.4 \pm 0.3 \text{ J/kg} (\times 10^5)$.

Data Title	Energy to Break (10^5 J/kg)
092200	1.1
101300	2.1
102000-1	1.3
102000_2	0.7
102000_3	1.2
111600_1	0.7
111600_2	0.7
111700_4	2.1
112200_1	1.9
112200_2	1.2
031001_4	2.1
031101_1	2.1
031101_2	1.4

Table 10 Comparison of baseline material properties between experimental data and literature values.

Material Property	Experimental Values	Literature Values
Maximum Strain (%)	24.1±2	24 - 40
Young's Modulus, E_i (GPa)	2.2±0.7	5.7 – 10.2
Final Modulus, E_f (GPa)	0.4±0.1	NA
Tensile Strength (UTS) (GPa)	1.2±0.2	1.06 - 1.6
Energy to Break (10^5 J/kg)	1.4±0.3	1 – 2.2

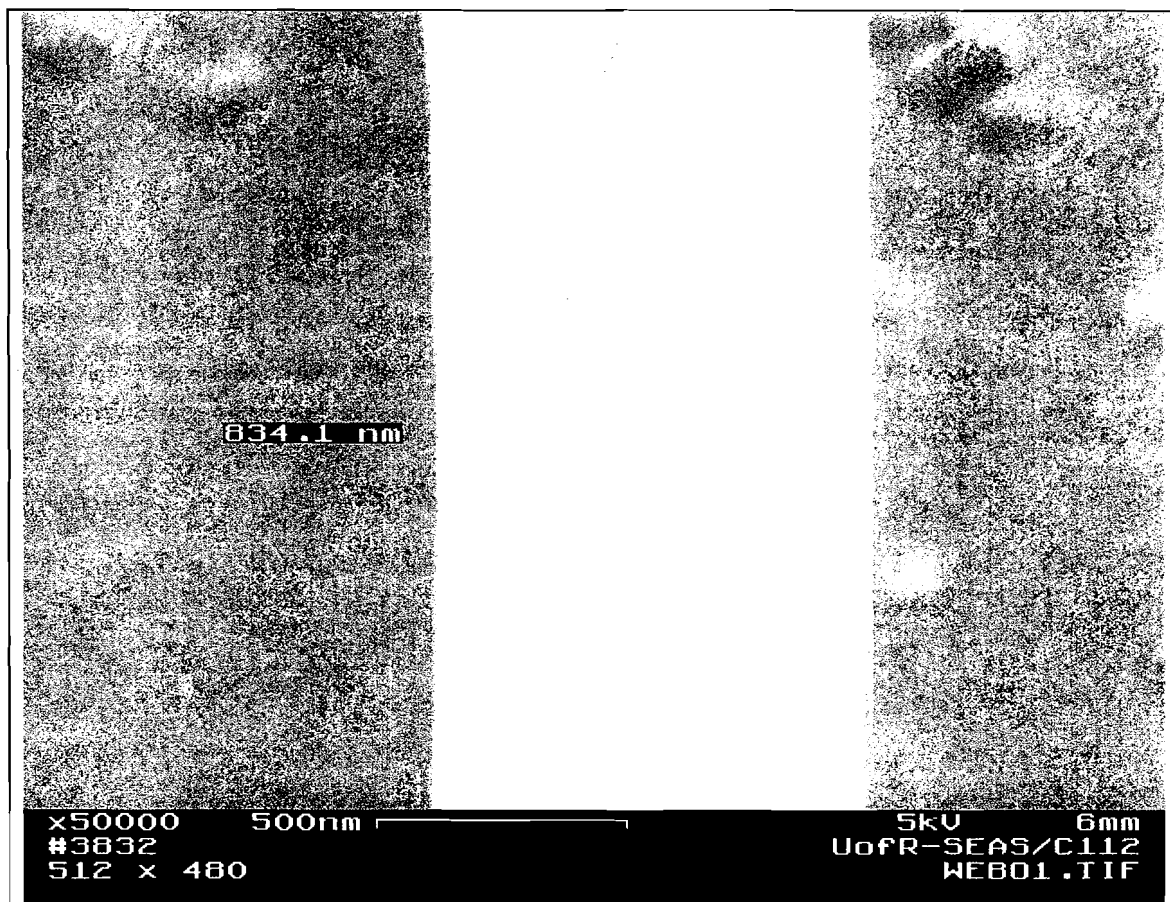


Figure 7 A single strand of spider silk shown at 50,000 times magnification. The diameter is 834.1 nm. The surface texture is difficult to image due to the low electrical conductivity of the silk. The upper limit is 10 keV; any more will burn through the sample.

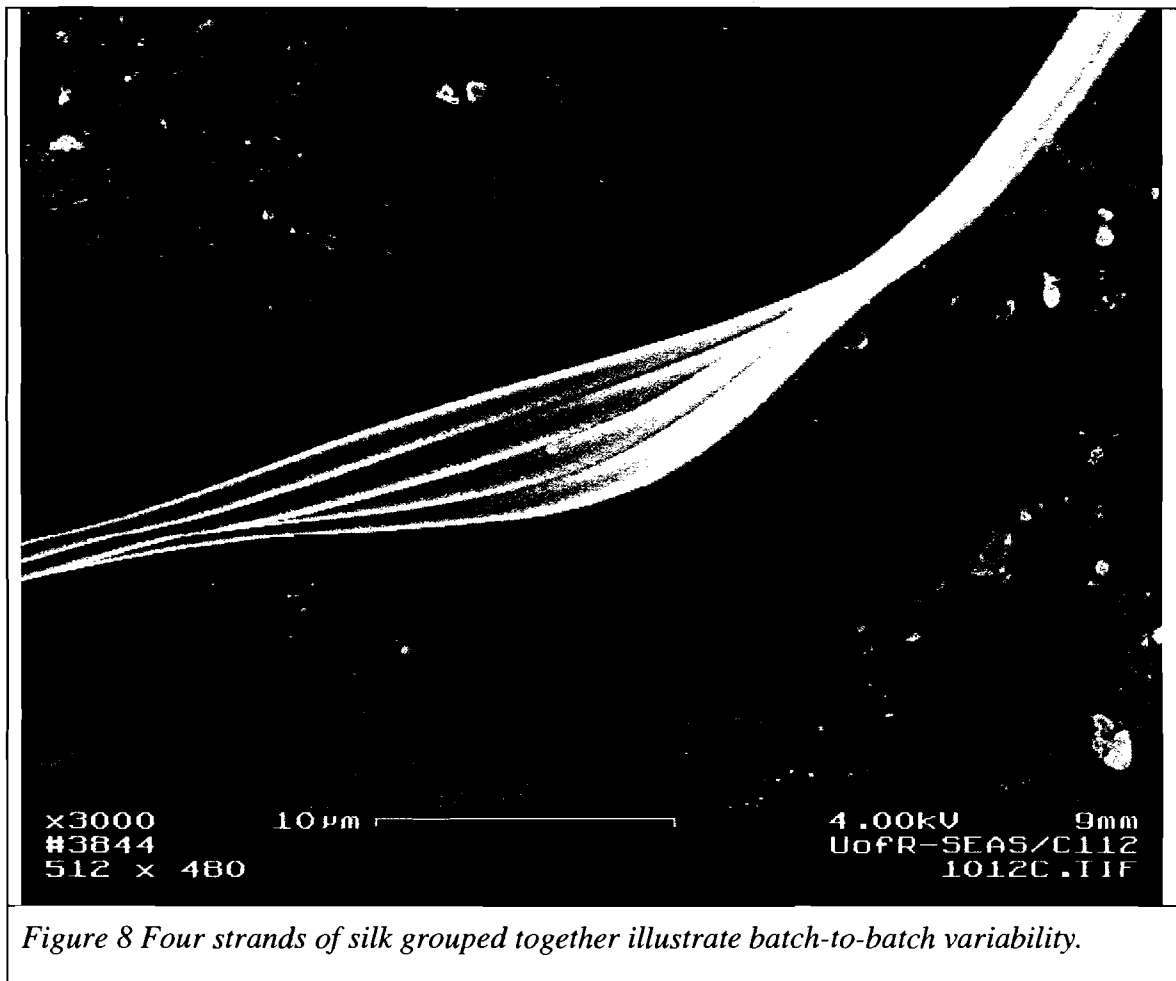
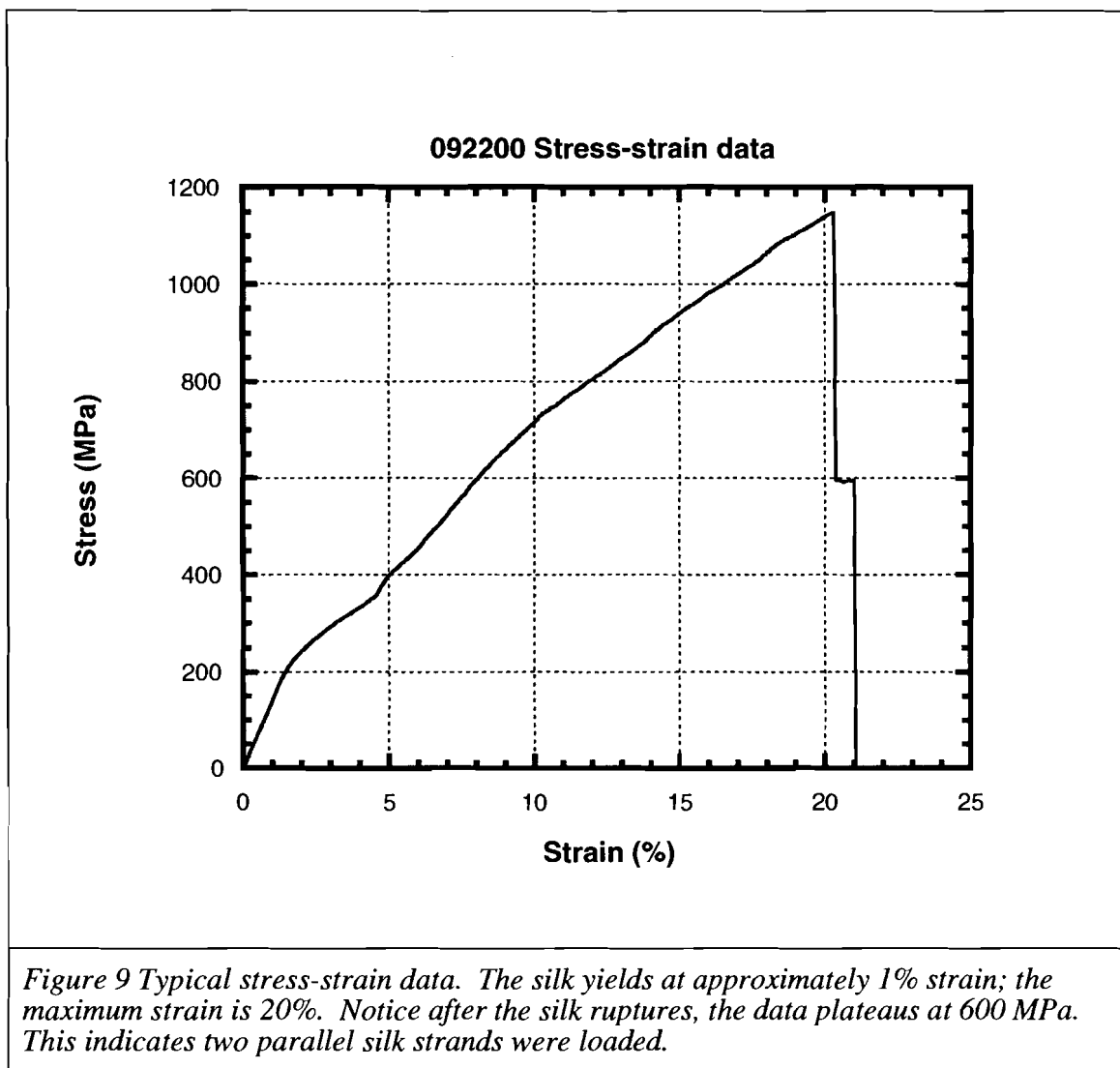
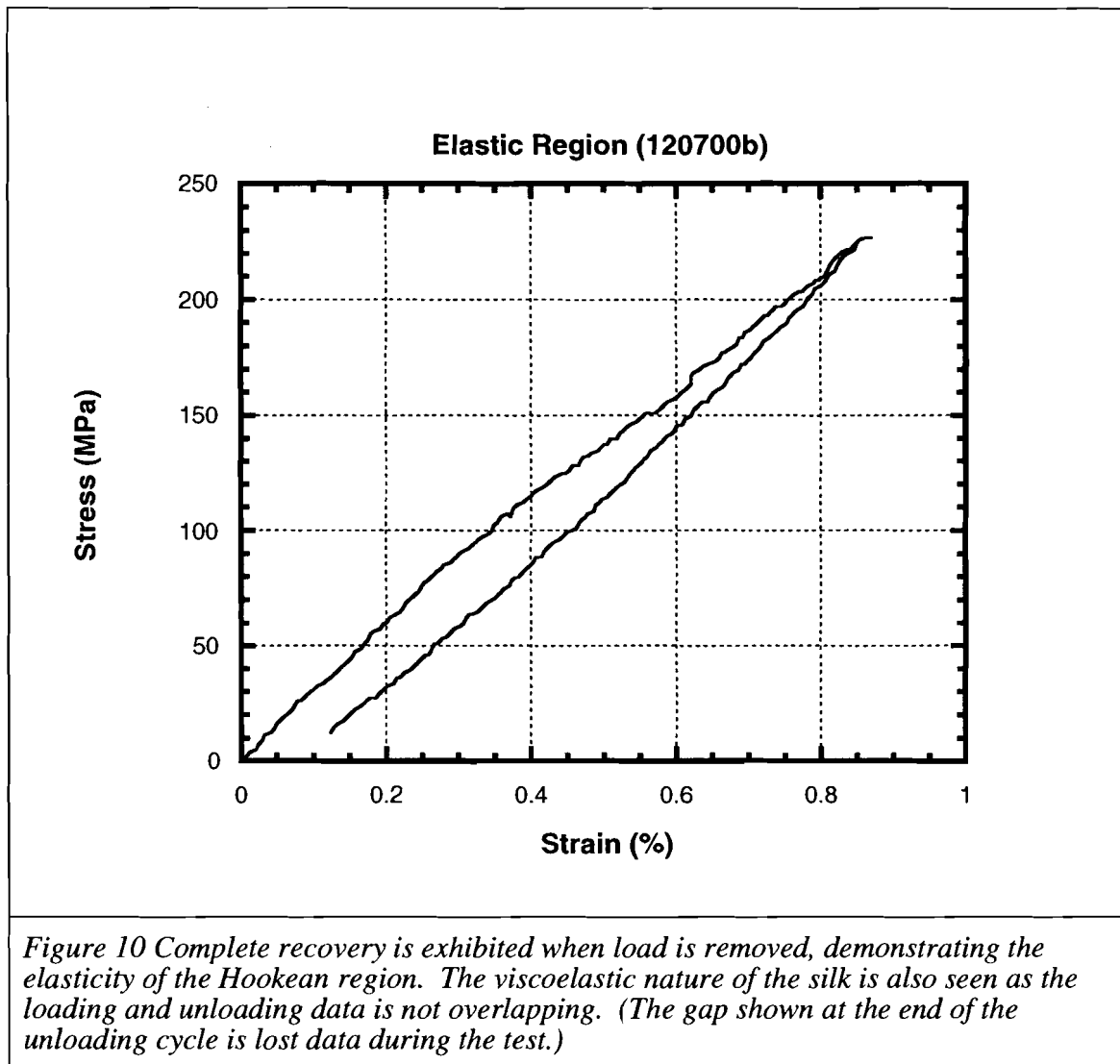


Figure 8 Four strands of silk grouped together illustrate batch-to-batch variability.





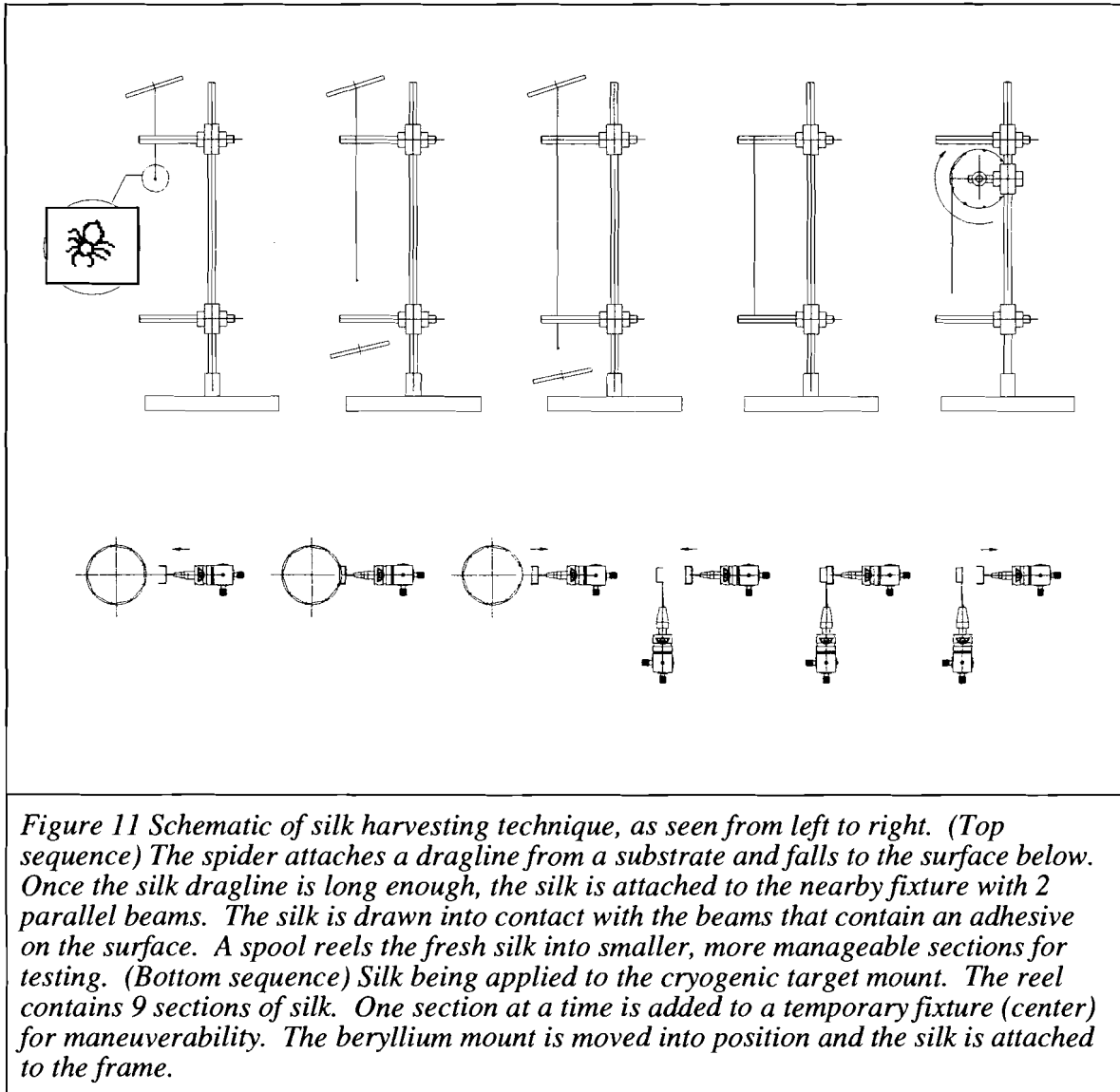


Figure 11 Schematic of silk harvesting technique, as seen from left to right. (Top sequence) The spider attaches a dragline from a substrate and falls to the surface below. Once the silk dragline is long enough, the silk is attached to the nearby fixture with 2 parallel beams. The silk is drawn into contact with the beams that contain an adhesive on the surface. A spool reels the fresh silk into smaller, more manageable sections for testing. (Bottom sequence) Silk being applied to the cryogenic target mount. The reel contains 9 sections of silk. One section at a time is added to a temporary fixture (center) for maneuverability. The beryllium mount is moved into position and the silk is attached to the frame.

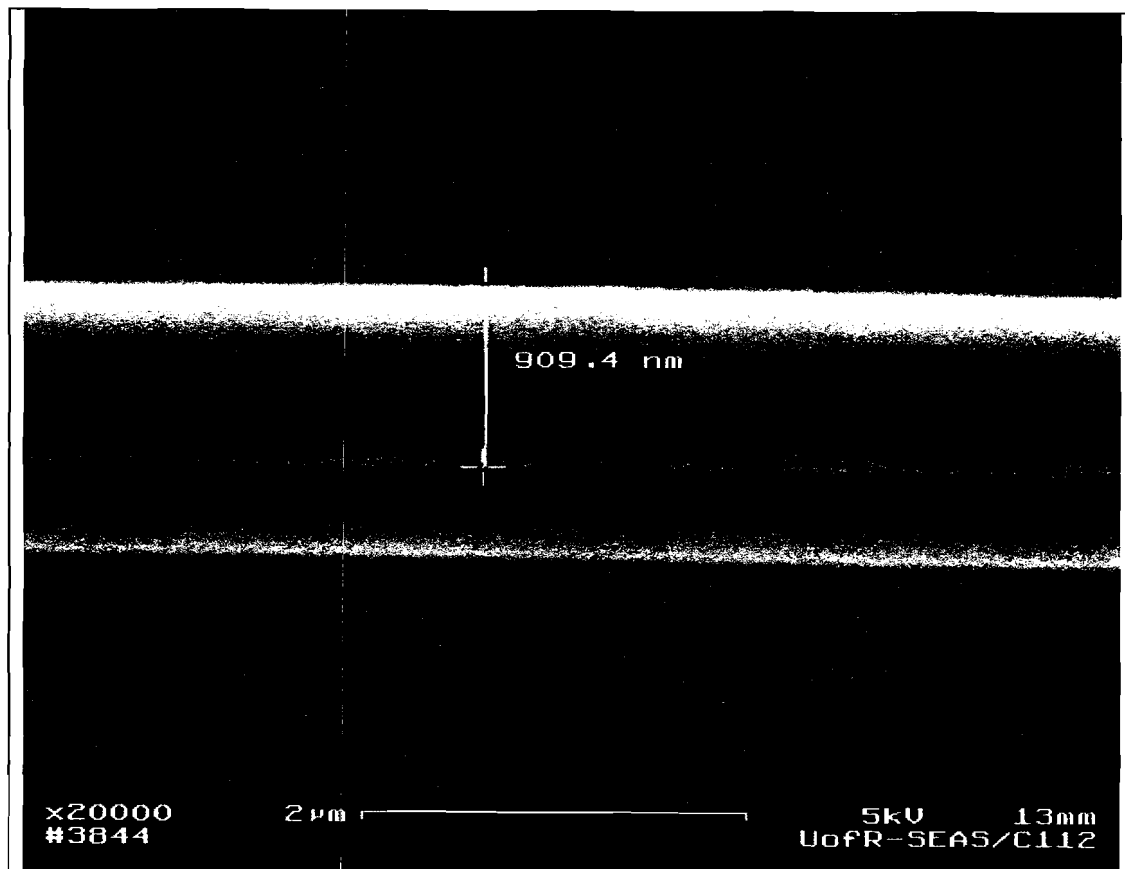
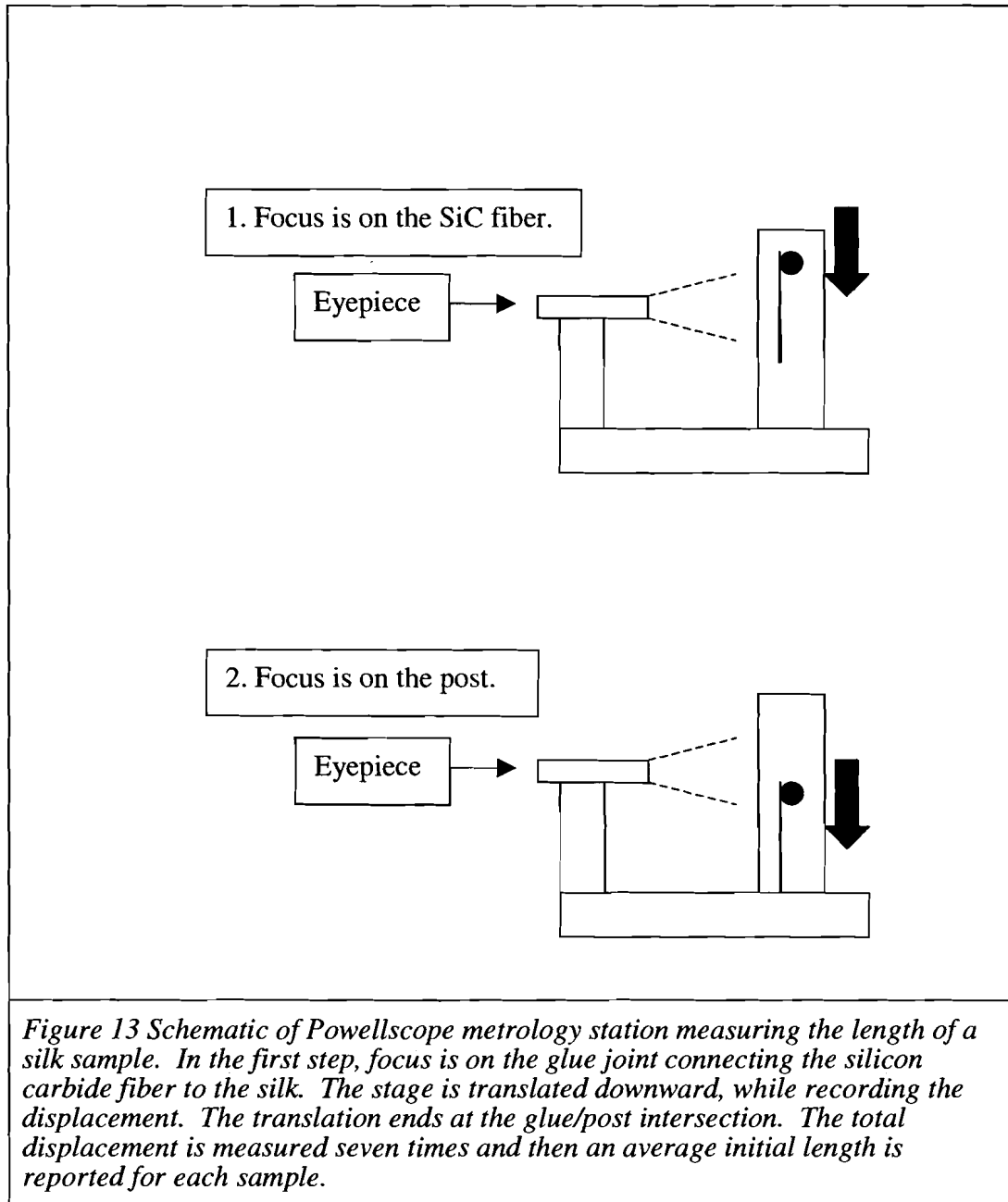
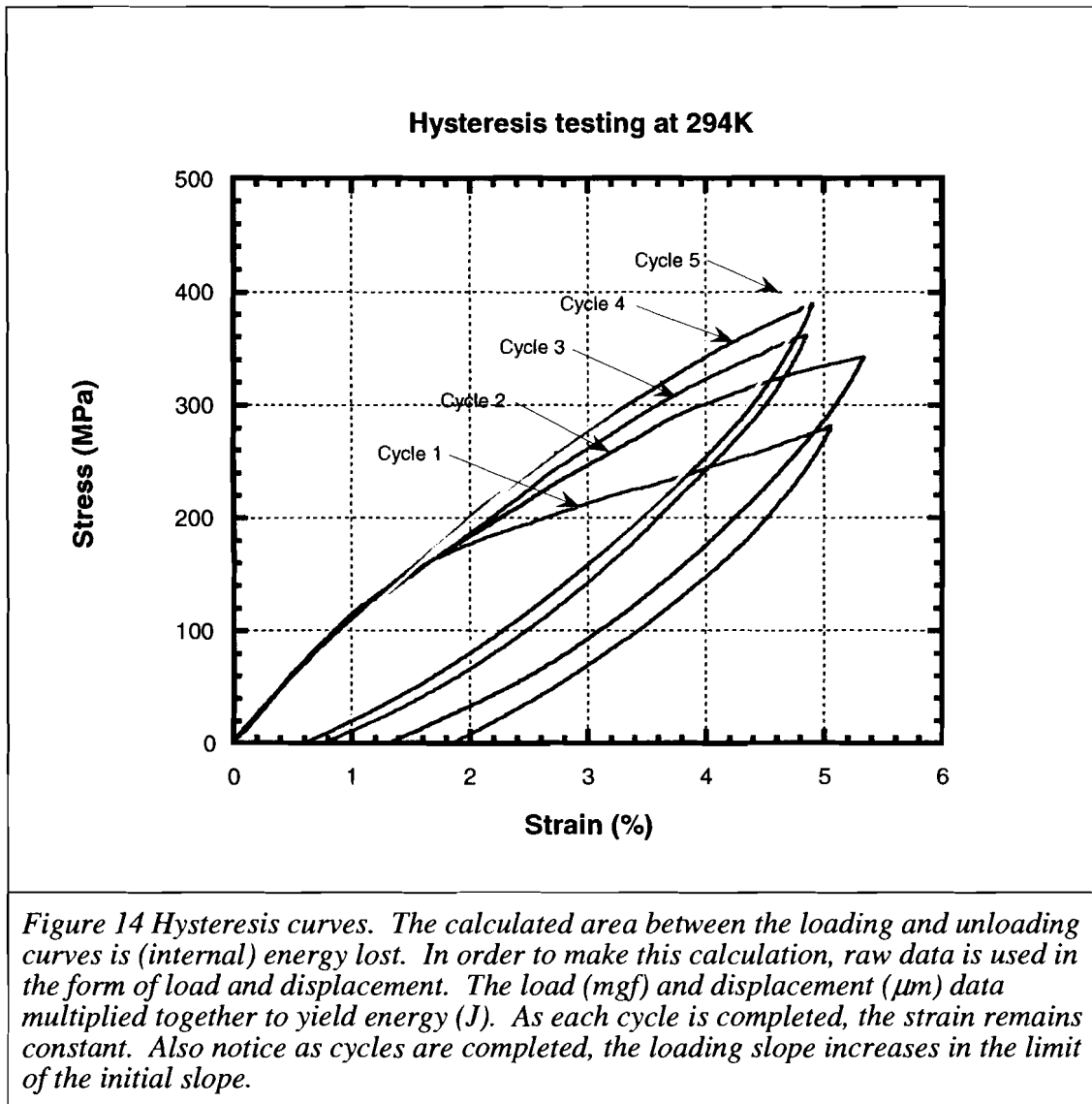
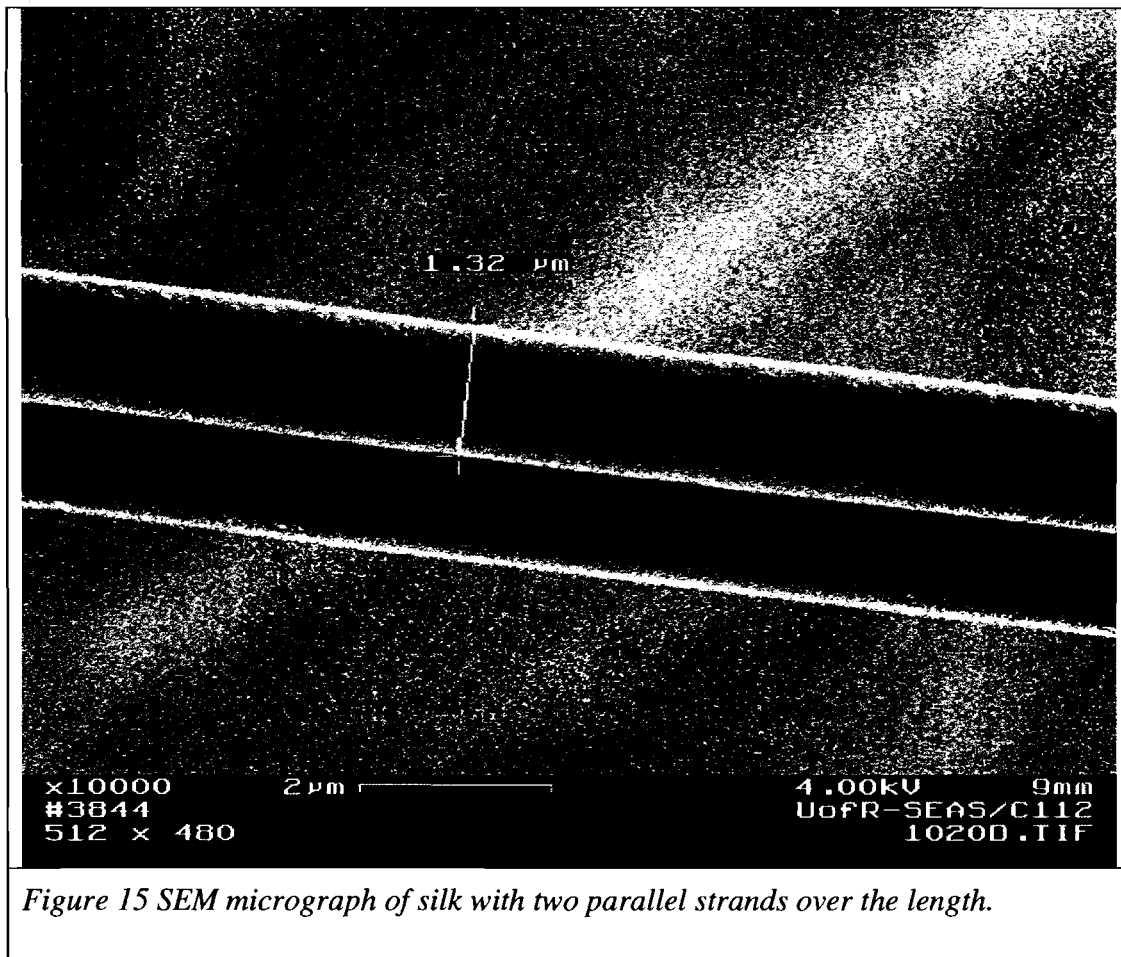


Figure 12 SEM micrograph showing one of the nine samples measured for quantifying the variation of silk diameter over a 30 cm strand. The micrograph shows 2 parallel strands of silk.







3.6 References

¹ Keith B. Guess and Christopher Viney, "Thermal analysis of major ampullate (drag line) spider silk: the effect of spinning rate on tensile modulus," *Thermochimica Acta*, **315**, 61-66, (1998).

² J.M. Gosline, et al., "The mechanical design of spider silks: from fibroin sequence to mechanical function," *The Journal of Experimental Biology*, **202**, 3295-3303 (1999).

³ Bo Madsen, et al., "Variability in the mechanical properties of spider silks on three levels: interspecific, intraspecific, and intraindividual," *International Journal of Biological Macromolecules*, **24**, 301-306, (1999).

⁴ B.Madsen and F.Vollrath, "Mechanics and Morphology of Silk Drawn from Anesthetized Spiders," *Naturwissenschaften*, **87**, 148-153 (2000).

⁵ John M. Gosline, et al., "The structure and properties of spider silk," *Endeavour*, **10**, no.1, (1986).

⁶ Robert W. Work, "The Force-Elongation Behavior of Web Fibers and Silks Forcibly Obtained from Orb-web Spinning Spiders," *Textile Research Journal*, 485-492, (July 1976).

⁷ Thomas H. Courtney, *Mechanical Behavior of Materials*, 2nd edition, McGraw Hill, 5 (2000).

⁸ Mark Denny, "The Physical Properties of Spider's Silk and Their Role in the Design of Orb-Webs," *Journal of Experimental Biology*, **65**, 483-506, (1976).

4.0 Elevated Temperature Testing

4.1 Introduction

The target filling process motivates for testing silk at an elevated temperature. The filling process is achieved by inserting a mounted capsule into a known volume. The gas is added to the volume and permeates into the capsule. If a capsule can be filled at an elevated temperature, the filling time can be greatly reduced because the permeation can be increased. To demonstrate this concept, gas permeability through a shell is described. The gas permeability time through a shell wall is dependent on the following: the shell dimensions (wall thickness and diameter), permeability of the shell material, and temperature, as shown in Equation 1-7:

$$\tau = \frac{WD}{6K_p RT}, \quad (1-7)$$

where W is the shell wall thickness, D is the outer diameter, R is the universal gas constant, T is the temperature. The temperature dependence of the gas permeability is expressed by the Arrhenius' relationship, where K_p is defined as:

$$K_p = A \exp\left(\frac{-E}{RT}\right). \quad (1-8)$$

A is a temperature independent pre-exponential factor and E is the activation energy for permeation. Equations 1-7 and 1-8 show that as the temperature increases, the

gas permeation time τ decreases, because both relations are temperature dependent. For example, a polyimide shell (920 μm diameter, 4 μm wall thickness) filled with helium at room temperature (294K) has a value K_p of 4×10^{-16} -mol $\text{m}/\text{m}^2 \text{ s Pa}$. This yields a permeation time-constant of 10 min. After five time constants, 99% of the gas equilibrates in the shell. If the shell is heated to 373K, K_p is 1.5×10^{-15} -mol $\text{m}/\text{m}^2 \text{ s Pa}$ and the filling time-constant decreases to 2 min.¹ The filling time is dependent on the buckle pressure, based on Equation 1-9:

$$\frac{dP}{dt} = \frac{P_{buckle}}{\tau}, \quad (1-9)$$

and the buckle pressure is

$$P_{buckle} = \frac{2E}{\sqrt{3(1-\nu^2)}} \left(\frac{w}{r} \right)^2, \quad (1-10)$$

where E is Young's modulus, ν is the Poisson's ratio, w and r are the wall thickness and radius of the capsule, respectively. Assuming the Young's modulus of the capsule is 3.2 GPa, the buckle pressure is 2.8 atm. At room temperature, the fill time is 60 h, while the elevated fill temperature takes 12 h. The shell can withstand a temperature of 373K, but the survivability of the silk-support is unknown. This poses the question whether silk will degrade in a heated environment.

4.2 Experimental Setup

The same tensile testing setup described in Chapter 3 was used. The silk samples were harvested and mounted in the same fashion as described in *Figure 11* and Appendix 2: Silk Preparation Overview. After the silk was mounted to the post, the samples were heat-treated. Initially, two silk samples were heated to

300°C for 24 h in an argon atmosphere. Upon removal from the oven, both pieces fractured. The silk was embrittled; it had lost all elastic properties. This observation agreed with the measurements made by Guess regarding the glass transition temperature (T_g) of major ampullate (MA) or dragline silk.² Dynamic mechanical analysis (DMA) indicates that dragline silk of *Nephila clavipes* (golden orb weaver) has a T_g 160°C. After that trial, the temperature schedule was changed to the following: ascending ramp rate of 0.2°C/min to hold at 100°C for 24 h and then a descending ramp of 0.5°C/min to ambient conditions. Upon a successful temperature cycle, the length, l_0 , of each sample was measured. Based on data from Chapter 3, only averaged silk diameters (1 μm per strand) are used in the calculations in the following sections.

4.3 Elastic Region

Young's modulus of the heated silk is shown in *Table 11*. Compared to the untreated silk in *Table 14*, heating the silk caused the modulus to decrease by a factor of four. According to Vollrath, the combination of the β -sheet crystalline structures in an α -helix matrix is what provide the stiffness of the dragline silk. Although it was not found in the literature, one explanation is that during the heating cycle, a fraction of the β -sheets either melted or dissolved in the microstructure. By removing part of the crystalline fraction in the composite, the overall material stiffness was reduced (see *Figure 16*). Comparing the untreated silk value to the heated silk values of initial modulus, a great reduction in stiffness is found: 2.2 ± 0.7 GPa to 0.6 ± 0.1 GPa.

The heated silk yield strain data is listed in *Table 12*. Compared to the untreated silk, the heated silk has the same measured value for yield strain. The thermal treatment has not changed the mechanical properties affecting the yield strain. The yield stress however has decreased due to the reduction in the elastic modulus, shown in *Figure 17*.

4.4 Inelastic Region

4.4.1 Percent Elongation

Percent elongation is listed in *Table 13*. The maximum percent elongation is $24\pm 5\%$ for silk that has been heat-treated. This is the same value found for untreated silk. Elasticity of dragline silk is independent of the baking temperature (up to 100°C).

4.4.2 Ultimate Tensile Strength

The ultimate tensile strength is also listed in *Table 13*. The experimental value is 0.4 ± 0.1 GPa for the heat-treated silk. This is a factor of three less than the untreated silk. The heat-treatment has reduced the stiffness in the silk matrix. According to Vollrath, the β -pleated sheets in *Figure 1* act as the stiffening mechanism in the silk³. Using the same logic in section 4.3, heat has broken down a portion of these crystalline structures and caused a greater mobility of the α -helices throughout the microstructure. As a result, when stressed, there is less internal resistance restricting the long rubber-like α -helices. The material can be loaded, but the slope is not as steep, resulting in a reduced UTS (see *Figure 17*).

4.4.3 Energy to Break

The energy to break for heat-treated silk is listed in *Table 13*. The experimental value is $4 \pm 2 \text{ J/kg (} \times 10^4 \text{)}$, which is a factor of 3.5 less than the untreated silk. Given the reduced UTS and the equivalent percent elongation, the energy to break scales accordingly.

4.5 Summary

In this chapter, silk was heated to 100C in an inert atmosphere for 24 h. Compared to the untreated silk, the properties related to strength were reduced, while the properties related to the elasticity were unchanged. It is theorized that the heating cycle changed the silk matrix by reducing the number of β -sheet crystals and thus reducing the strength. The α -helices are long and robust chains that the heat did not alter, as seen by the elasticity in the maximum strain shown in *Table 14*.

4.6 Tables and Figures

Table 11 The silk heated to 100°C for 24 h. has a Young's modulus of 0.6 ± 0.1 GPa. The final modulus (after yielding) is 0.2 ± 0.05 GPa.

Data Title	Young's Modulus (GPa)	Final Modulus (GPa)
100300	0.6	0.2
100400	0.4	NA
100500	0.5	0.1
110600	0.6	0.07
110700_2	0.5	0.2
111700_2	0.8	0.2
111700_3	0.5	0.08
120100_1	0.7	0.2
120100_2	0.7	0.2

Table 12 Strain at the yield point for silk heated to 100°C for 24 h is 1.2+/-0.2%.

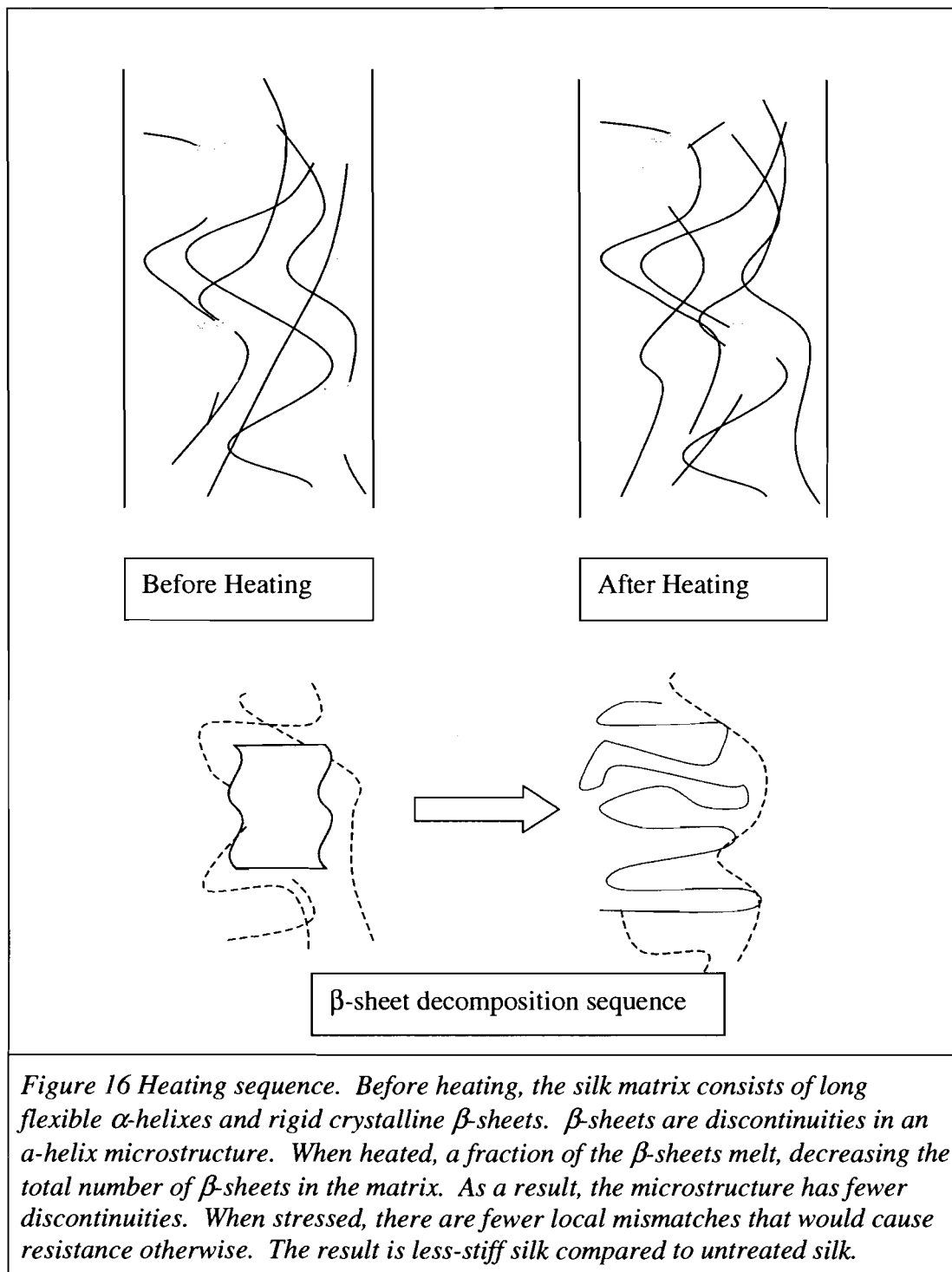
Data Title	Strain at Yield Point (%)
100300	1.3
100400	1.7
100500	1.2
110600	1.6
110700_2	0.9
111700_2	1.3
111700_3	0.7
120100_1	1.3
120100_2	1.2

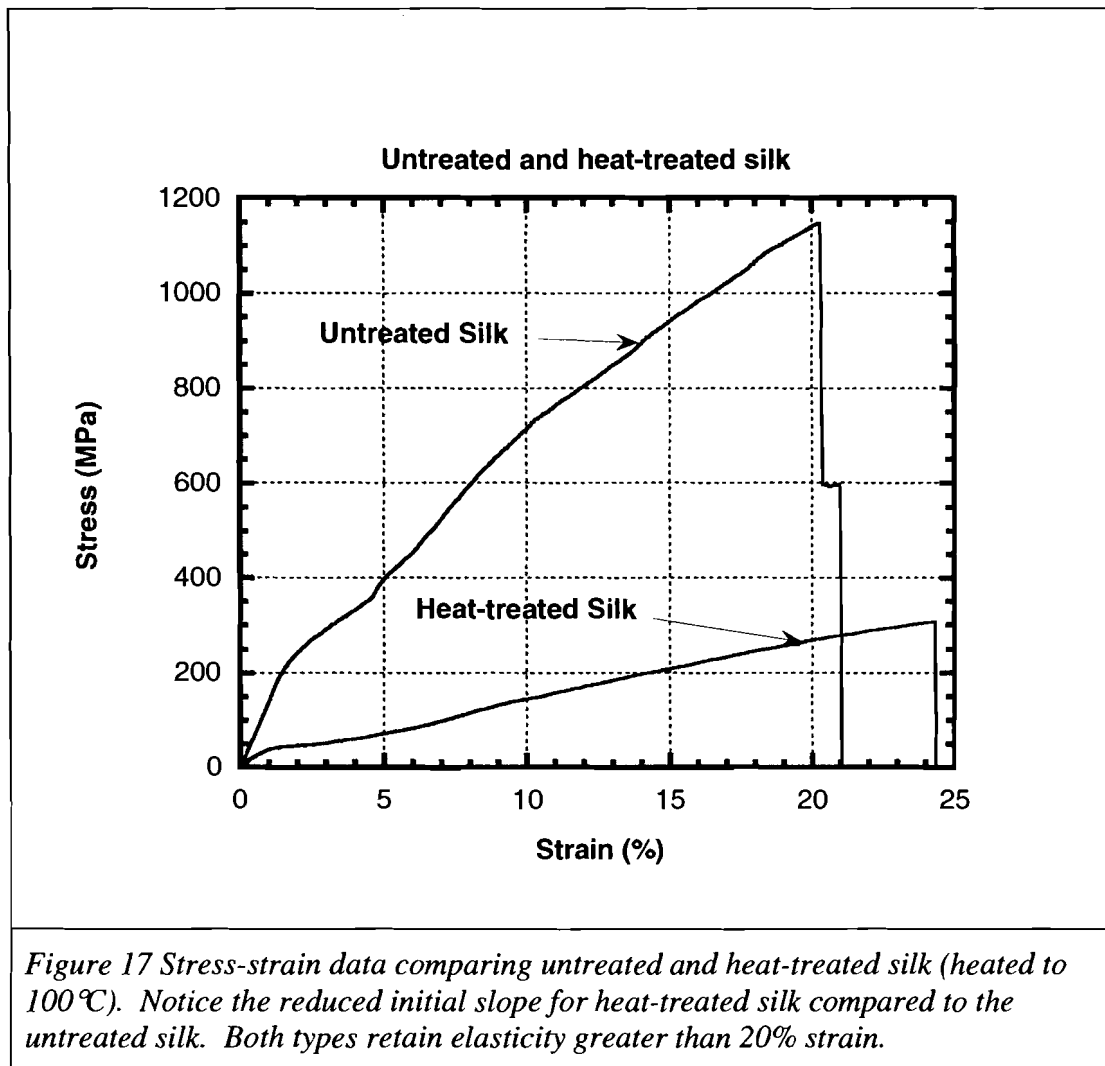
Table 13 Properties of silk heated to 100°C for 24 h. The averaged experimental values are the following: percent elongation, $24.3 \pm 4.6\%$, ultimate tensile stress, 0.4 ± 0.1 GPa, energy to break, $4 \pm 2 \times 10^5$ J/kg.

Data Title	Percent Elongation (%)	Ultimate Tensile Stress (GPa)	Energy to Break (10^5 J/kg)
100300	29	0.5	0.58
100400	29	0.4	0.23
100500	24.3	0.3	0.18
110600	26.4	0.3	0.42
110700_2	9.8	0.2	0.06
111700_2	25.4	0.5	0.54
111700_3	23.2	0.2	0.2
120100_1	28.5	0.6	0.75
120100_2	23	0.6	0.63

Table 14 Dragline silk material properties between untreated and heat-treated silk (100°C for 24 h.)

Material Property	Untreated Silk	Heat-treated Silk
Young's Modulus, E_i (GPa)	2.2±0.7	0.6±0.1
Strain at Yield Point (%)	1.4±0.2	1.2±0.2
Final Tensile Modulus, E_f (GPa)	0.4±0.07	0.2±0.05
Strain at Maximum Load (%)	24.1±2	24.3±5
Ultimate Tensile Strength (MPa)	1244±214	382±122
Energy to Break (10^5 J/kg)	1.4±0.3	0.4±0.2





4.7 References

¹ F. Y. Tsai, T. N Blanton, D. R. Harding, and S.H Chen, "Temperature dependence of the properties of vapor-deposited polyimide," *Journal of Applied Physics*, **93**, No. 7, 3760-3764 (1 Apr 2003).

² Keith B. Guess and Christopher Viney, "Thermal analysis of major ampullate (drag line) spider silk: the effect of spinning rate on tensile modulus," *Thermochimica Acta*, **315**, 61-66 (1998).

³ F. Vollrath, "Spider Webs and Silks," *Scientific American*, 70-76 (March 1992).

5.0 Summary

In conclusion, the objectives for this study have been met. First of all, a load cell and strain gauge were identified and assembled to perform tensile testing in the appropriate loading range. Secondly, procedures were developed over the course of the project in handling dragline spider silk samples and measuring the material properties at room temperature. Finally, experimental data was collected for silk exposed to 100°C temperature. Data from room temperature showed a Young's modulus of 2.2 ± 0.7 GPa, ultimate tensile strength of 1244 ± 214 MPa and an energy to break of $1.4 \pm 0.3 \times 10^5$ J/kg. For heat-treated silk, Young's modulus is 0.6 ± 0.1 GPa, the ultimate tensile strength is 382 ± 122 MPa, and the energy to break is $0.4 \pm 0.2 \times 10^5$ J/kg. The properties of yield strain and maximum strain for untreated silk were 1.4 ± 0.2 and $24.1 \pm 2\%$, respectively. Heat-treated silk showed the same respective values: $1.2 \pm 0.2\%$ and $24.3 \pm 5\%$. These data support the theory that the heating cycle selectively damaged the silk strengthening mechanism, without changing the elasticity.

Due to the nature of the target-mounting scheme, vibration of the capsule is an issue. The following expression relates the natural frequency of the silk to the applied tensile force:

$$f = \left(\frac{1}{ld} \right) \sqrt{F/\rho\pi} \text{ (Hz)} \quad (1-11)$$

where l is the length of the silk, F is the tensile force, and ρ is the material density. As the tension in the silk increases, the frequency increases. In this application, pre-stressing the silk before adding a capsule adds tension to an already stiff fiber. The length of each strand is 16 mm. Based on data from this work, silk can conservatively withstand a 10%-15% (1.6mm to 2.4mm) elongation before rupturing. Following this procedure for each target increases the resonant frequency and reduces lateral displacement. Although it was not measured, the stiffness of the silk will increase as the target is cooled to 20K, because stiffness generally increases as a function of temperature. The silk remains in tact at these low temperatures.

Silk has been chosen for the ICF capsule mount for many reasons. Its size is a benefit not only for the implosion point of view, but also from a vibration standpoint. A 1.00 μm diameter fiber attached tangentially to a capsule is the smallest practical fiber of its kind. Compared to other materials such as Kevlar or rubber, its strength and elasticity over the 20K to 373K temperature range make it the best material for this application.

Appendix 1: Tensile testing data

A1.1 Calculations

Untreated Data

Data title	Initial length (cm)	Strain (%)	Max load (mg)
90800			152.5
92200	1.186	20.3	184.1
101200-2	1.29	22.5	171.7
101300	1.3464	26.6	122.9
102000-1	1.7959	27.2	311.3
102000-2	1.1223	19.8	216.1
102000-3	1.5938	24.6	319.7
111600-1	0.9905	21.5	112.9
111600-2	1.0246	22.2	104.1
111700-4	0.8774	31.9	122
112200-1	0.9834	24.2	134.6
112200-2	0.9953	21.4	99
031001_4	0.9595	26.1	187.9
031101_1	0.9358	26.6	180.9
031101_2	0.9933	23	139.8
mean_strain		24.1	170.6
n_strain		14	15
stdev_strain		3.3	68.0
t		2.2	2.1
95% t*stdev/sqrt(n)		1.9	37.7

Baked Data	Initial length (cm)	Strain (%)	Max load (mg)
100300	1.3783	29	79.9
100400	1.5132	29	56.2
100500	1.1434	24.3	49.2
110600	0.7185	26.4	47.9
110700-2	1.2645	9.8	24.5
111700-2	0.9499	25.4	76.2
111700-3	0.8847	23.2	31.3
120100-1	0.9626	28.5	93.4
120100-2	0.8319	23	93
average		24.3	61.3
n		9	9
stdev		5.9	25.5
t		2.306	2.306
95% t*stdev/sqrt(n)		4.6	19.6

UTS Calculations

UTS factor 1.00E+06
 G 9.8 m/s²
 average silk OD 1 um

Untreated data	#silk	OD(um)	Max load (mg)	area (um ²)	UTS (Pa)	UTS(MPa)
90800	1	1	152.5	0.785398	1.9E+09	1902.9
92200	2	1	184.1	1.570796	1.15E+09	1148.6
101200-2	4	0.73	171.7	1.674155	1.01E+09	1005.1
101300	2	0.72	122.9	0.814301	1.48E+09	1479.1
102000_1	2	1.36	311.3	2.905345	1.05E+09	1050.0
102000_2	2	1.36	216.1	2.905345	7.29E+08	728.9
102000_3	2	1.36	319.7	2.905345	1.08E+09	1078.4
111600_1	2	1	112.9	1.570796	7.04E+08	704.4
111600_2	2	1	104.1	1.570796	6.49E+08	649.5
111700_4	1	1	122	0.785398	1.52E+09	1522.3
112200_1	1	1	134.6	0.785398	1.68E+09	1679.5
112200_2	1	1	99	0.785398	1.24E+09	1235.3
031001_4	2	0.842	187.9	1.113638	1.65E+09	1653.5
031101_1	2	0.842	180.9	1.1	1.59E+09	1591.9
031101_2	2	0.842	139.8	1.1	1.23E+09	1230.2
	average		170.6 mg		average	1244
	stdev		68.0 mg		stdev	386.1
	95%				n	15.0
					t	2.1
					95%	213.8

Baked data	#silk	OD(um)	Max load area		UTS (Pa)	UTS(MPa)
			(mg)	(um2)		
100300	2	1	79.9	1.570796	4.98E+08	498.5
100400	2	1	56.2	1.570796	3.51E+08	350.6
100500	2	1	49.2	1.570796	3.07E+08	307.0
110600	2	1	47.9	1.570796	2.99E+08	298.8
110700_2	2	1	24.5	1.570796	1.53E+08	152.9
111700_2	2	1	76.2	1.570796	4.75E+08	475.4
111700_3	2	1	31.3	1.570796	1.95E+08	195.3
120100_1	2	1	93.4	1.570796	5.83E+08	582.7
120100_2	2	1	93	1.570796	5.8E+08	580.2
			61.3		average	382.4
			25.5		stdev	159.2
					n	9
			3.253282		t	2.306
			19.6151		95%	122.4

Untreated Silk, $E_{i,f}$ Measurements

average silk diameter

Data Title	1 μm						SI conversion 1.0E+06			
	Initial slope			Final slope			Silk			
	dmass (mg)	dstrain	slope	dmass (mg)	dstrain	slope	#silk	OD (μm)	E_i	E_f
92200	200	0.0851	2350	60	0.088	682	2	1	1.5E+09	4.3E+08
101200_2	180	0.108	1667				2	0.73	2E+09	0
101300	140	0.087	1609	20	0.086	233	2	0.72	1.98E+09	2.9E+08
102000_1	350	0.091	3846	150	0.142	1056	2	1.36	1.32E+09	3.6E+08
102000_2	250	0.03	8333	100	0.116	862	2	1.36	2.87E+09	3E+08
102000_3	350	0.078	4487	150	0.116	1293	2	1.36	1.54E+09	4.5E+08
111600_1	120	0.075	1600	60	0.133	451	2	1	1.02E+09	2.9E+08
111600_2	120	0.081	1481	60	0.156	385	2	1	9.43E+08	2.4E+08
111700_4	140	0.077	1818	80	0.209	383	1	1	2.31E+09	4.9E+08
112200_1	160	0.033	4848	80	0.165	485	1	1	6.17E+09	6.2E+08
112200_2	120	0.062	1935	60	0.142	423	1	1	2.46E+09	5.4E+08
031001_4	200	0.079	2532	100	0.16	625	2	0.842	2.27E+09	5.6E+08
031101_1	200	0.077	2597	120	0.21	571	2	0.842	2.33E+09	5.1E+08
031101_2	160	0.0657	2435	60	0.162	370	2	0.842	2.19E+09	3.3E+08
Averages			2967			601			2.21E+09	4.2E+08
stdev			1889			305			1.27E+09	1.2E+08
n	14						MPa		2208	416
							ratio		5	
							n		14	13
							t		2.160	2.179
							95%		7.4E+08	7.4E+07

Energy to Break Calculations

Gravity constant 9.8 m/s² silk OD 1 um

silk density 1.2 g/cc

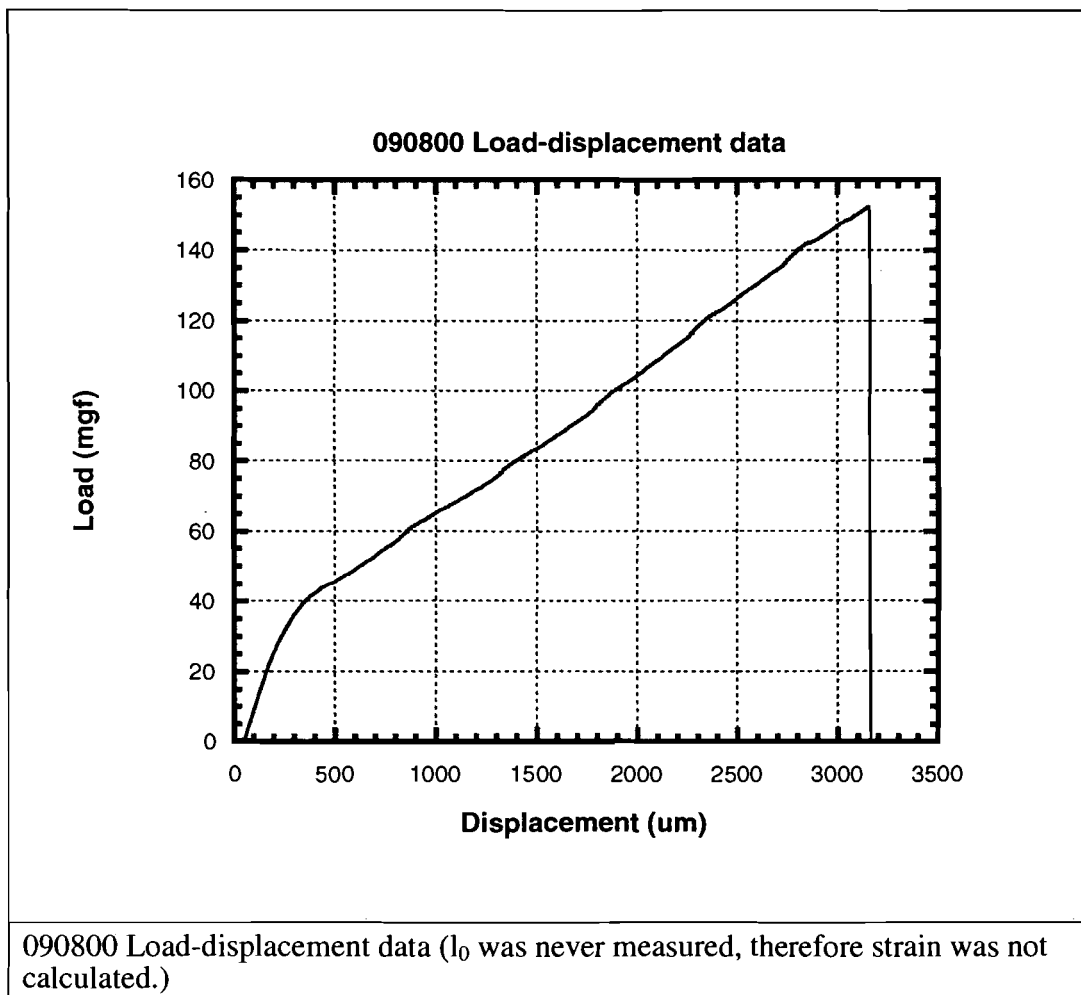
mass factor 1.00E-11

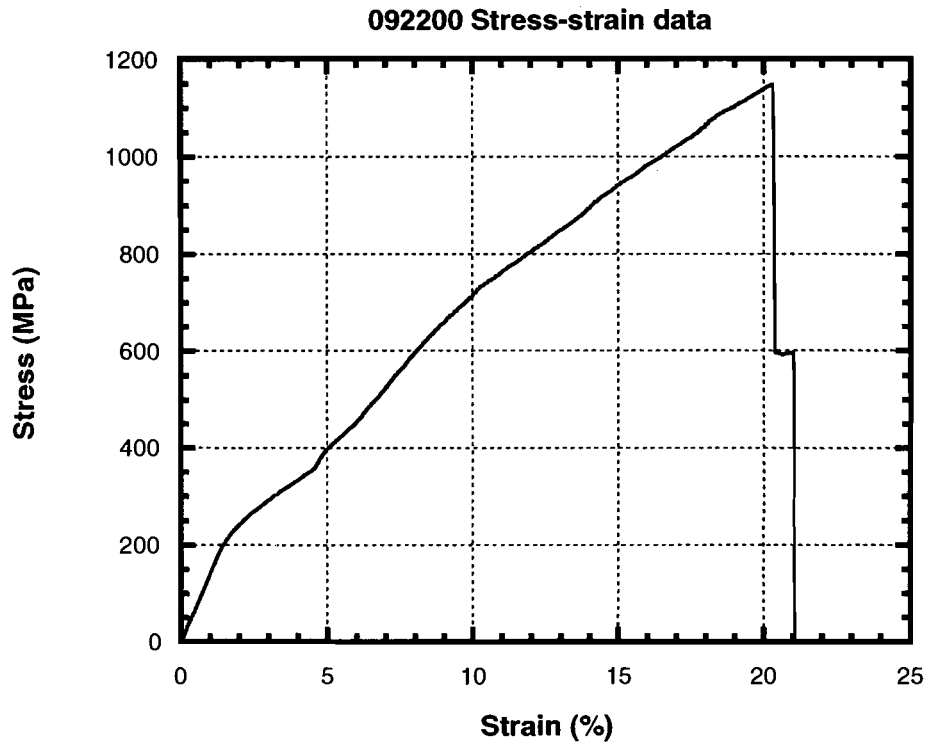
Untreated data title	Area under Curve (kg m)**	#silk	OD (um)	Total cross- sectional area(um ²)	Initial length (cm)	Silk Mass(kg)	Energy to Break (J/kg)
92200	2.6E-07	2	1	1.57	1.186	2.2E-11	1.1E+05
101300	2.8E-07	2	0.72	0.81	1.3464	1.3E-11	2.1E+05
102000_1	8.4E-07	2	1.36	2.91	1.7959	6.3E-11	1.3E+05
102000_2	2.8E-07	2	1.36	2.91	1.1223	3.9E-11	7.1E+04
102000_3	6.6E-07	2	1.36	2.91	1.5938	5.6E-11	1.2E+05
111600_1	1.4E-07	2	1	1.57	0.9905	1.9E-11	7.3E+04
111600_2	1.4E-07	2	1	1.57	1.0246	1.9E-11	7.2E+04
111700_4	1.8E-07	1	1	0.79	0.8774	8.3E-12	2.1E+05
112200_1	1.8E-07	1	1	0.79	0.9834	9.3E-12	1.9E+05
112200_2	1.2E-07	1	1	0.79	0.9953	9.4E-12	1.2E+05
031001_4	2.8E-07	2	0.842	1.11	0.9595	1.3E-11	2.1E+05
031101_1	2.7E-07	2	0.842	1.11	0.9358	1.3E-11	2.1E+05
031101_2	1.9E-07	2	0.842	1.11	0.9933	1.3E-11	1.4E+05
						average	1.4E+05
						min	7.1E+04
						max	2.1E+05
						stdev	56445
						t	2.179
						95%	3.41E+04

Baked Data Title	Area under Curve (kg m)**	#silk	OD (um)	Total cross-sectional area(um ²)	Initial length (cm)	Silk Mass(kg)	Energy to Break (J/kg)
100300	1.5E-07	2	1	1.57079633	1.3783	2.6E-11	5.8E+04
100400	6.6E-08	2	1	1.57079633	1.5132	2.9E-11	2.3E+04
100500	4.0E-08	2	1	1.57079633	1.1434	2.2E-11	1.8E+04
110600	5.8E-08	2	1	1.57079633	0.7185	1.4E-11	4.2E+04
110700_2	1.5E-08	2	1	1.57079633	1.2645	2.4E-11	6.1E+03
111700_2	9.9E-08	2	1	1.57079633	0.9499	1.8E-11	5.4E+04
111700_3	3.5E-08	2	1	1.57079633	0.8847	1.7E-11	2.0E+04
120100_1	1.4E-07	2	1	1.57079633	0.9626	1.8E-11	7.5E+04
120100_2	1.0E-07	2	1	1.57079633	0.8319	1.6E-11	6.3E+04
						average	4.0E+04
						min	6.1E+03
						max	7.5E+04
						stdev	23937.049
						t	2.306
						95%	1.8E+04

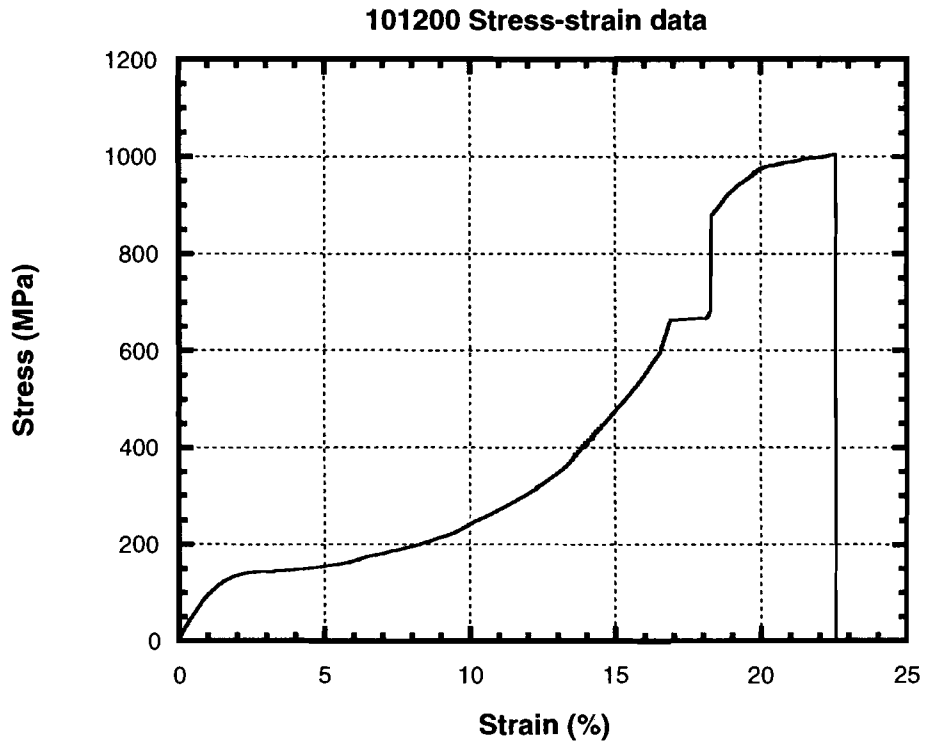
A1.2 Untreated data

{Note: All the following data (untreated, heat-treated, Hysteresis) is shown in a load-strain format. This format was chosen because the silk diameter was unknown at the time of the test.}

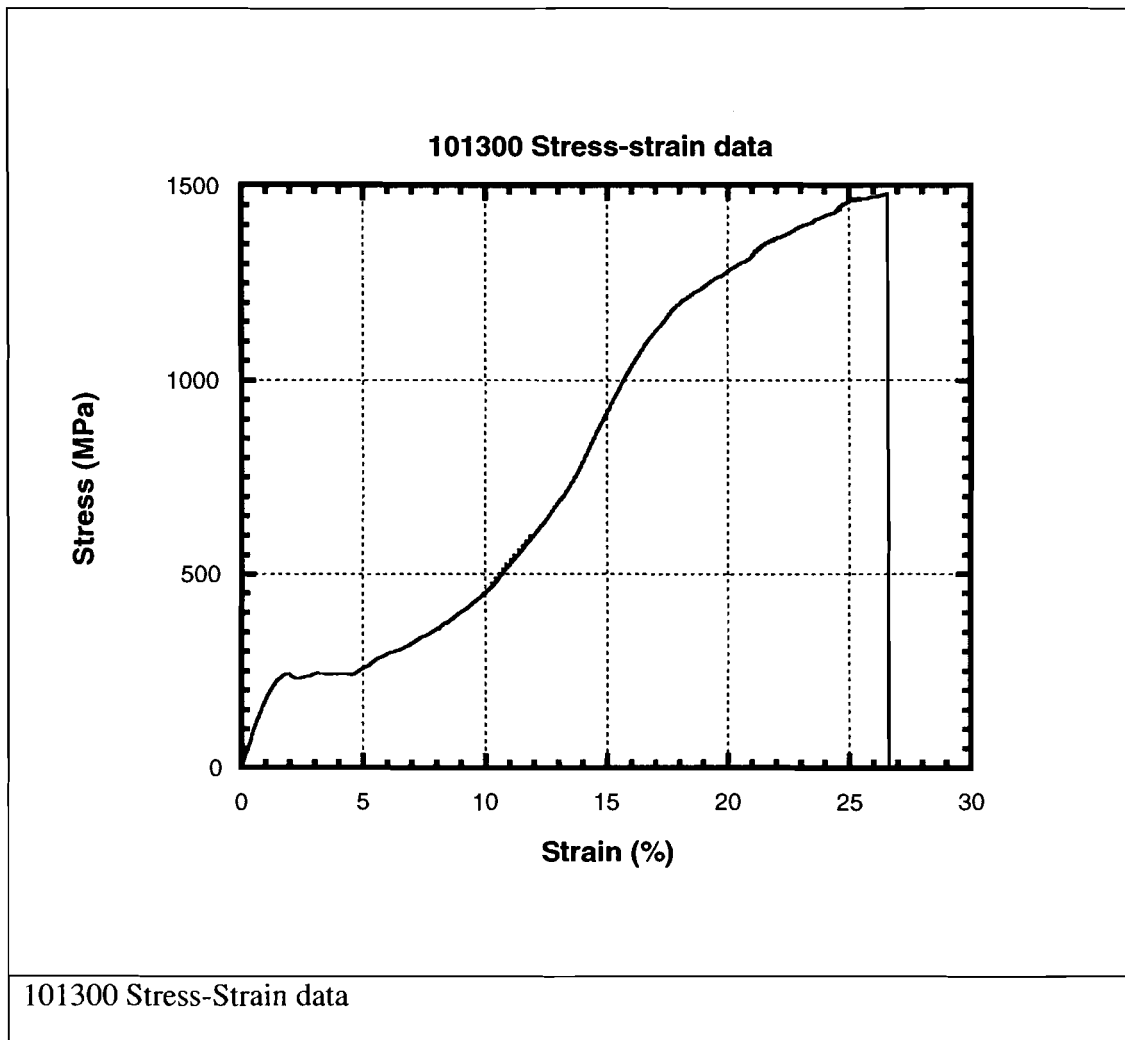


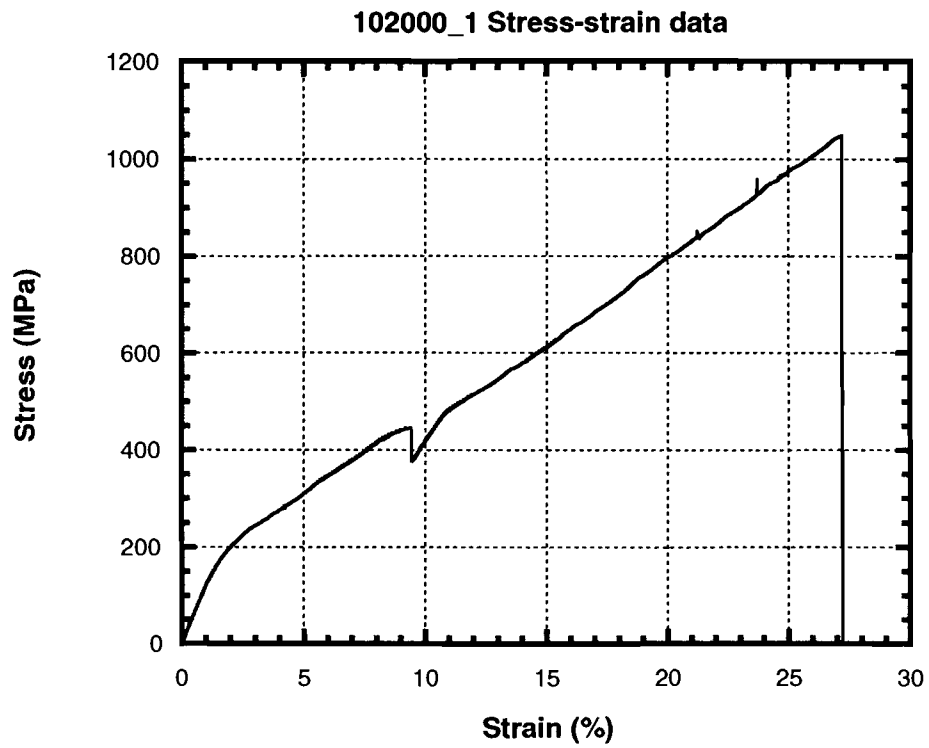


092200 Stress-Strain data

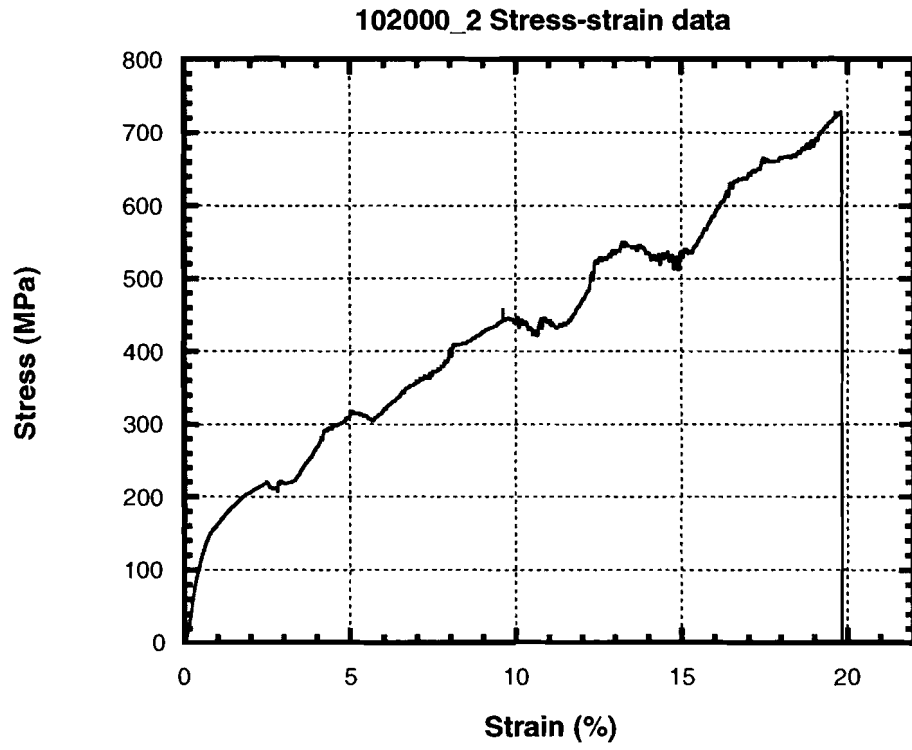


101200_2 Stress-Strain data. (Computer data fallout between 16.8% and 18.1% strain)

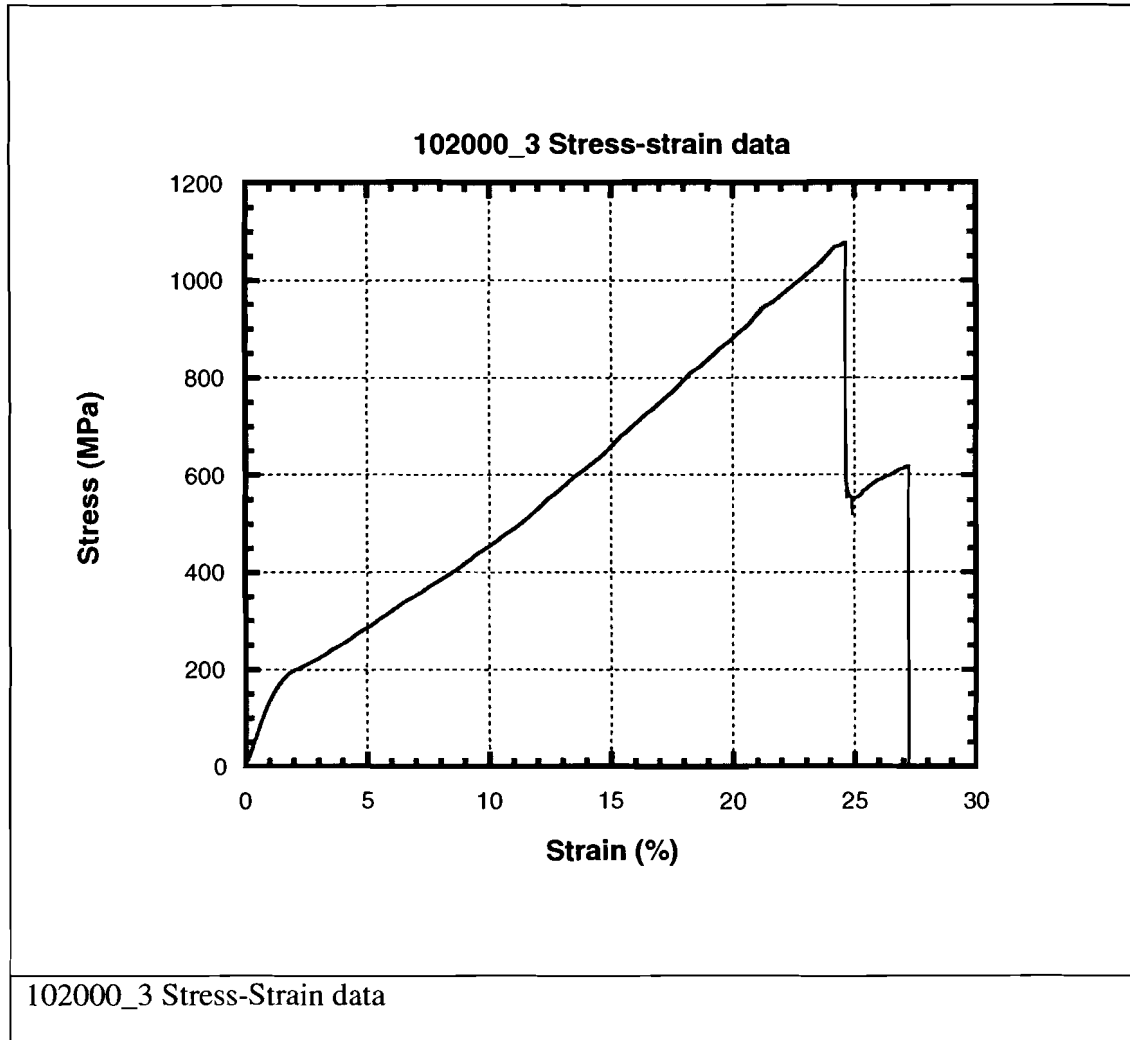


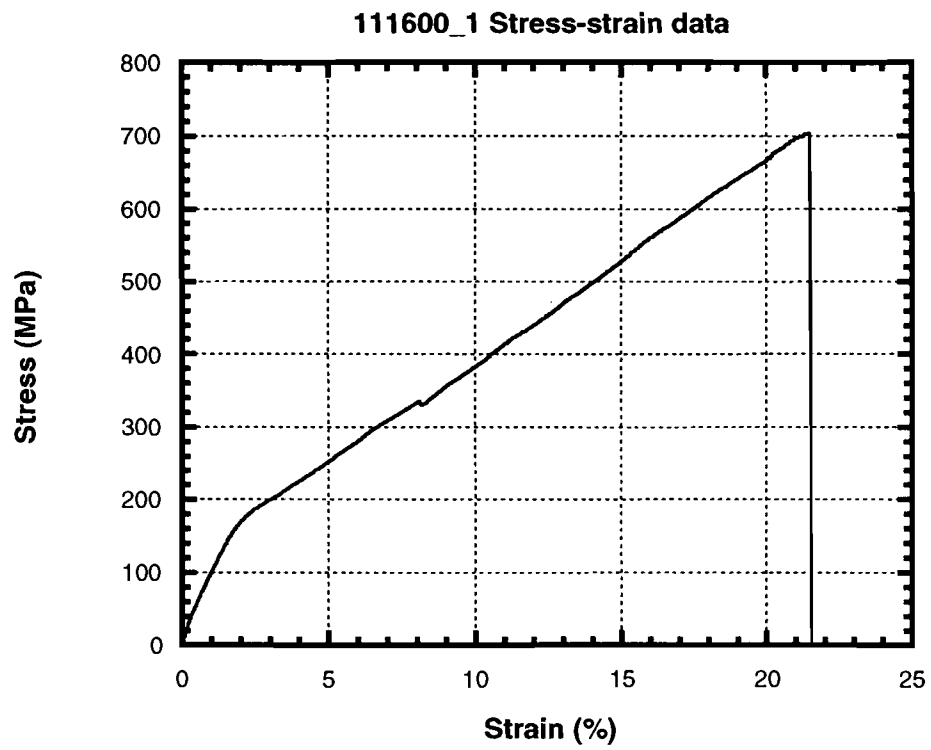


102000_1 Stress-Strain data

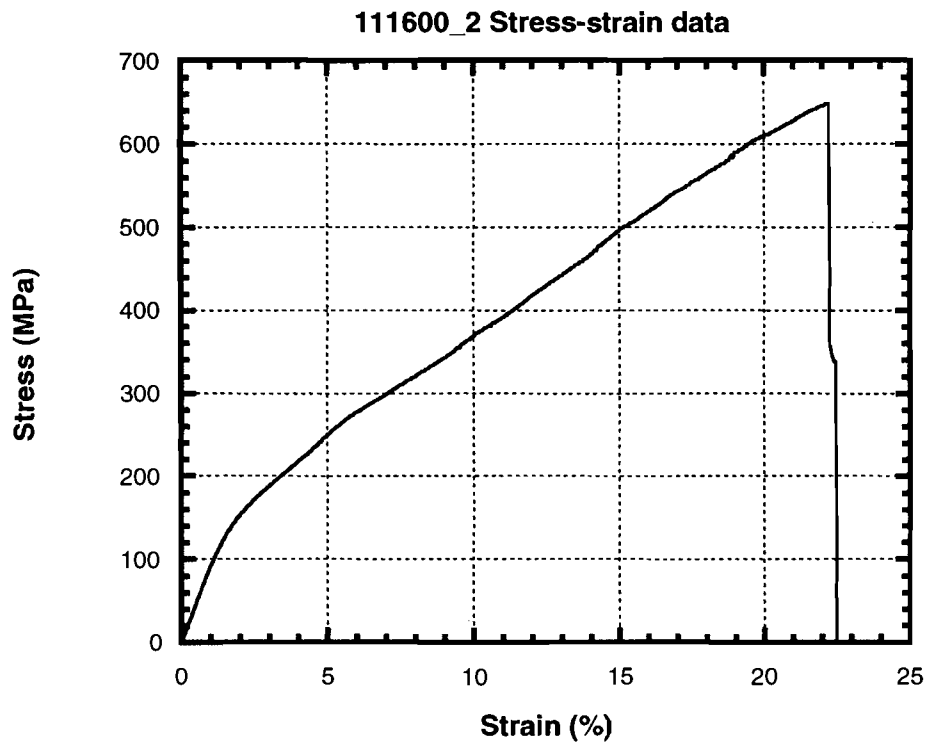


102000_2 Stress-Strain data

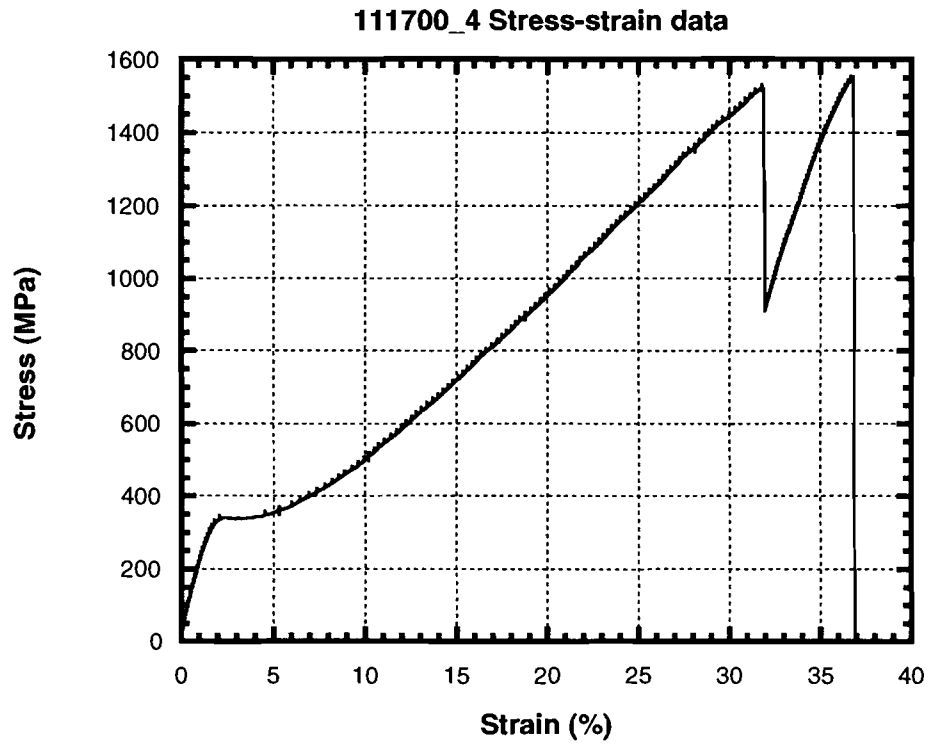




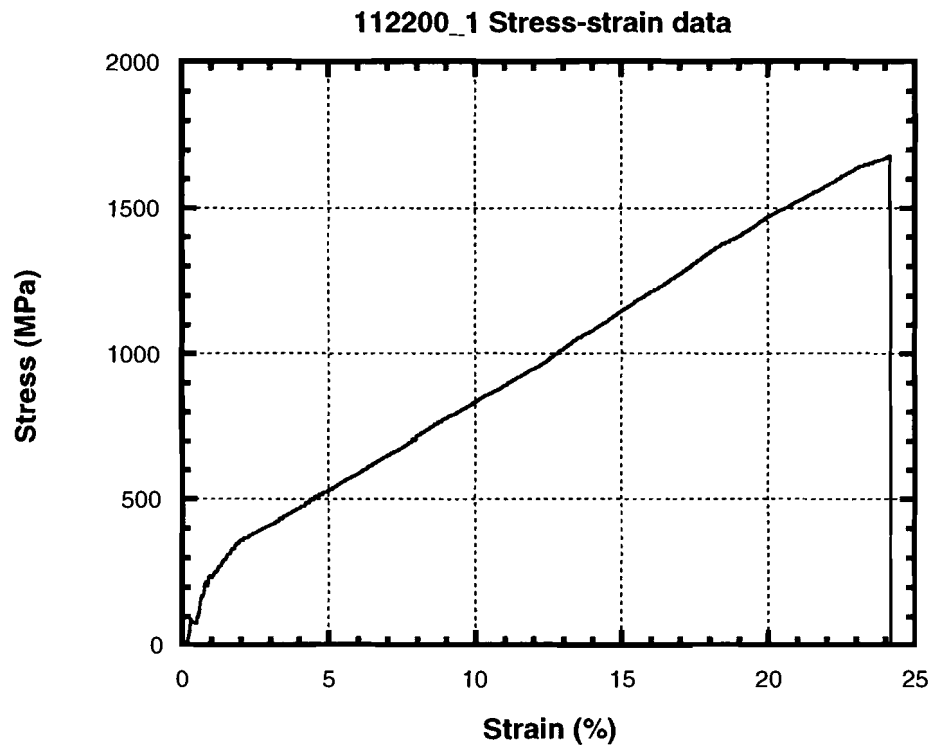
111600_1 Stress-Strain data



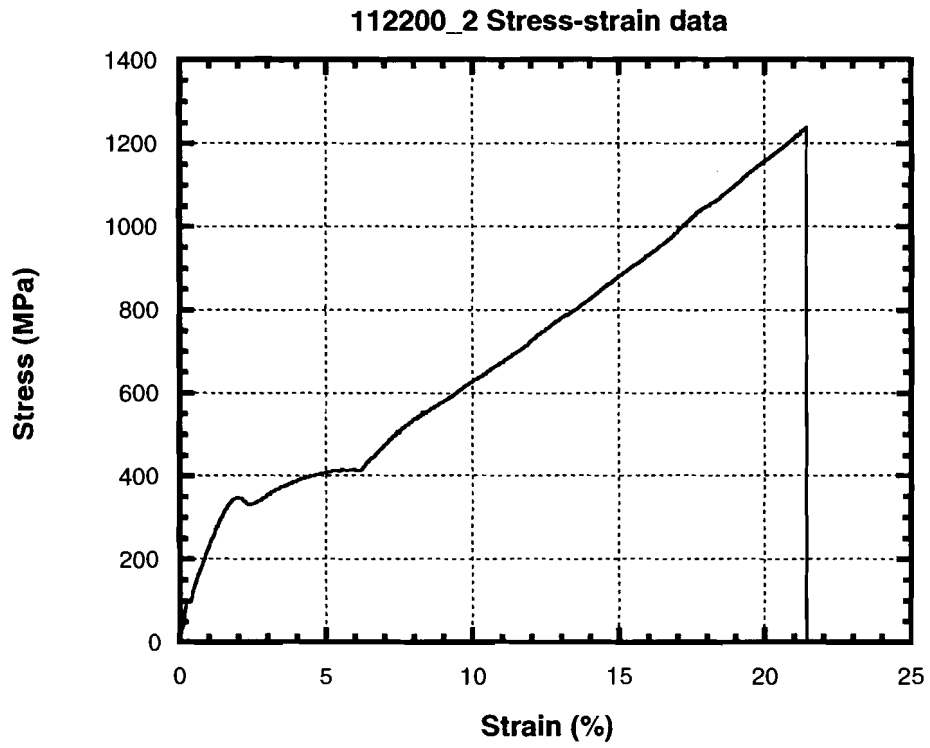
111600_2 Load-Strain data



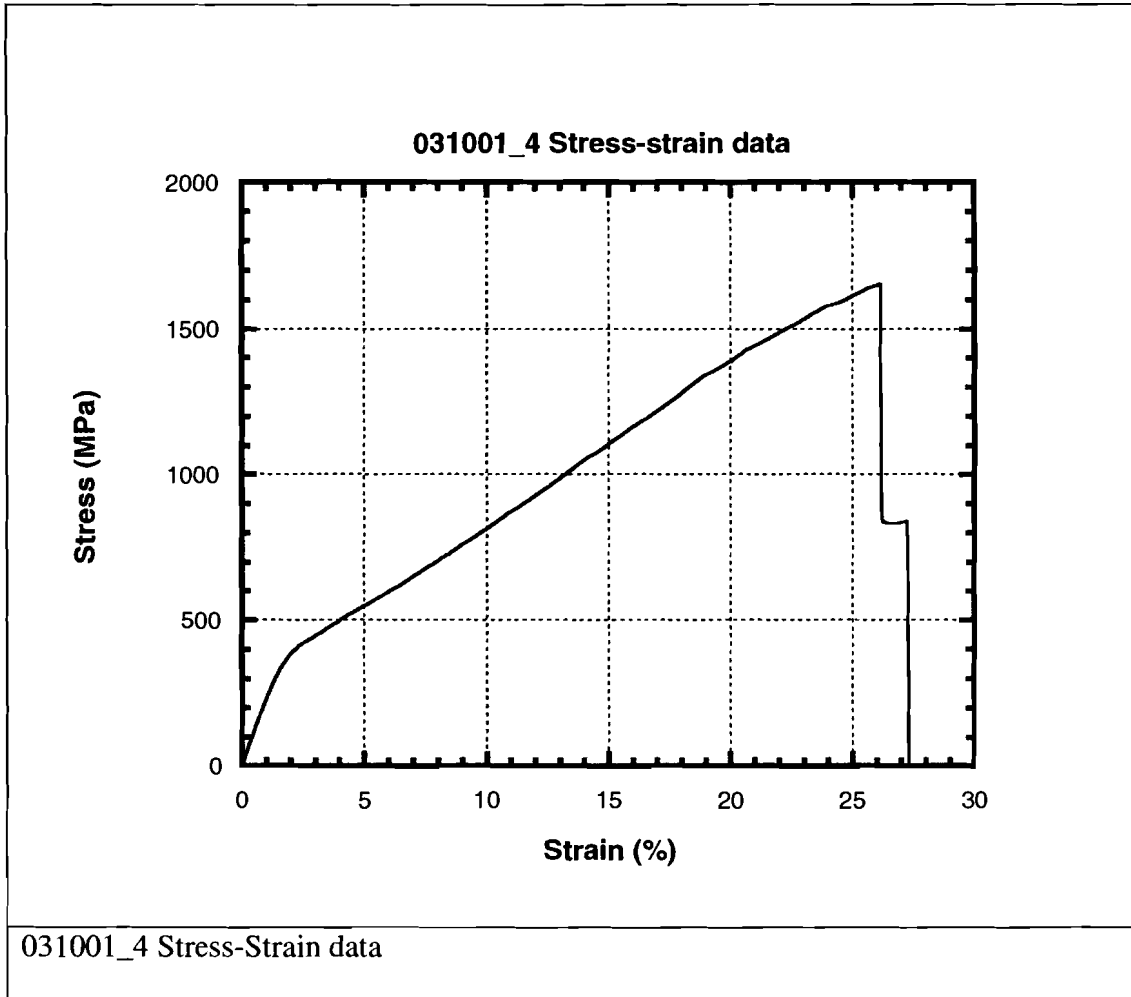
111700_4 Stress-Strain data

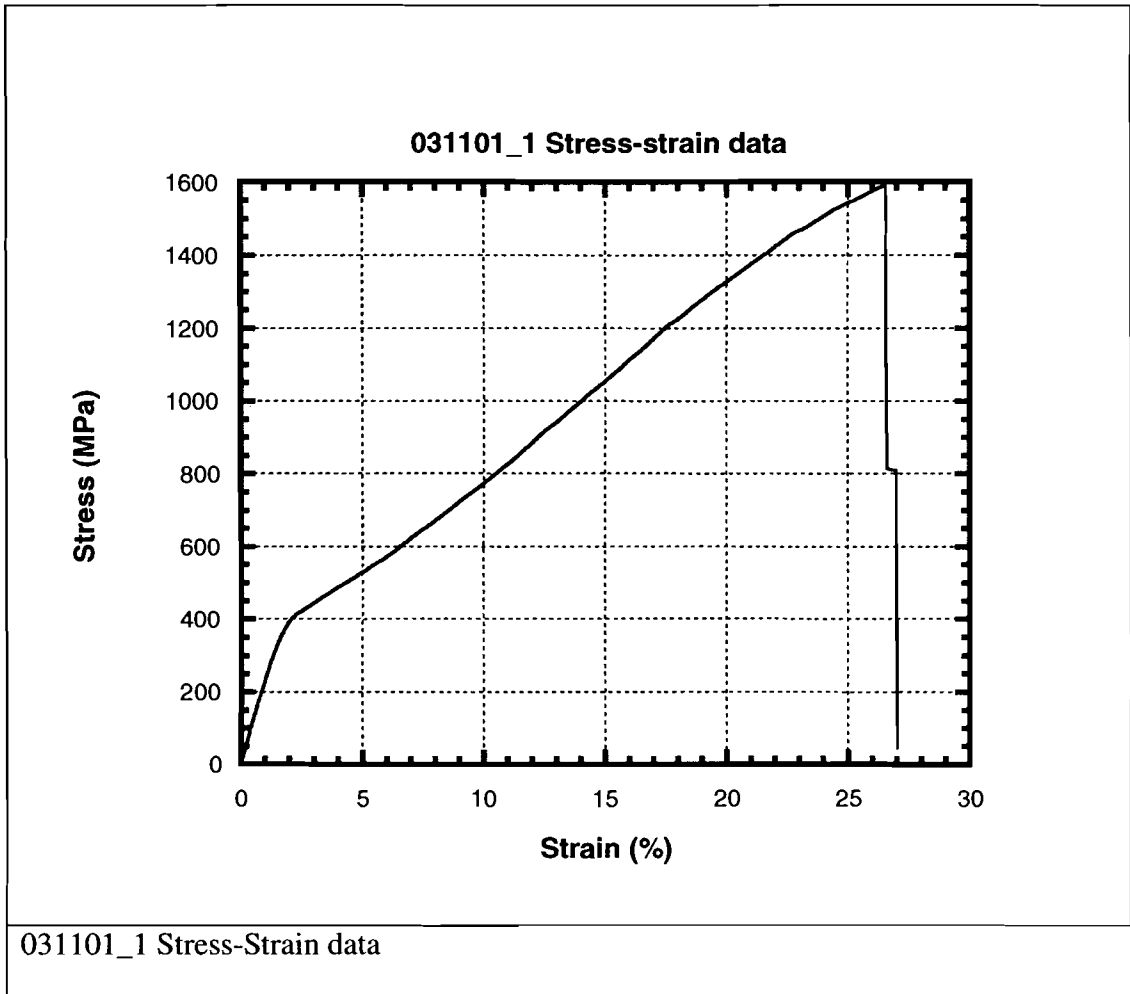


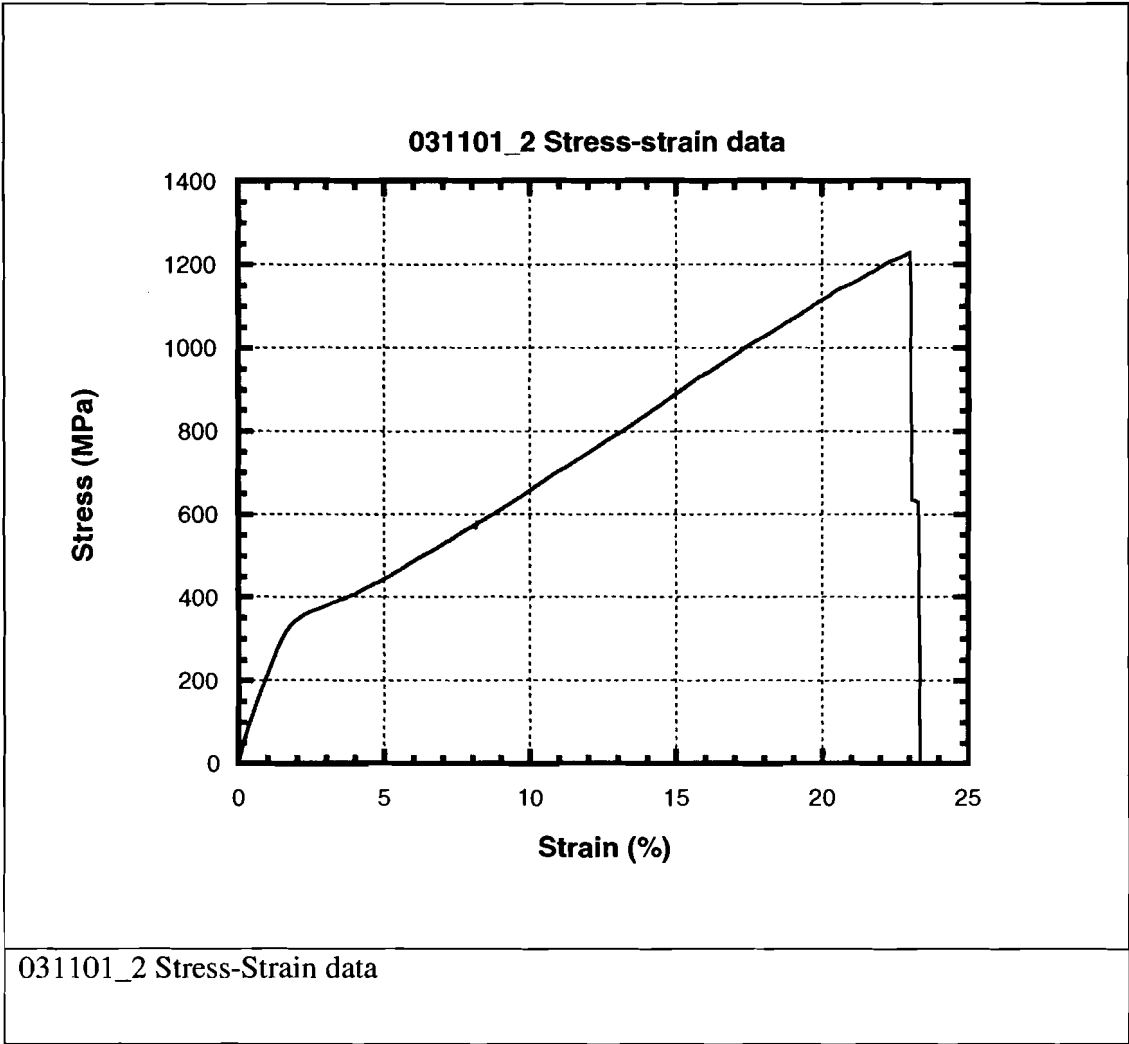
112200_1 Stress-Strain data



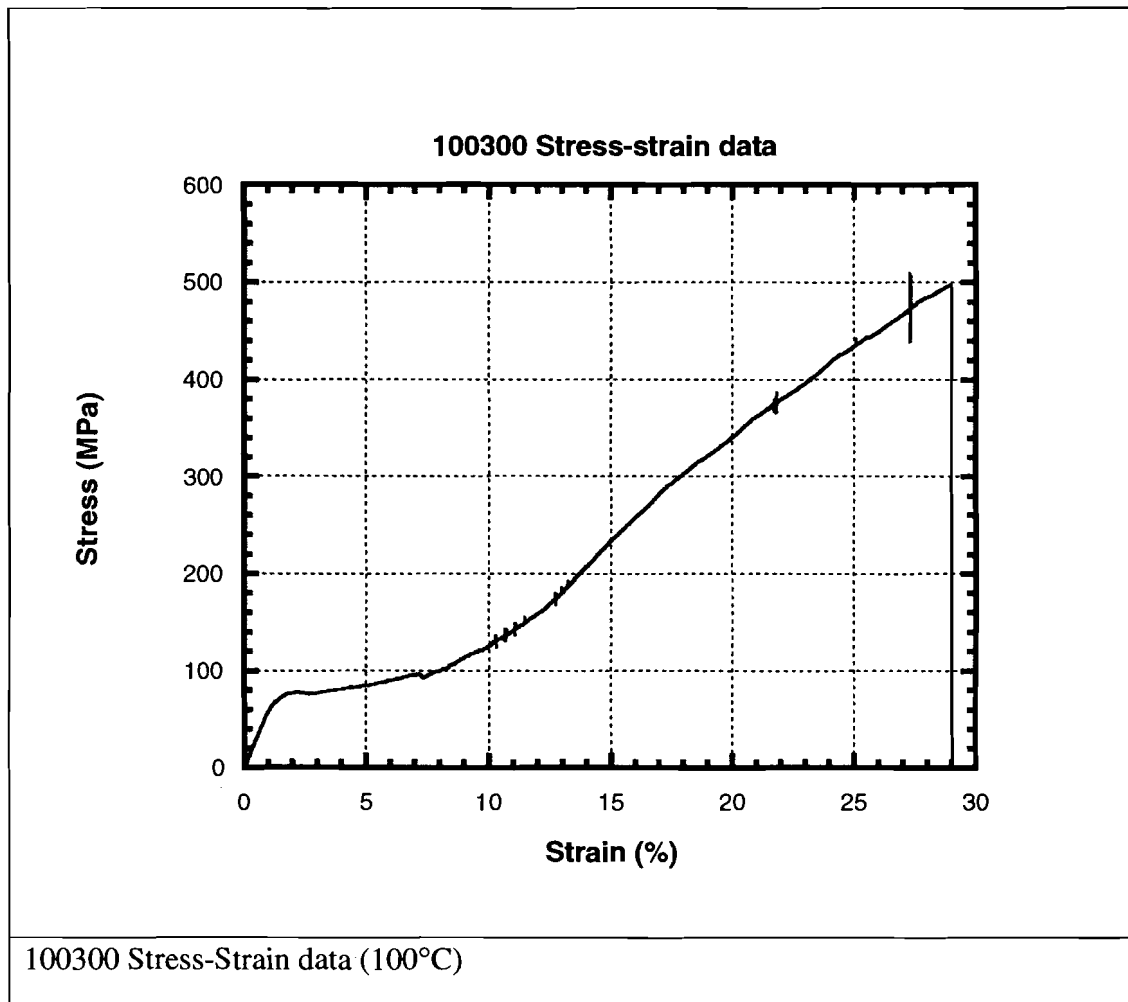
112200_2 Stress-Strain data

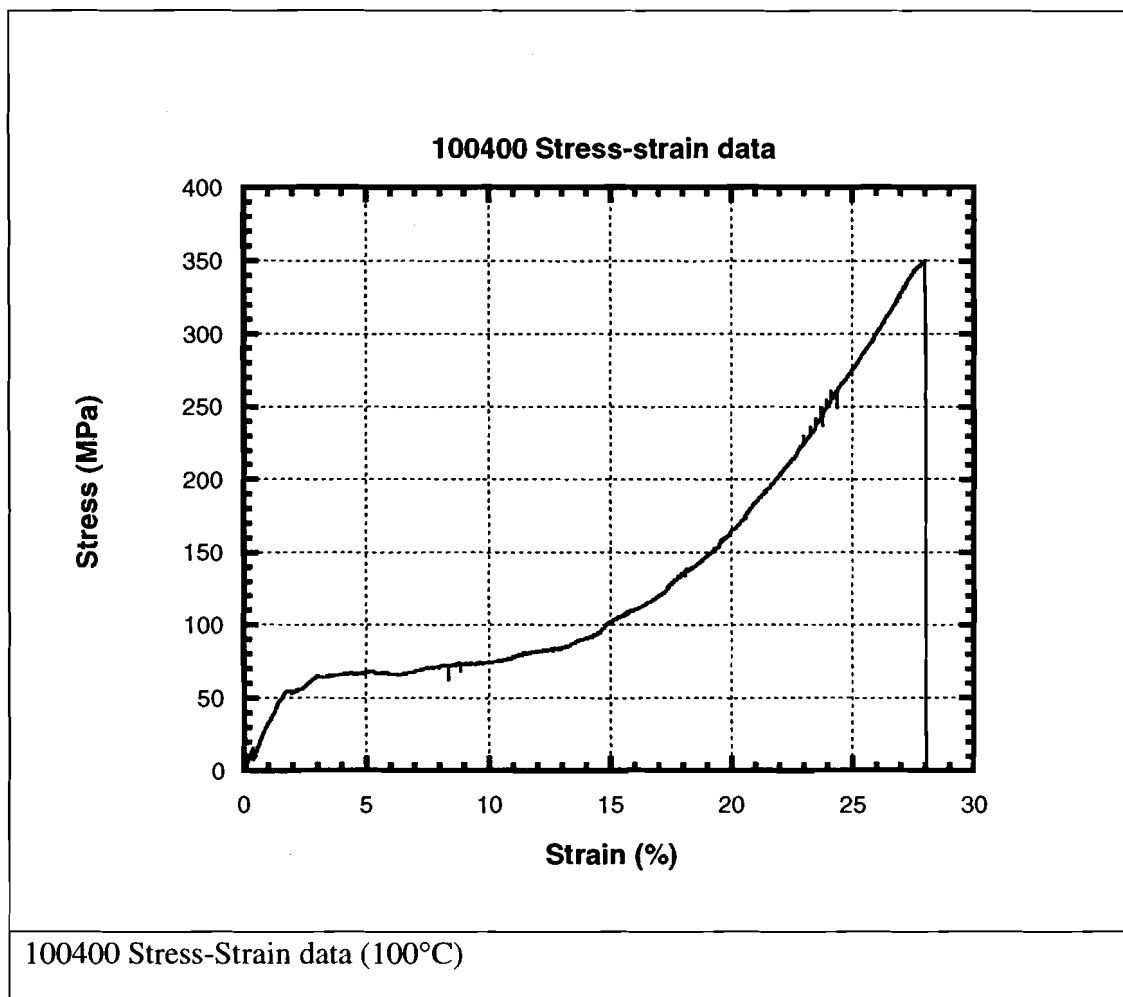


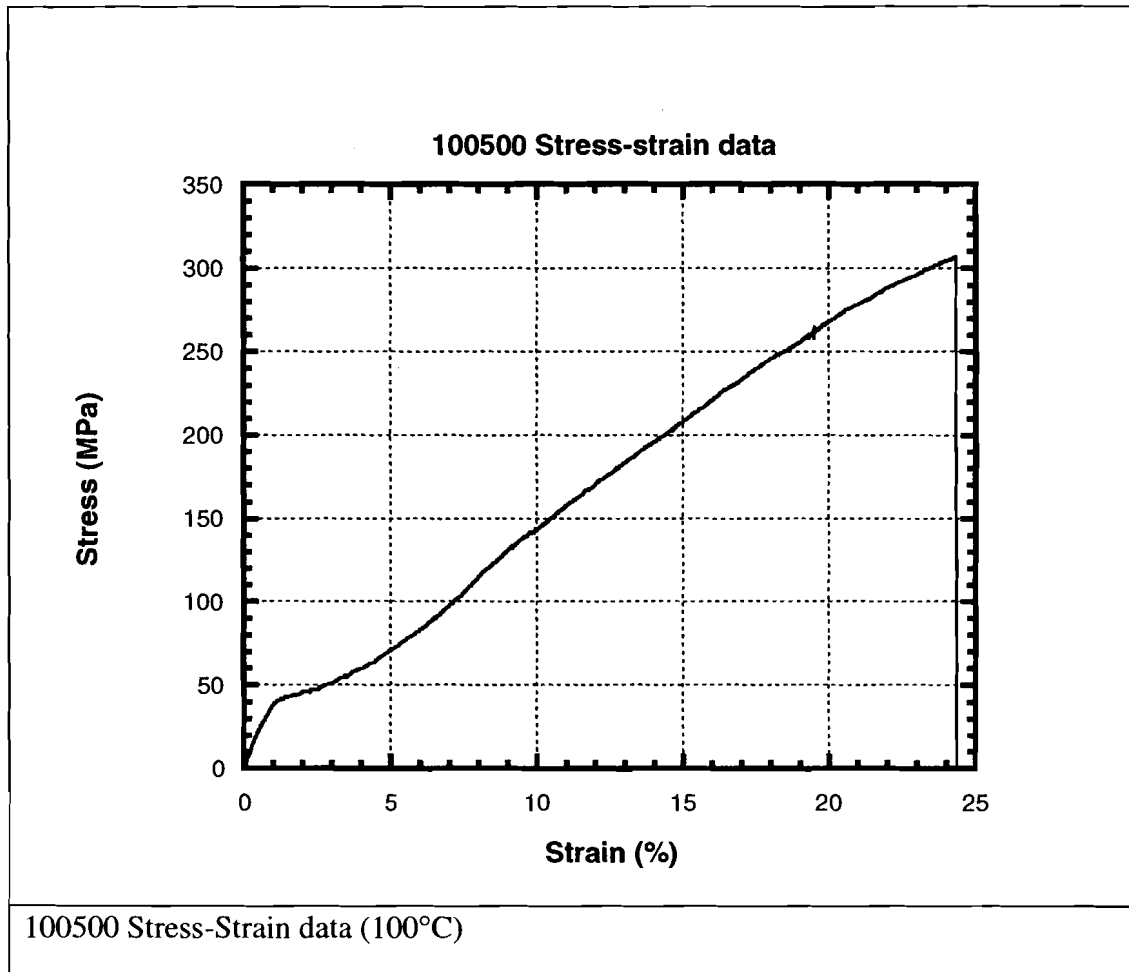


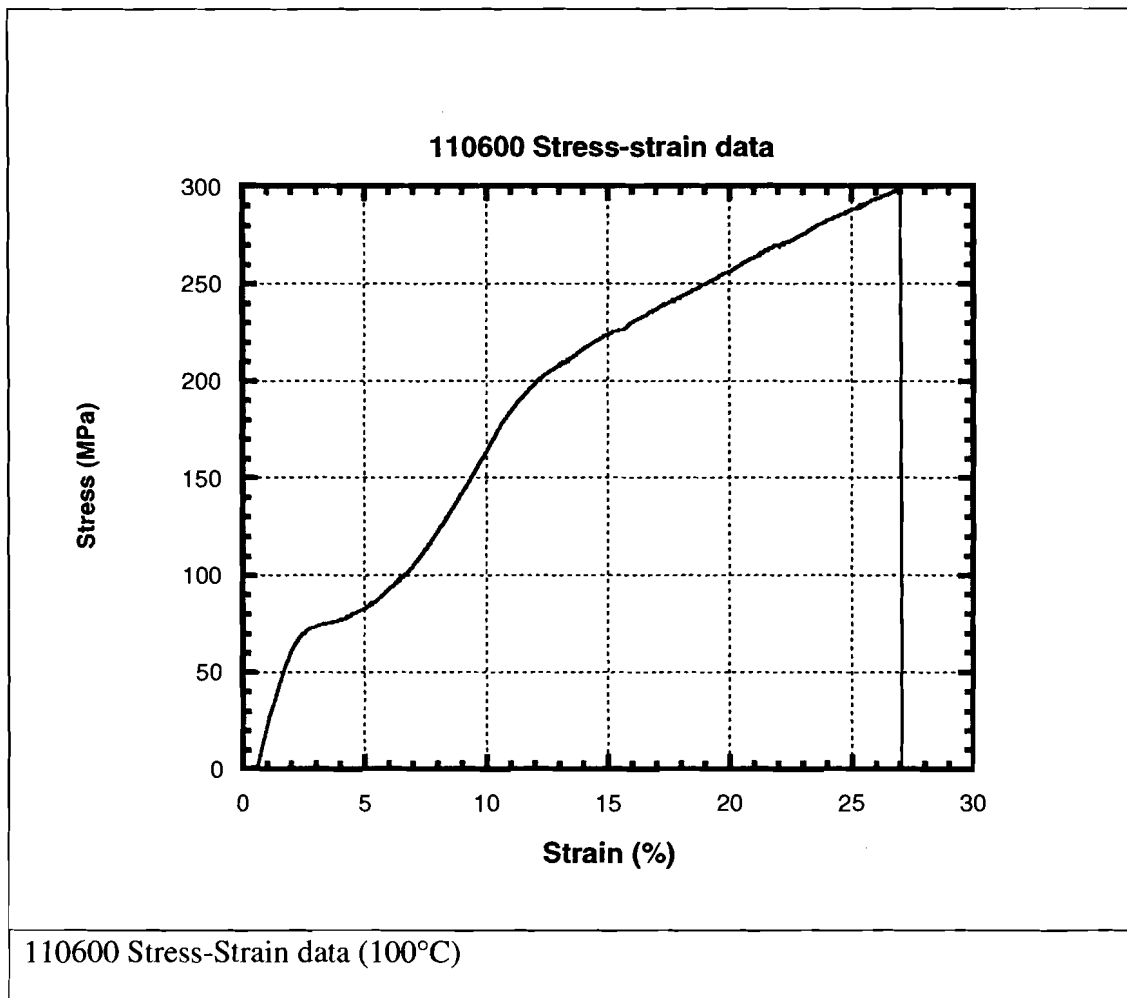


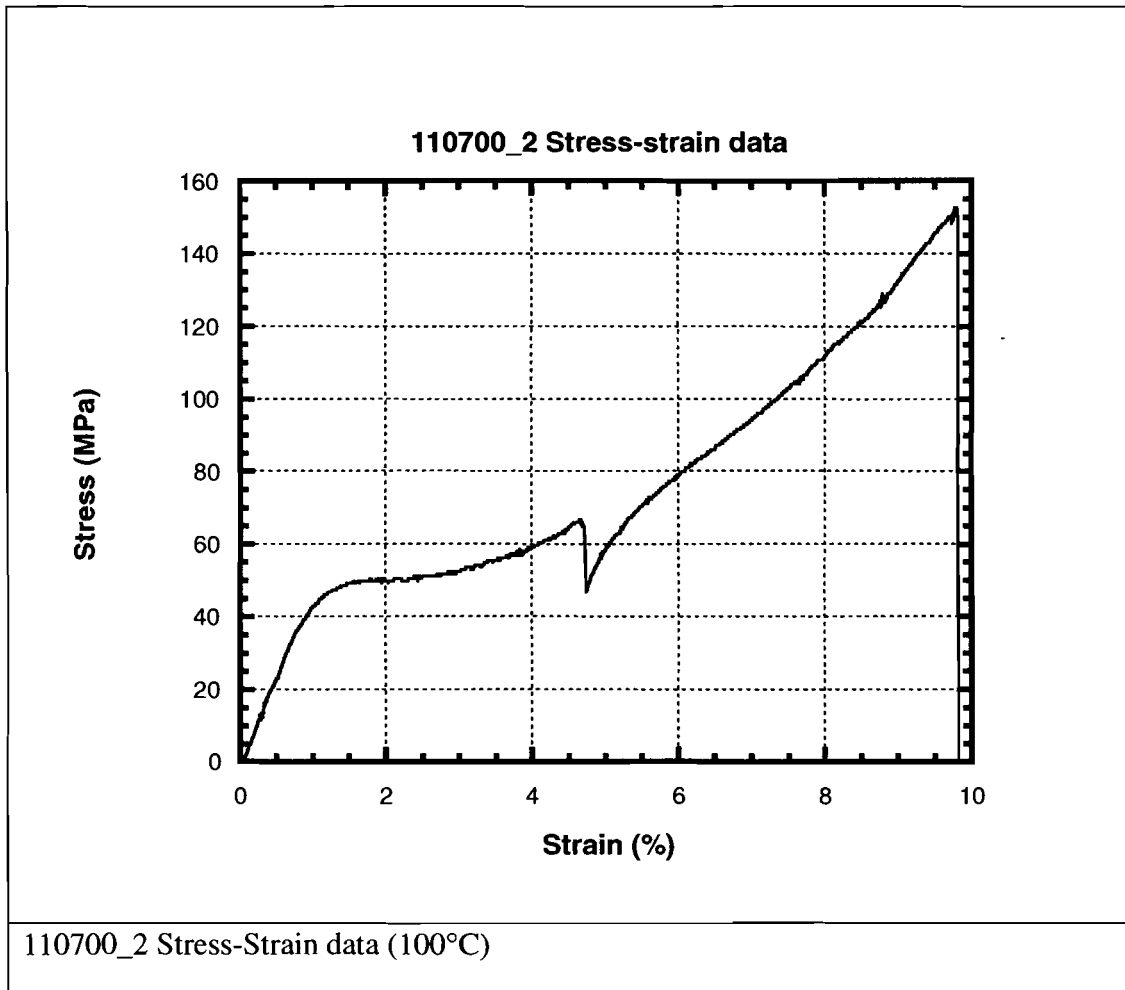
A1.3 Heat-treated data

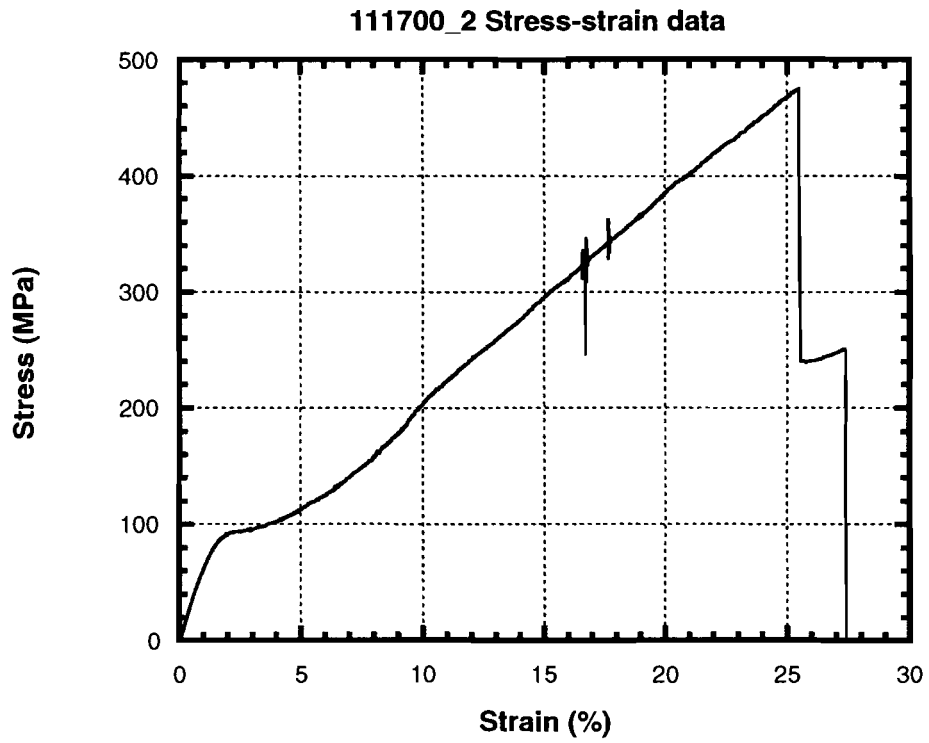




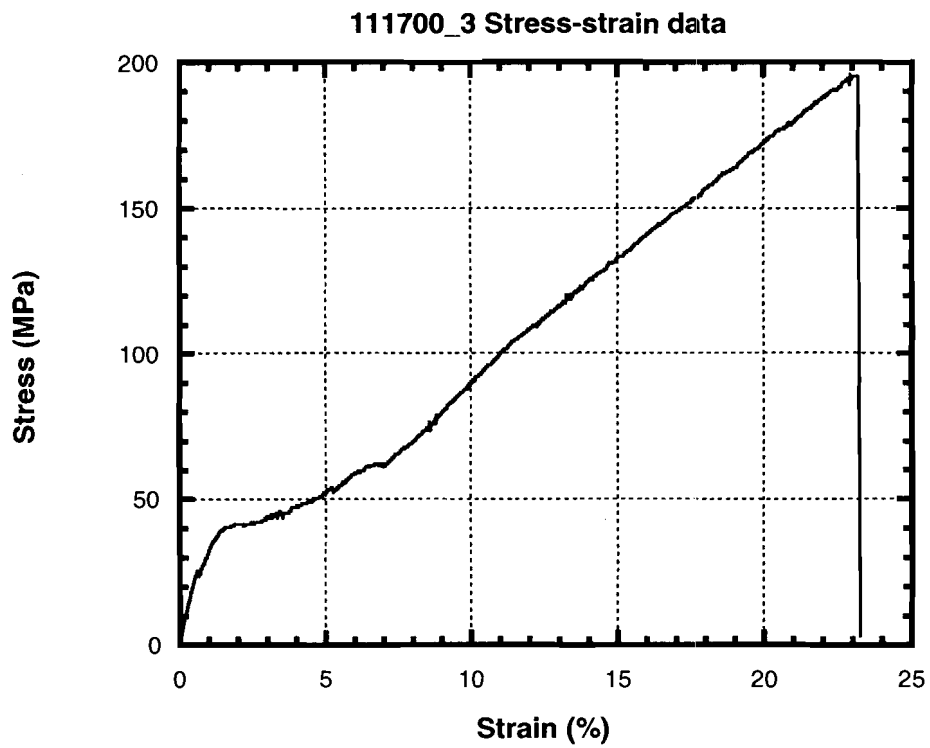




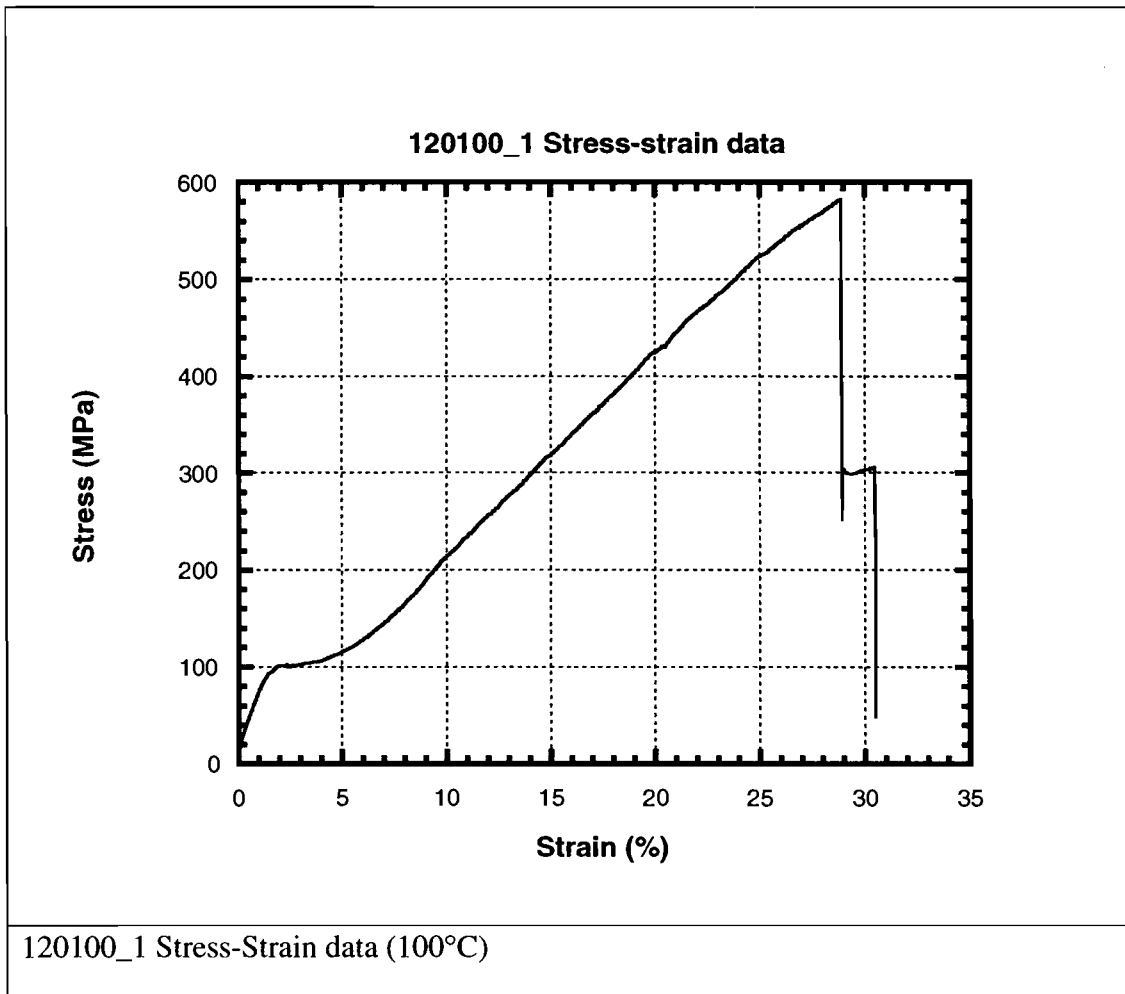


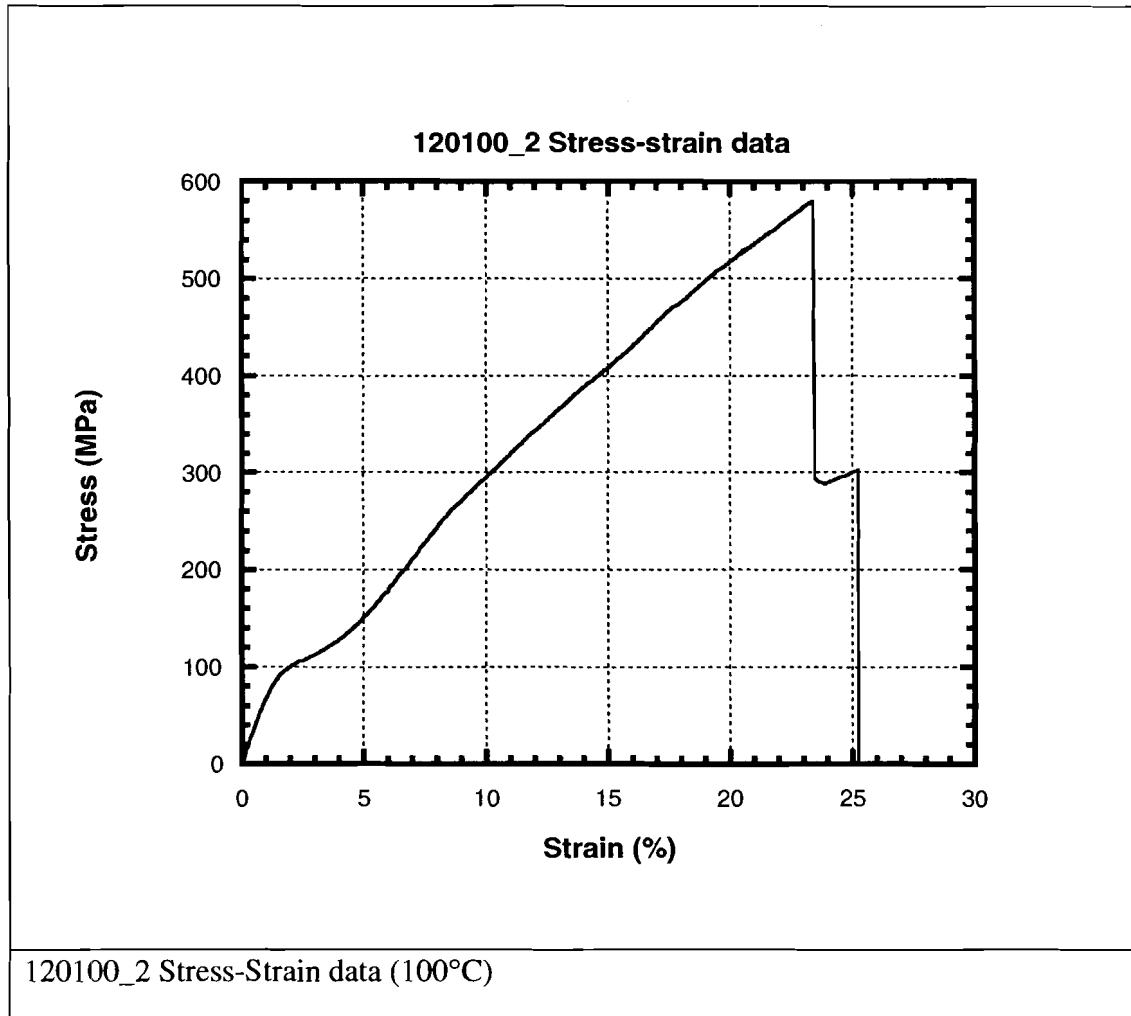


111702_2 Stress-Strain data (100°C)

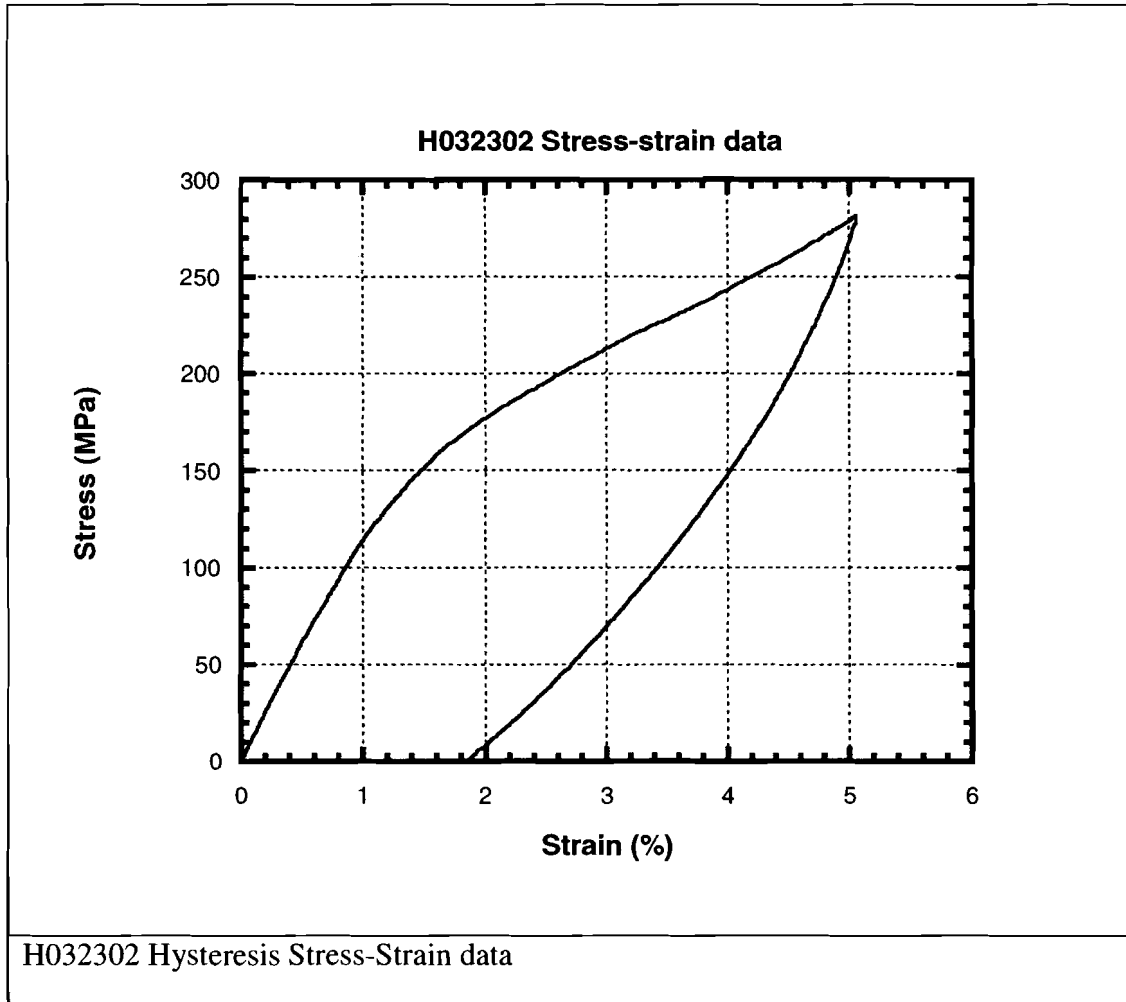


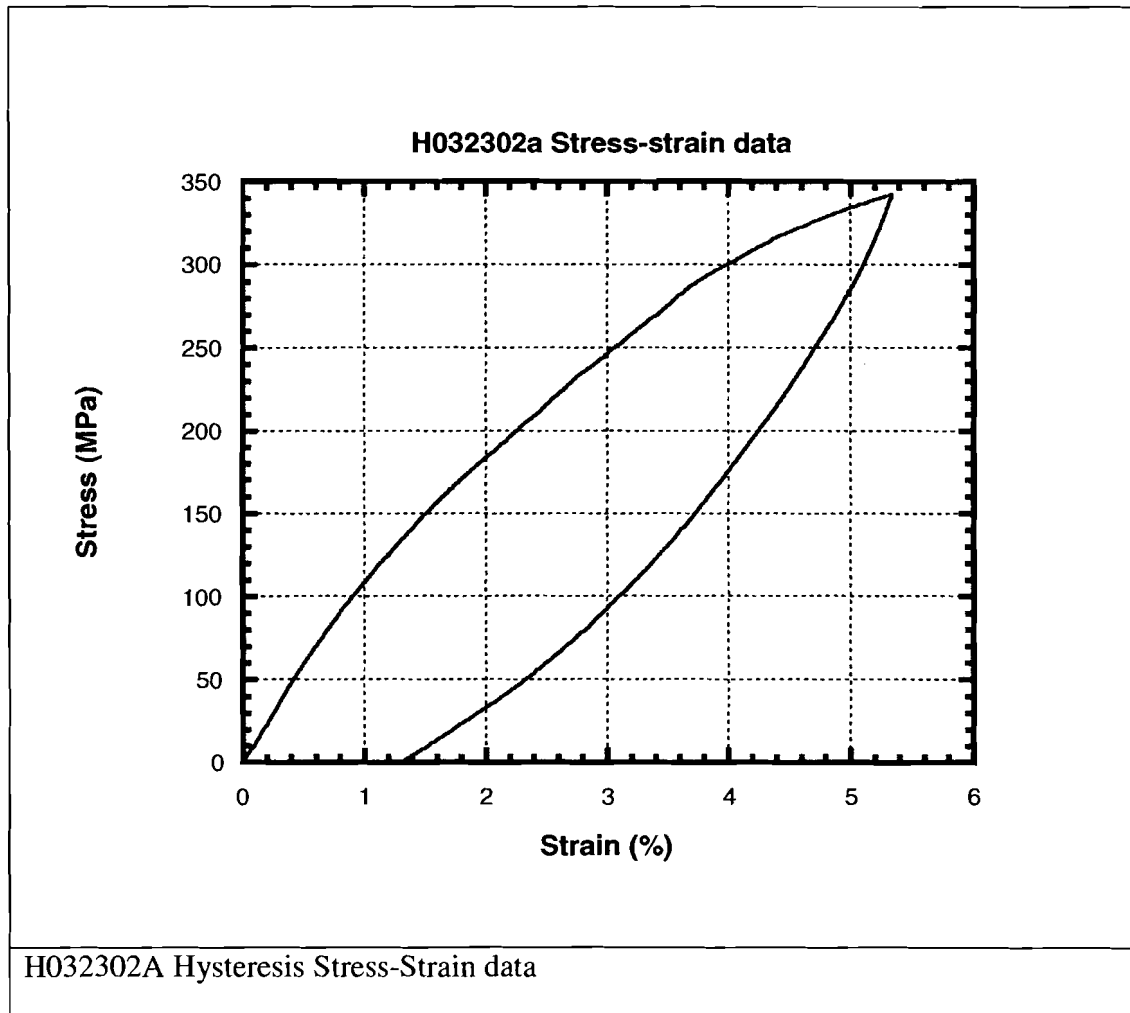
111700_3 Stress-Strain data (100°C)

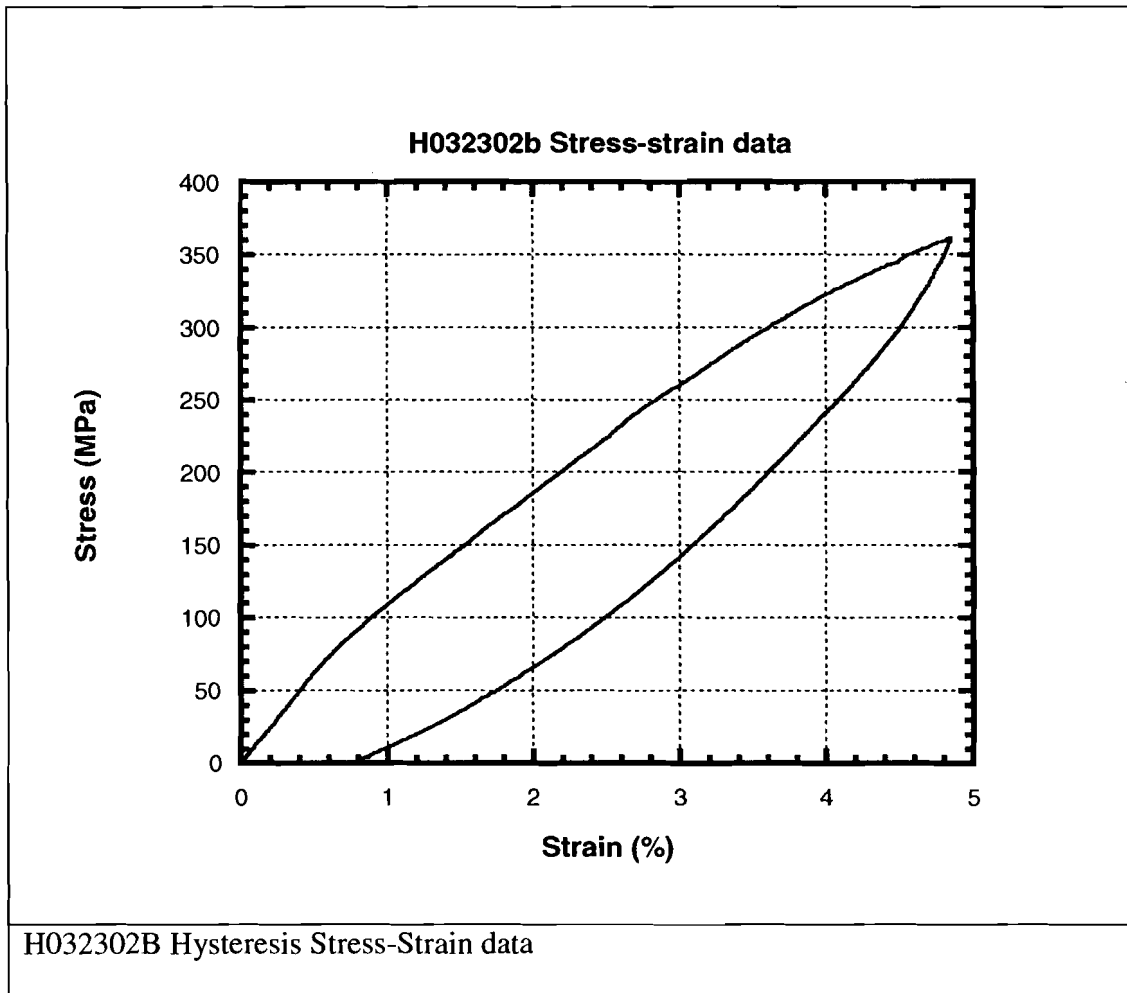


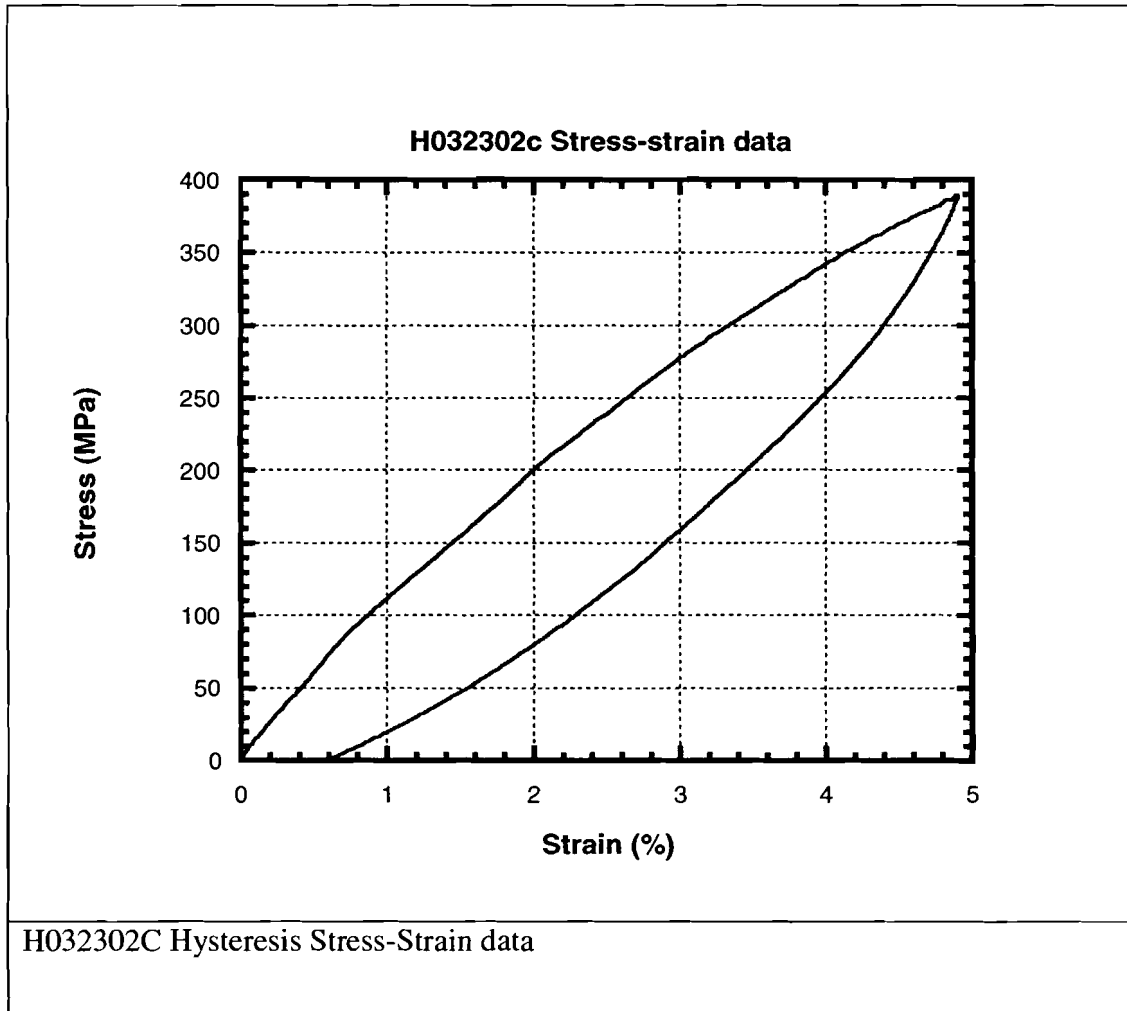


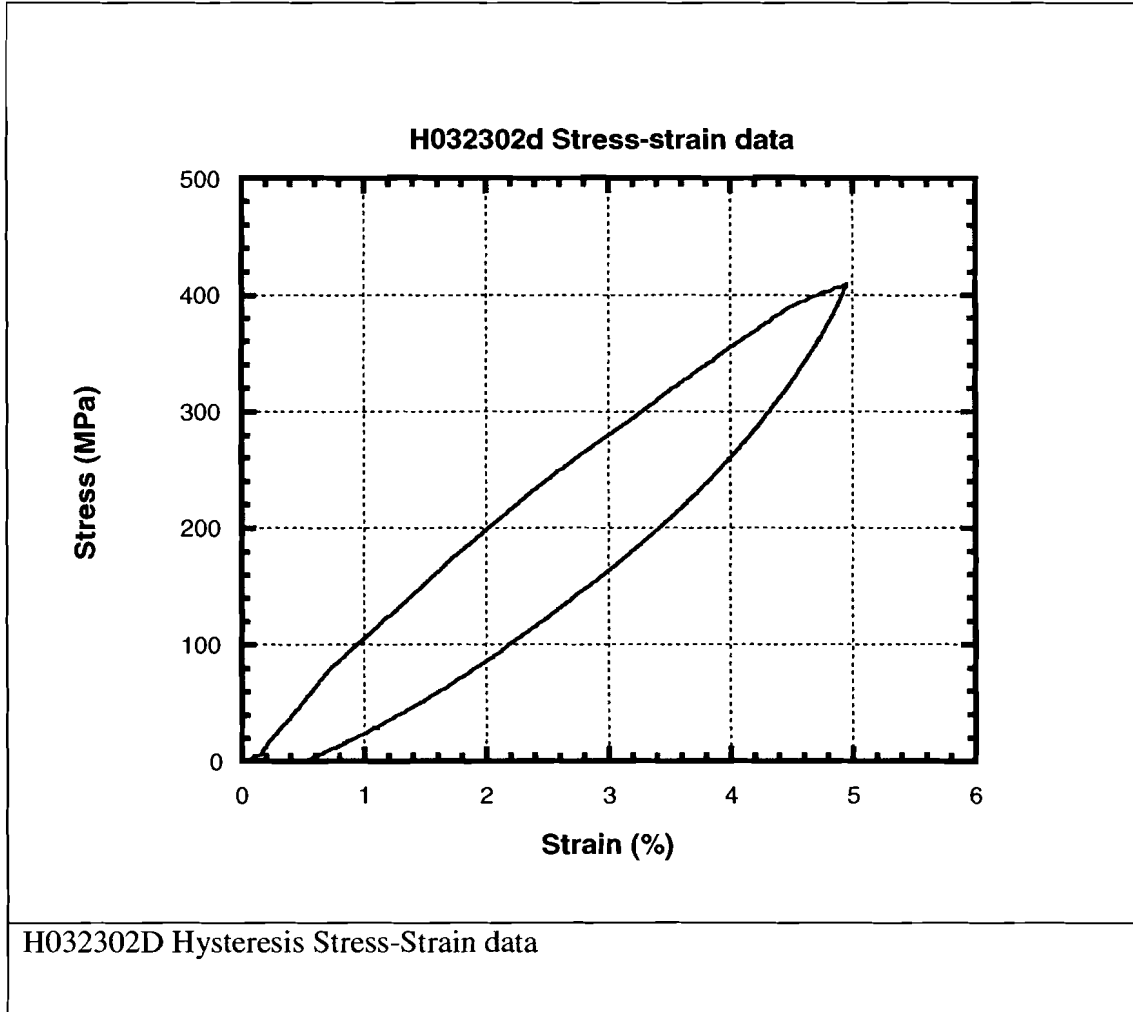
A1.4 Hysteresis Data

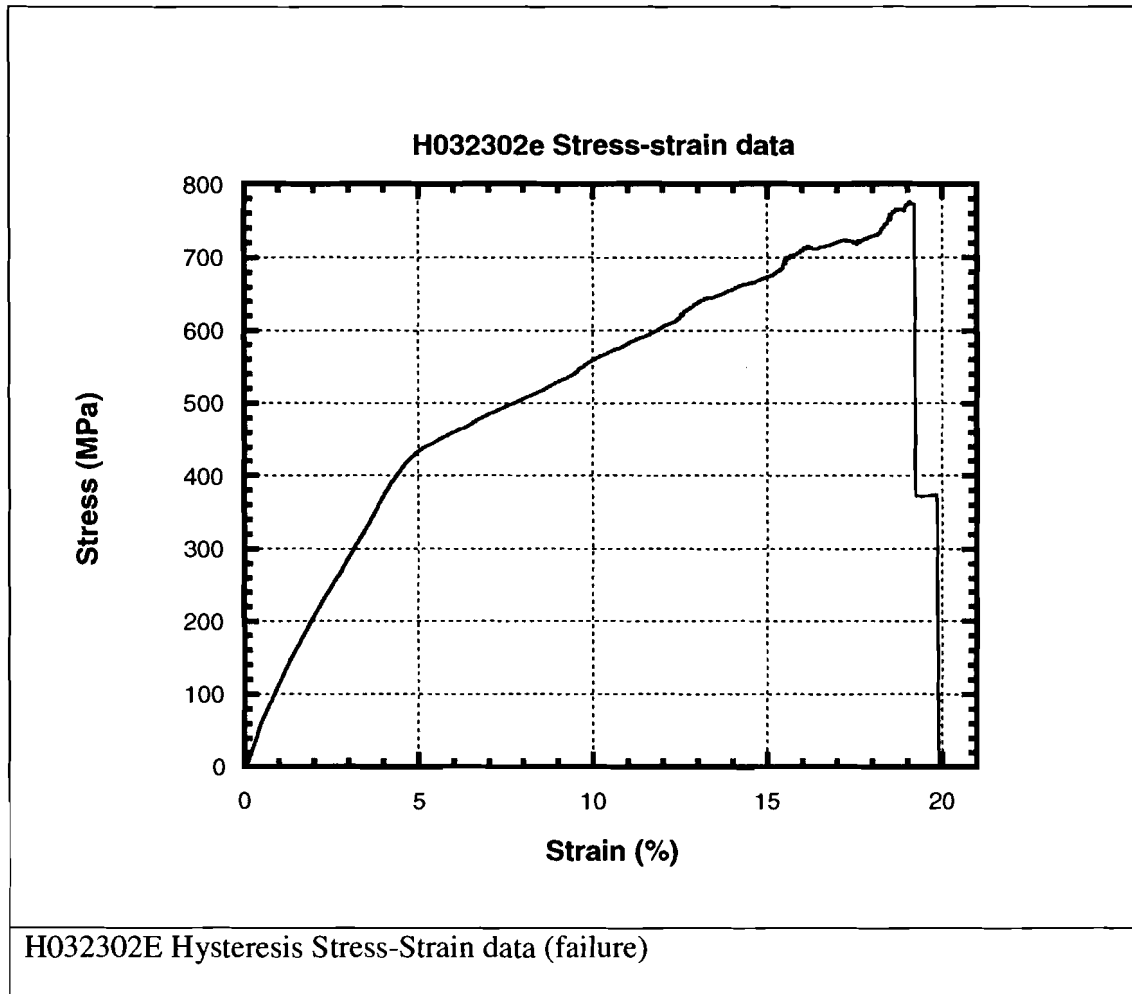












Appendix 2: Silk Preparation Overview

A2.1 Sample Preparation

Silk extraction is more of an art than science. Although coercing a spider to draw dragline silk is an acquired technique; all the following techniques have been streamlined for a target production setting.

Statoda triangulosa, a common, brown, house arachnid, is the type of spider used at LLE since the early 1980's. This species was chosen because of its availability and size. It commonly dwells in the Northeastern United States and is found in basements or garage corners. It is safe to keep in the lab since it is a non-poisonous variety. The mass of the spider ranges between 40 mg and 45 mg.

The procedure begins by drawing the silk from the spider. The drawing process is achieved by getting the spider to fall from a petri dish towards the countertop. In doing so, the dragline silk is produced. Once the spider nears the countertop, the silk is moved towards the ring stand assembly. The two parallel bars are used to capture the silk temporarily. Dragline silk does not possess glue like other types of silk. Therefore, two-sided tape is used for adhesion to the parallel bars.

Once the silk is secured between the bars, it is transferred to another temporary fixture. The "Ferris wheel" is a spool for thread. The wheel rotates on an axle and collects the harvested silk. One 30 cm long strand is divided into nine smaller sections of silk, making the job more manageable. The sections are the correct length for the beryllium "C-mount" for the target support, as well as for the test samples.

The next step is mounting the silk to the aluminum post assembly. One-quarter inch diameter thick-walled aluminum tubing acts as the upper grip assembly, or post. The tubing is a rigid fixture that is large enough (2.5" length) to be handled using your fingers. On the other end of the test sample is a 70 μm silicon carbide (SiC) fiber. It is 3 ± 0.1 mm long and has a mass of 0.1 mg. The SiC fiber acts like a plumb bob, using the silk as the connecting wire. The silk is positioned into place and secured by UV curing glue (Norland 65, Edmund Scientific). After the glue is cured, the remaining silk is cut from the Ferris wheel using stainless steel surgical scissors. The result is a silk test sample dangling from the aluminum post, as shown in *Figure 18*.

It is worth mentioning that assembly-mounting station is the foundation for the entire setup procedure. Shown below, the platform has vacuum capability in six places. Standing three inches tall, the mounting station fits underneath a Wild microscope, which is used during the whole process as well. The two micro-positioning stages utilized on the mounting station have four degrees of motion control: x, y, z, and rotation about the z-axis. These stages have the fine control necessary for mounting the silk test samples.

The baseline mechanical properties were established testing silk samples within 8 days after harvesting. This timeframe is practical, since during the production of cryogenic target mounts silk is generally used after 8 days. The silk does contain a protein which changes the pH to a slight acid, according to an article entitled "The spider web and thread," by Ed Nieuwenhuys (Mar. 1999). The acidity wards off bacteria from attacking the silk, thus giving it a longer shelf life. Although

the expiration date is not exactly known, measurements have been made greater than 8 days after harvesting and have not shown a reduction in the properties.

A2.2 Characterization

Initial length and diameter data are measured after the mounting procedure. The length of the silk is measured using the Powellscope metrology station. This device is run by a Newport MM3000 motor controller, which has 1-micron resolution for the x, y, and z-axes. The system is interfaced through the computer via the keyboard commands. A microscope is featured as part of the system for magnified views. A video monitor is also employed to relieve the user's eyestrain from the monocular microscope. Focusing on the silk/glue intersection, the user sets the origin and translates the test assembly until stopping at the second intersection. Seven measurements are taken and the average value is reported with an associated standard deviation.

Diameter measurements require much higher resolution. The Institute of Optics lends time for making these measurements using the scanning electron microscope operated by Brian McIntyre (Institute of Optics). One section of silk is measured per long strand (statistics are used to calculate an average diameter). The diameter changes slightly over the section length.

A2.3 Test Setup

Finding an off-the-shelf item such as a load cell with 0.1 mg resolution was an impasse. A device that had the resolution necessary to perform accurate measurements on a very small scale was designed and fabricated. The Mettler microbalance is a 15 g maximum scale, accompanied by an interfacing unit to the

data-storing computer. The driving unit for pulling the test sample was also fabricated in-house. A motor-controller driving an Oriel motor mike pulls the silk uniaxially. The controller readout has 0.1 μm units, and the crosshead rate is varied using a tunable dial.

The testing concept is as follows. A test sample mounted to the post assembly is inserted into an aluminum block, secured by a nylon setscrew. The block is attached to the translating motor mike stage. On the bottom end of the test sample, the SiC fiber attaches to an aluminum anchor, via 5-minute curing epoxy, that rests on the Mettler scale. As the sample is pulled upwards, the anchor (mass is 2.836 ± 0.001 g) is slowly being lifted off the scale. The load and displacement readings are read into a communication port and a data acquisition board respectively. The data is then written to an Excel file using Labview software, specifically created for this application. Labview was chosen for its straightforward programming format and hardware compatibility. The program vi's (virtual instruments) are shown in *Figure 5* and *Figure 6*. The front panel displays the raw load and displacement data.

Hardware components worth mentioning are the Kohu color camera, light source and Ectrohome monitor. These devices are utilized during final setup and all throughout the test cycle for viewing the test samples.

The test is over when the test sample has ruptured. The Labview program, controller and Mettler balance are manually turned off. The analysis is then finalized using Excel and Kaleidagraph software packages.

A2.4 Appendix Figures

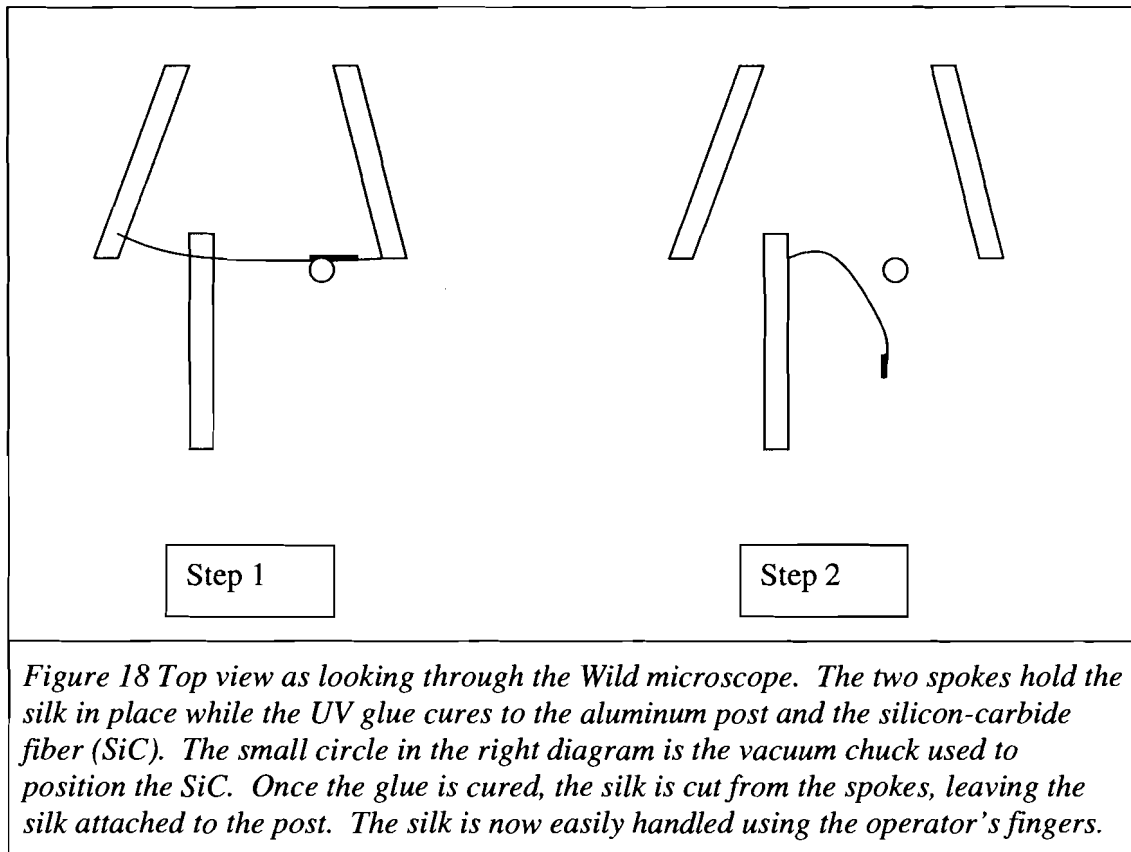


Figure 18 Top view as looking through the Wild microscope. The two spokes hold the silk in place while the UV glue cures to the aluminum post and the silicon-carbide fiber (SiC). The small circle in the right diagram is the vacuum chuck used to position the SiC. Once the glue is cured, the silk is cut from the spokes, leaving the silk attached to the post. The silk is now easily handled using the operator's fingers.

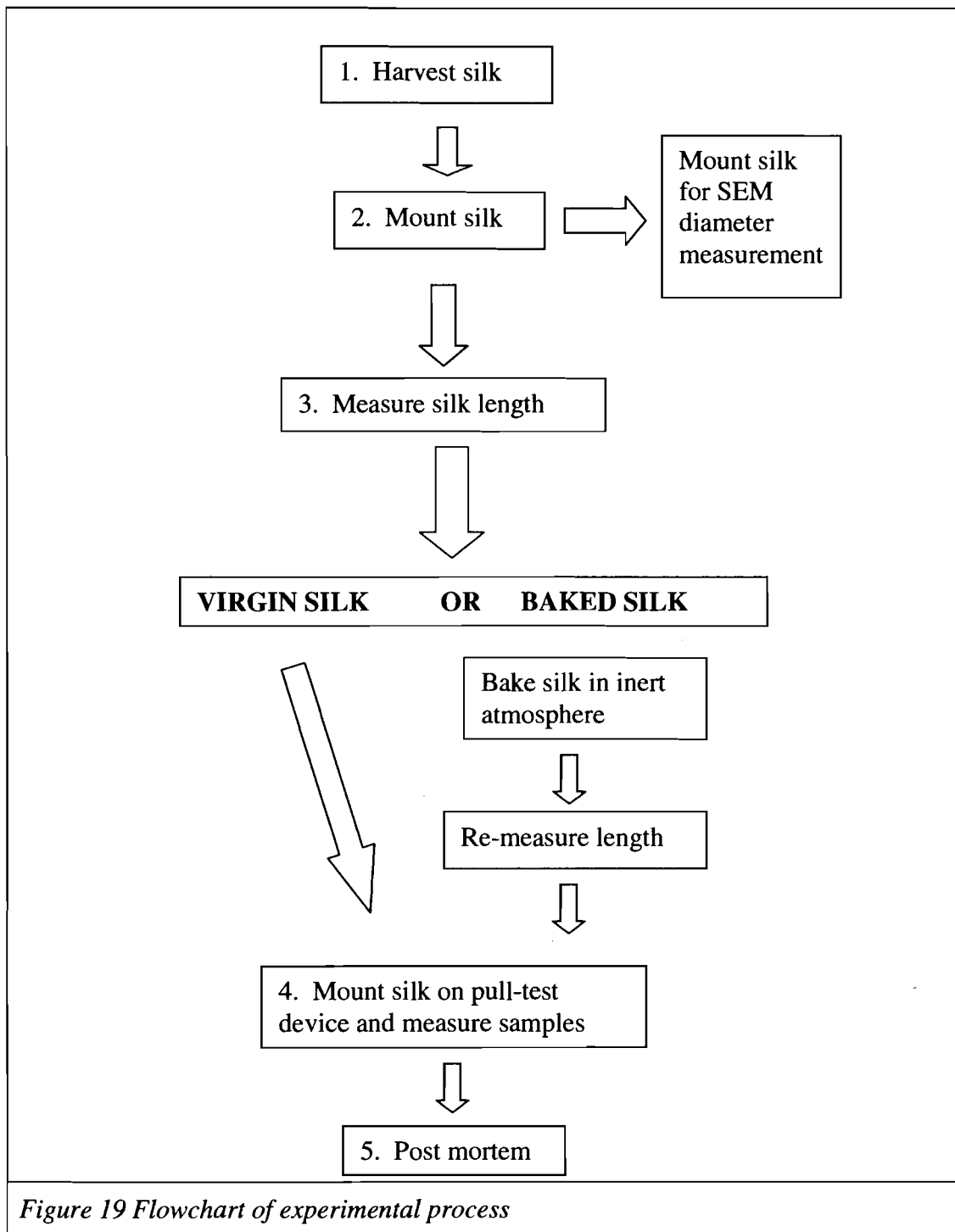


Figure 19 Flowchart of experimental process